IMPROVING ULTIMATE RECOVERY IN THE GRANITE POINT FIELD TYONEK C SANDS

By

Thomas L. Nenahlo, B.S. ChE

A Dissertation Submitted in Partial Fulfillment of the Requirements for the Degree of

Master of Science

in

Petroleum Engineering

University of Alaska Fairbanks

December 2018

APPROVED:

Dr. Abhijit Dandekar, Committee Chair

Dr. Shirish Patil, Committee Co-Chair

Dr. Samson Ning, Committee Member

Abstract

The objective of this research is to determine how the ultimate recovery of the Granite Point field can be improved. An understanding of the depositional setting, structure, stratigraphy, reservoir rock properties, reservoir fluids, aquifer, and development history of the Granite Point field was compiled. This was then leveraged to provide recommendations on how the ultimate recovery can be improved.

The Granite Point field Tyonek C sands are located on an anticline structure at 8,000' to 11,000' SSTVD within the offshore Cook Inlet basin. These sands were deposited in a fluvial environment with the source material provided by the Alaska Range to the northwest. Due to uplifting, the Tyonek C sands are of relatively low porosity for their depth. The sands thin, become more numerous, and are of generally lower porosity from southwest to northeast. Oil quality is excellent and displacement efficiency of the reservoir rock with water flood exceeds 50% at breakthrough. Although displacement efficiency is high, the relative permeability to water is extremely low. The fracture gradient of the reservoir rock is on the order of magnitude of 1.0 psi/ft.

Many initiatives were undertaken throughout the history of the Granite Point field to improve the rate and resource recovery, all of which were met with negligible success with the exception being the introduction of horizontal wells that were first drilled in the early 1990's. The underlying reason for the lack of success of these other initiatives is the low effective permeability to oil and the extremely low effective permeability to water. Secondary recovery with water injection was successful in the early stage of development, and can be in the future, but only when applied between wells that are connected by a sand of acceptable porosity.

The results of this research indicate that to improve the ultimate recovery of the Granite Point field a thorough quantification of aquifer and injection water movement must first be understood, then horizontal wells can be placed in appropriate locations to improve the offtake and leverage the weak aquifer drive to provide pressure support.

Table of Contents

Page

Table of Contents (Continued)

Page

List of Figures

Page

List of Figures (Continued)

Page

List of Figures (Continued)

Page

List of Tables

Page

List of Equations

Page

Chapter 1: Field Overview and Project Objective

1.1 Field Development History

The Granite Point field is located in the offshore Cook Inlet basin of southcentral Alaska (Figure 1). Granite Point field was discovered by the Pan American Tyonek State 18742-1 well in July of 1965, with the discovery confirmed by the Mobil Granite Point-1 well. The primary oil sands encountered were the Tyonek C sands, a series of stacked fluvial sands that are at depths of 8,000-11,000' Sub Sea True Vertical Depth (SSTVD), with the Hemlock encountered as a secondary target of limited productivity.

The Granite Point, Anna, and Bruce production platforms were installed in 1967 with first oil production beginning in March of that year. The Tyonek C sands were developed first with Hemlock being brought into production in the 1990's. The focus of this research will be upon the improvement of the ultimate recovery of the Tyonek C sands.

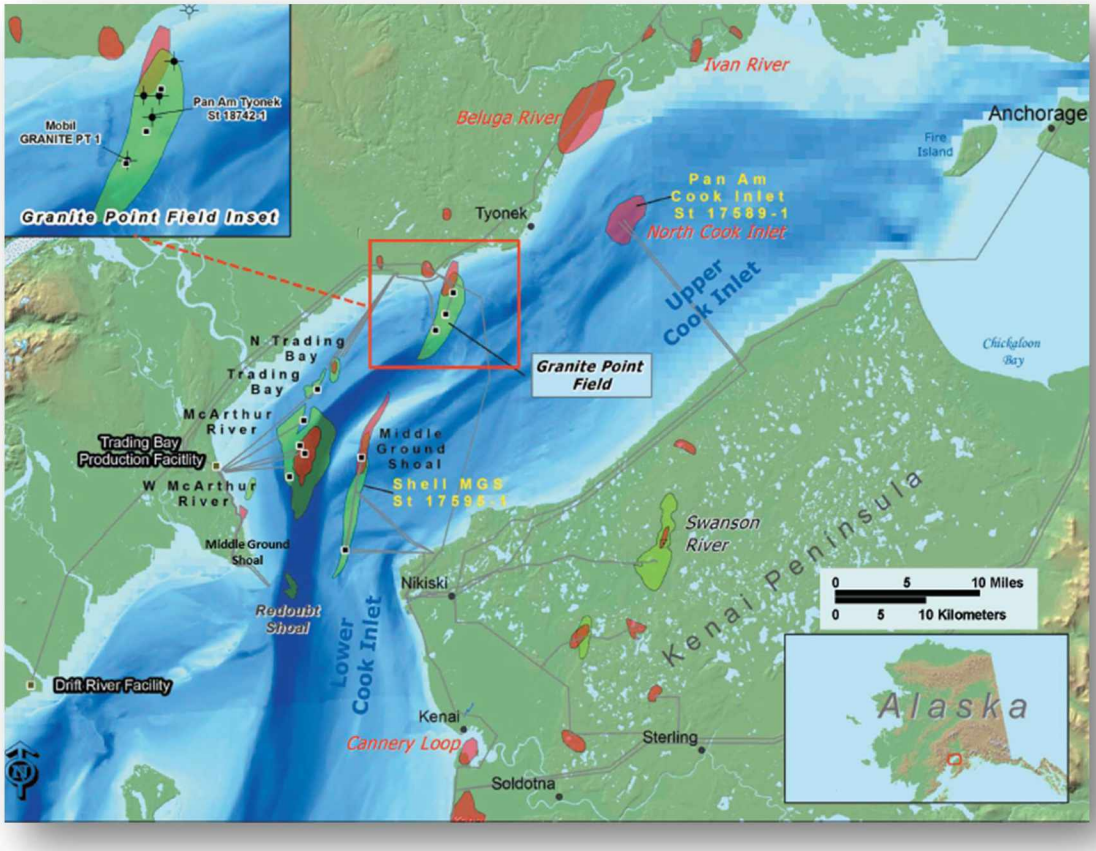

Figure 1: The Granite Point Field, Cook Inlet, Alaska. Reprinted from "The Granite Point Field, Cook Inlet, Alaska" by M.J. Frankforter and J.C. Waugaman, 2013, in D.M. Stone and D. M. Hite, ed., Oil and gas fields of the Cook Inlet Basin, Alaska: AAPG Memoir 104, p. 263–290.

With the completion of the Granite Point, Anna, and Bruce production platforms, the first phase of development began. This first phase of development consisted of drilling slant producing wells targeting the Tyonek C sands. Single and dual-string completions were used, with all oil-bearing Tyonek C sands present in the well cased, cemented, and perforated. The Tyonek C sands were produced commingled. For artificial lift the Granite Point Platform utilizes gas lift while the Anna and Bruce Platforms utilize a power oil jet pump system that cycles dead crude through a downhole jet pump.

In 1970 peak production was achieved at nearly 53,000 BOPD. A steep oil rate decline was realized, prompting the initiation of a waterflood in the early 1970's. Oil production remained flat through the 1970's as a result of this waterflood and a second round of development that began in 1975 and ended in 1983. After completion of a brief development program in the late 1980's from the Anna platform the operator Amoco, along with the group of owners known as the Chakachatna Group (Getty, Phillips, ARCO, and Chevron), sold their interest in the Anna and Bruce platforms to Unocal, the operator of the Granite Point platform. Unocal initiated a third round of development that began in 1990 and ended in 1998 and introduced the first horizontal wells to the Granite Point field, as well as development of the Hemlock formation. During this third round of development waterflood was re-activated, although to a limited extent, at all three platforms (Figures 2 and 3).

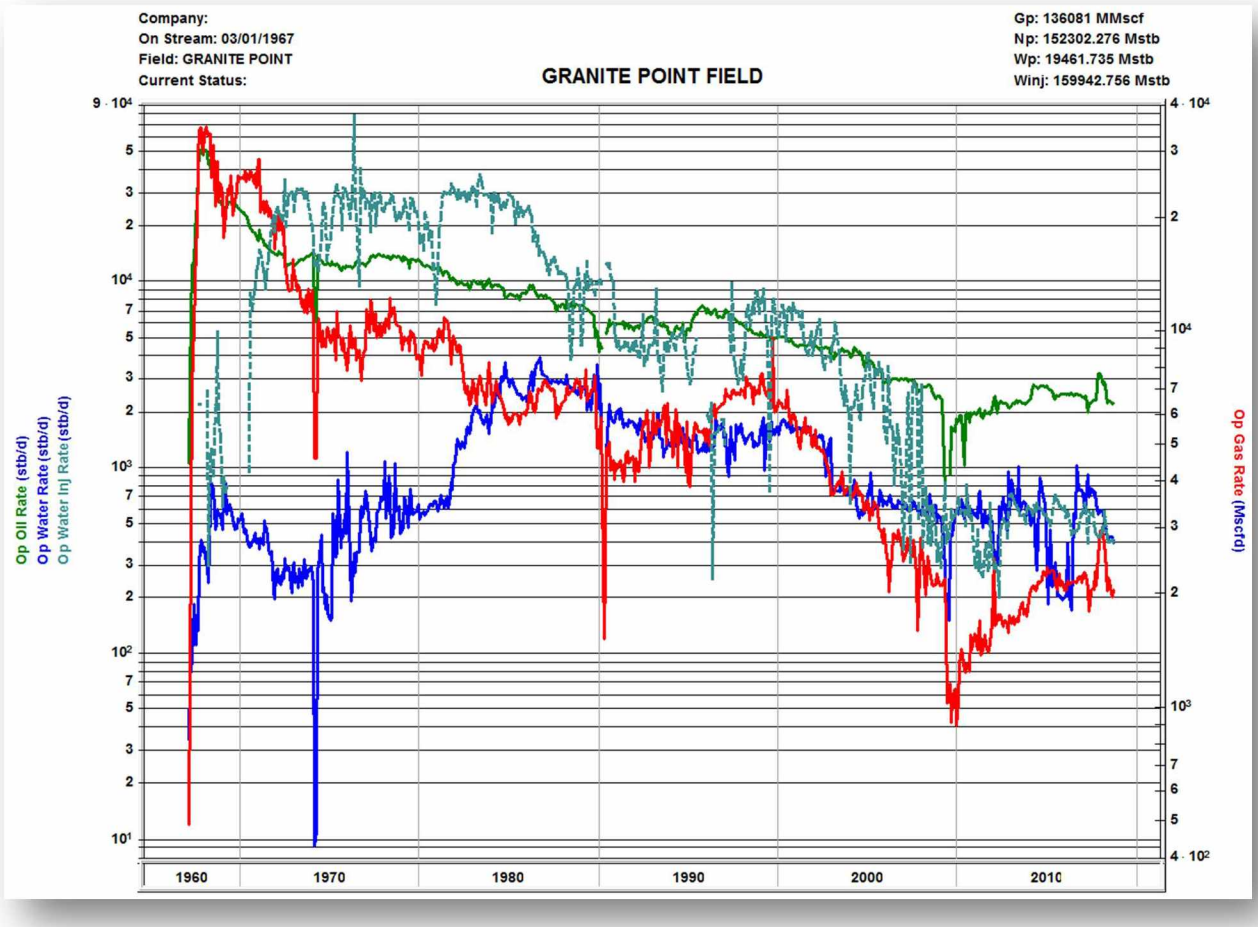

Figure 2: Granite Point Field Production History.

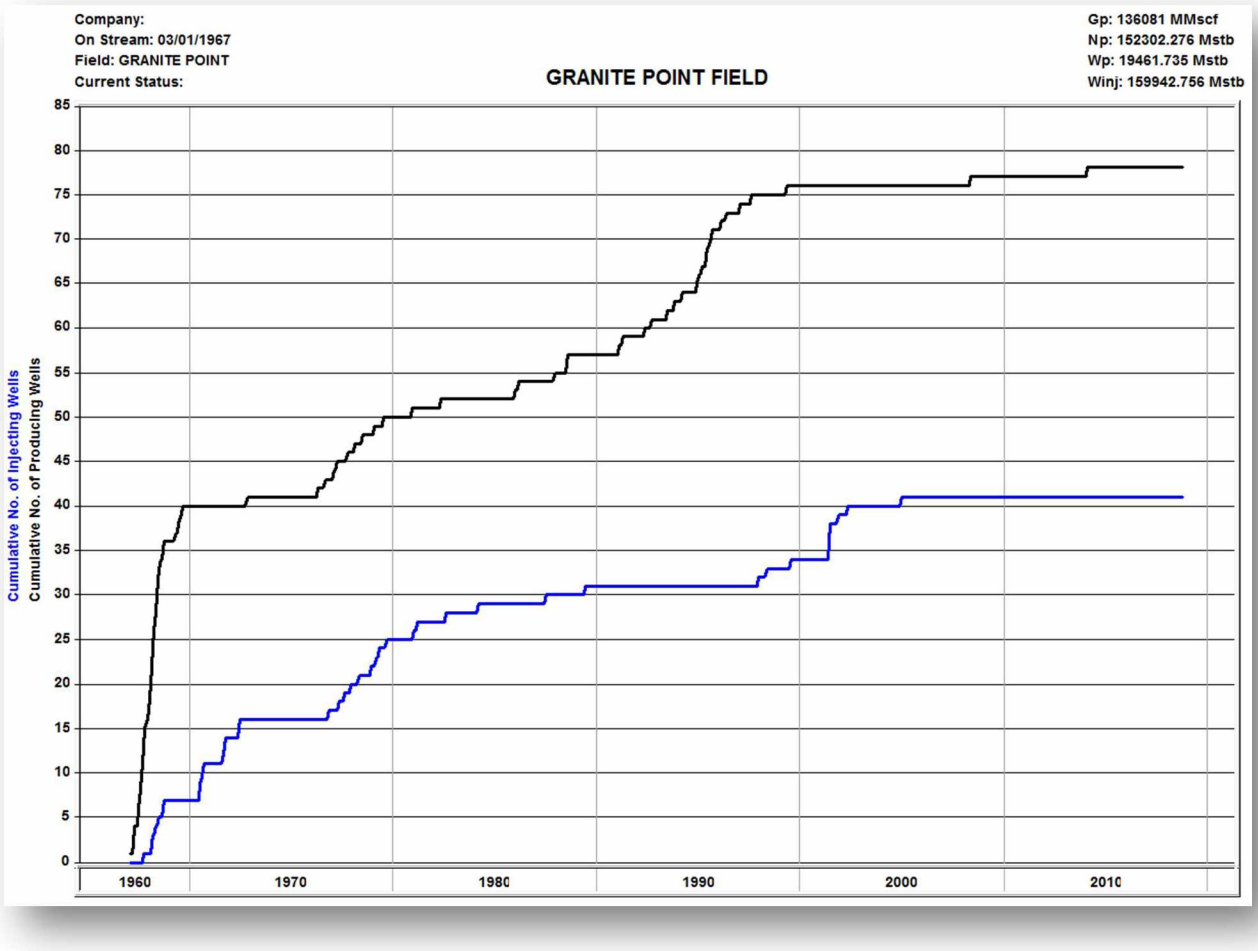

Figure 3: Granite Point field producing and injecting wells. Three major phases of development occurred, with the third phase that occurred in the 1990's introducing the first horizontal wells.

From 1998 to 2008 no new development wells were drilled. In 2005 Unocal was acquired by Chevron, that as operator drilled two development wells in 2008 targeting the east and west flanks of the field from the Anna platform, neither resulting in a commercial success.

In 2011 Chevron sold the Granite Point field to Hilcorp Energy Company, which drilled its first development well from the Anna platform in 2015, targeting the Hemlock formation. In 2017 a three horizontal well development program was undertaken in 2017 targeting the Tyonek C sands on the east flank of the field from the Granite Point platform.

1.2 Project Objective

The Granite Point field has produced a cumulative 151 MMSTBO as of year-end 2017, with nearly all of this being produced from the Tyonek C sands. Initial oil in place estimates from previous operators are in excess of 700 MMSTBO.[1] At current production rates the estimated recovery factor will be less than 25%. The purpose of this study is to assess the Granite Point field's Tyonek C sands to determine how to improve the ultimate recovery of the field.

Chapter 2: Geology

2.1 Geology Section Preface

The first fundamental step required in any field study is to thoroughly understand the geologic setting. The Granite Point field was discovered in 1965 and this author has the luxury of being able to leverage 53 years' worth of studies undertaken by the many operators and joint interest owners of the Granite Point field. The fundamental interpretations of the geology have changed little since the initial development phase was completed, but each new well, core study, petrophysical analysis, seismic study, and the continued accumulation of production data has provided an ever clearer understanding of the Granite Point field.

In 2013 a comprehensive paper by Frankforter and Waugaman was published that addressed each component of the geology of the Granite Point field. This paper was published in the American Association of Petroleum Geologists Memoir 104. It is truly the cornerstone for understanding the geologic setting as it compiles all of the geology work done over the life of the field in a clear and concise format. This work, along with the references that it was built upon, is leveraged to provide the reader the necessary geologic background that supports the reservoir engineering work done to determine how the ultimate recovery can be improved.

It must be noted that this author agrees with the interpretations summarized by Frankforter and Waugaman with one key difference. Frankforter and Waugaman state that sensitivity to aqueous fluids introduced through drilling mud or water flooding is not an issue in the field. This author disagrees with this statement and the subject is critical for understanding how to improve the ultimate recovery of the field. This subject will be further explored in Chapter 3.

2.2 Tectonic Setting and Geologic History

The geologic history of the Cook Inlet area can be divided into two distinct phases associated with the Mesozoic and Cenozoic eras (Figure 4).[1]

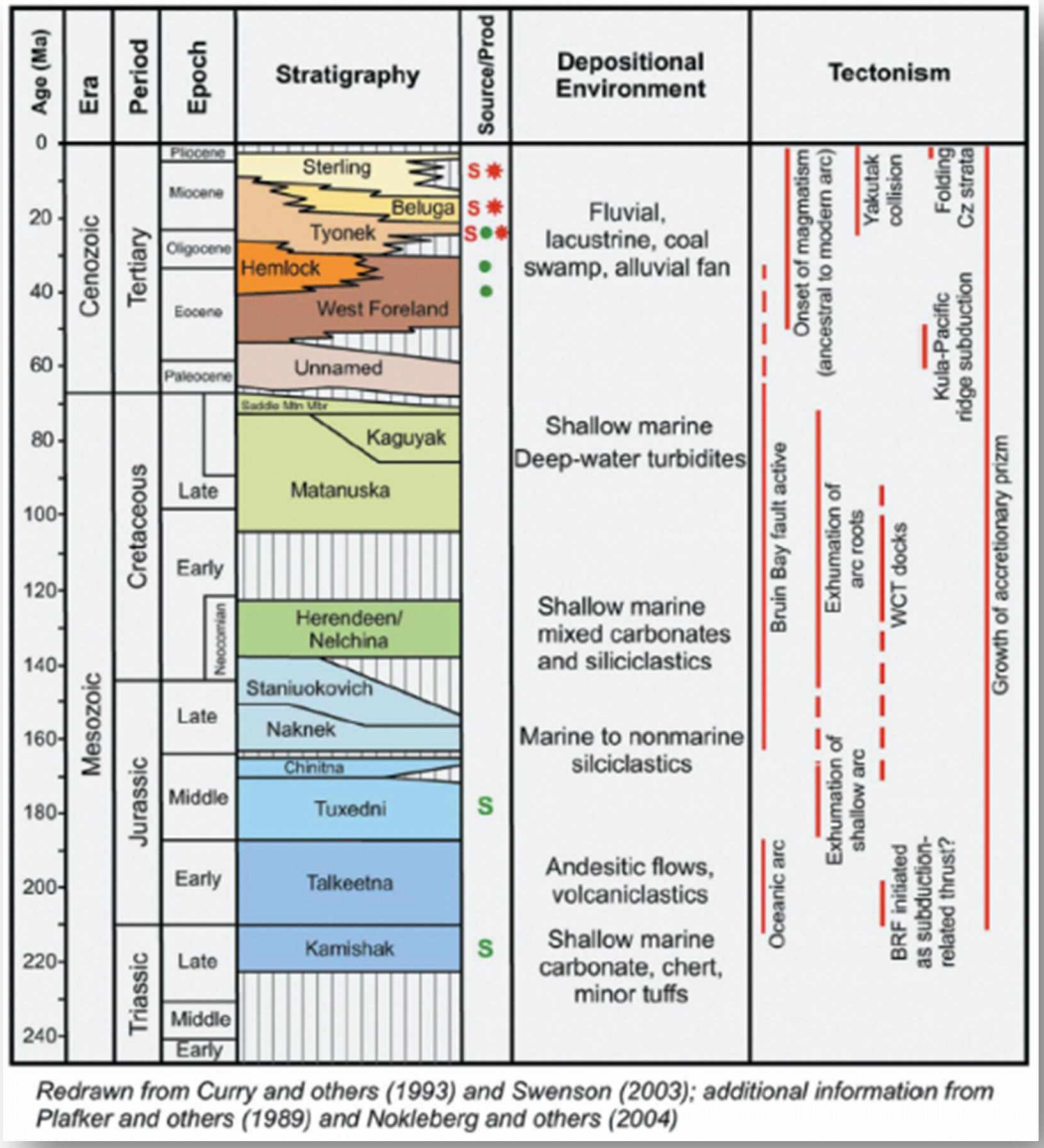

Figure 4: Cook Inlet Basin Stratigraphic Column. Reprinted from "The Granite Point Field, Cook Inlet, Alaska" by M.J. Frankforter and J.C. Waugaman, 2013, in D.M. Stone and D. M. Hite, ed., Oil and gas fields of the Cook Inlet Basin, Alaska: AAPG Memoir 104, p. 263–290.

The Cook Inlet Basin is, in present time, in a forearc setting bounded on the northwest by the rising Alaska Range Complex, to the north by the Talkeetna Range, and by fault contact with the accreted Mesozoic deep marine deposits of the Chugach Terrane to the southeast.

The terranes that form the foundation of the basin were depositing and accreting throughout the Paleozoic and Mesozoic eras along the western North American continental plate margin that was advancing over the oceanic

Farallon, Kula, and Pacific plates.[2] The placement of these terranes was complete by the mid-Cretaceous, followed by a late-Cretaceous period of mostly marine deposition across the entire basin. The early Cenozoic was marked by a period of counterclockwise rotation of the Cook Inlet area and reorienting plate motions. What was once a northwesterly-trending oblique margin between plates became an acute margin trending southwesterly as the oceanic plate began subducting steeply beneath the accreted continental terranes. At this time a strike-slip component of stress developed across the Alaska region, resulting in the Castle Mountain and Bruin Bay faults that are located along the northwest edge of the basin (Figure 5).[1]

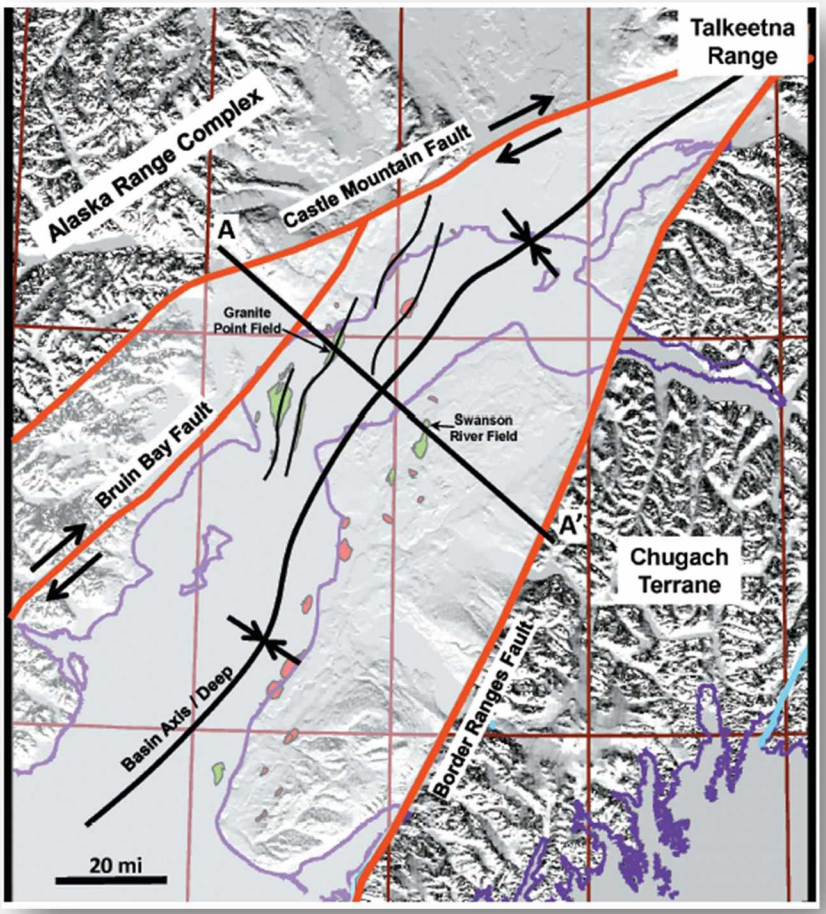

Figure 5: Major tectonic elements of the upper Cook Inlet Basin. Reprinted from "The Granite Point Field, Cook Inlet, Alaska" by M.J. Frankforter and J.C. Waugaman, 2013, in D.M. Stone and D. M. Hite, ed., Oil and gas fields of the Cook Inlet Basin, Alaska: AAPG Memoir 104, p. 263–290.

During the Tertiary period the basin continued to subside. With the Alaska Range Complex uplifting at this time, accommodation space for fluvial deposits was created. Although it is theorized that marine flooding occurred

periodically during this time, there is no definitive evidence of marine deposits. Climatic variations, periodic uplift, and shifting of the channel belts are believed to be the cause of the repetitive sequences of sand, claystone, and coal observed in the sedimentary section.[1]

Due to a regional east-west right lateral stress component combining with a northwest-southeast oriented compression from subduction, the basin was placed in a transpressional stress regime. The structural characteristics indicate a strong compressional component where anticlines formed along a northeast-southwest trend. The Granite Point Field is situated along the crest of one of these northeast-southwest trending anticlines. The field is steeply dipping to the west and it is extremely difficult to image this steep west flank seismically.[1] An effort was undertaken by Frankforter, et al. to understand the kinematic origin of the structure in order to guide interpretations in areas with minimal well control along this west flank. Figure 6 shows the results of this work, a balanced dip section across the central part of the field and its corresponding reconstructed section. This work indicates that the Granite Point field is associated with a high-angle reverse fault along its west flank associated with a large-scale basement step feature. A series of large, predominantly down-to-the-northeast faults in the shallow Beluga and Tyonek section also developed in the northern part of the field.[1]

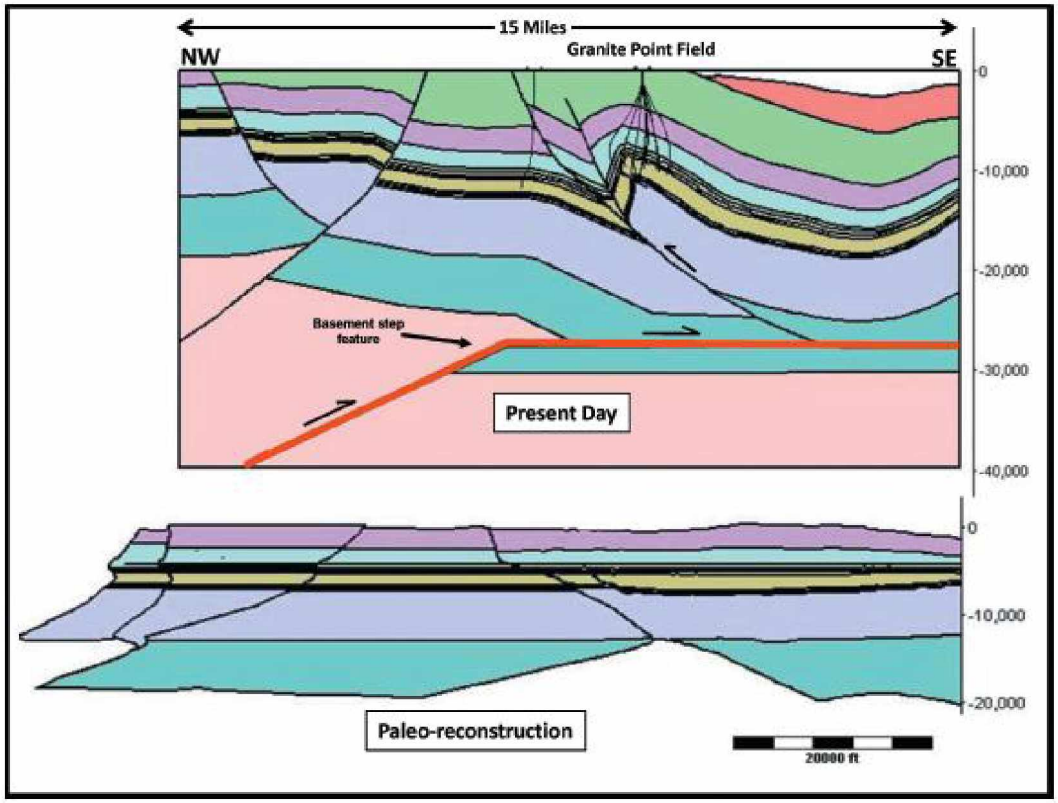

Figure 6: Diagramattic balanced cross section. Top image is the balanced cross section constructed in dip direction across Granite Point field. Major bend in basement thrust plane is highlighted in red. Bottom image is flexural-slip paleo-reconstruction of top image section. The paleo-reconstruction is flattened on the Tyonek reservoir interval. Reprinted from "The Granite Point Field, Cook Inlet, Alaska" by M.J. Frankforter and J.C. Waugaman, 2013, in D.M. Stone and D. M. Hite, ed., Oil and gas fields of the Cook Inlet Basin, Alaska: AAPG Memoir 104, p. 263–290.

2.2 Stratigraphy

The Tyonek C sands at Granite Point field lay within an interval of sequences of sandstone, conglomerate, claystone, and coal. Previous operators have divided the Tyonek C sands into ten zones, the C1 through C10 as shown in Figure 7 below. Within these ten major zones are several sub-zones. These zone definitions are carried throughout this project report.

These sands are amalgamated fluvial deposits of sand, conglomerate, and silt with a fining upward characteristic. The coals present within the Tyonek C sands are predominantly laterally continuous, providing excellent hydraulic barriers and geologic markers.

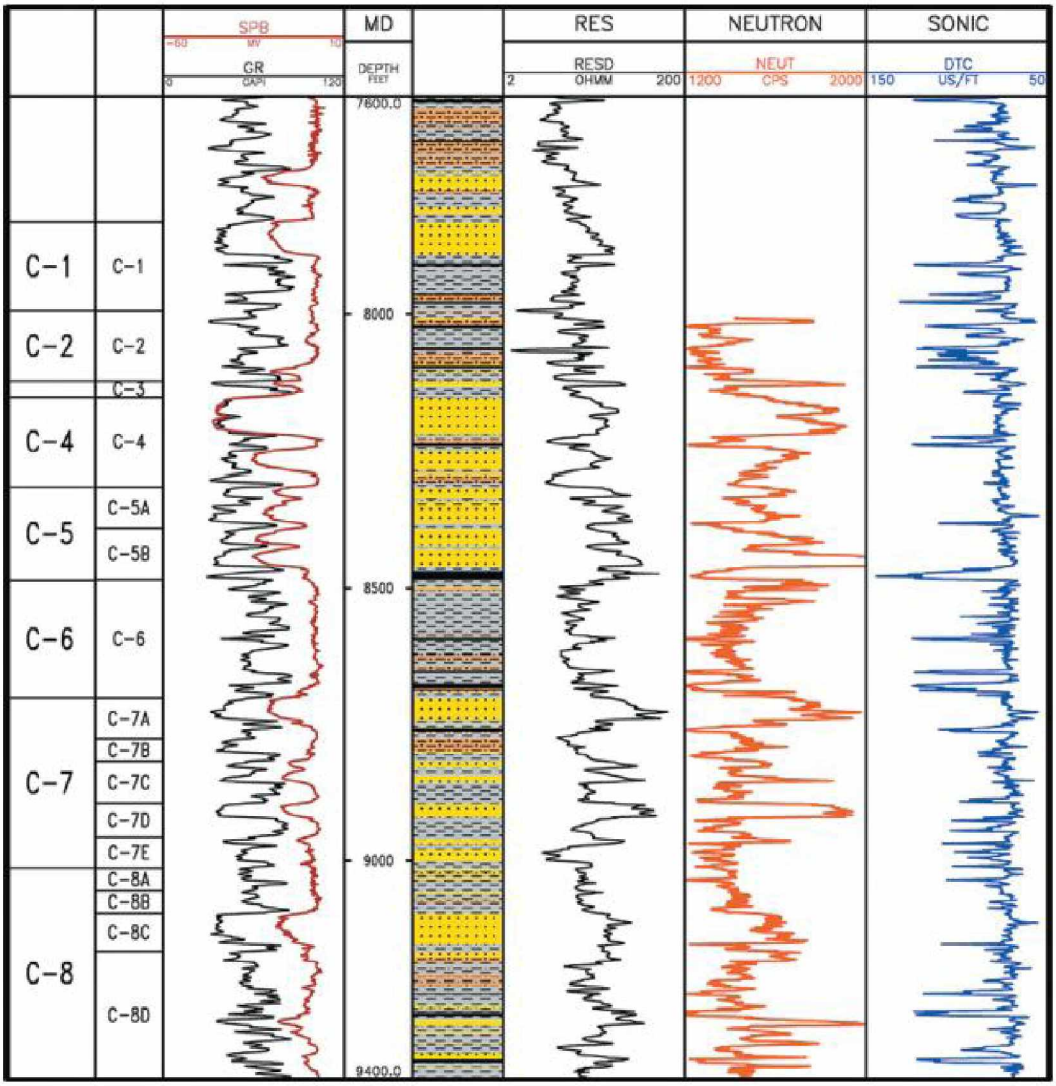

Figure 7: Log response from example Tyonek C zones from the Unocal AN-03 well. Reprinted from "The Granite Point Field, Cook Inlet, Alaska" by M.J. Frankforter and J.C. Waugaman, 2013, in D.M. Stone and D. M. Hite, ed., Oil and gas fields of the Cook Inlet Basin, Alaska: AAPG Memoir 104, p. 263–290.

2.3 Reservoir Characterization

The Tyonek C sands are fluvial deposits with the sediment having been derived primarily from the Alaska Range to the northwest and a smaller amount from the Talkeetna Range to the northeast. A modern analog to the deposition environment is the Susitna River Valley. In present day the Susitna River is depositing channels that are hundreds of feet wide and tens of feet thick. This is analogous to the Tyonek C sands that range from less than 10 feet up to 200 feet thick. These thicker sand packages are believed to be amalgamated channels.[1]

The sands are composed of fluvial clastics ranging from fine grained sandstone to conglomerate. Siltstones are also present, and where present tend to degrade reservoir quality. Within the sandstones the clay content is low, as shales tend to be confined to the channel overbank and channel abandonment environments.[1]

From well control the channel orientations align along a general northwest-southeast trend, conforming to the expected sediment source, the Alaska Range. Variation in channel orientation amongst the Tyonek C sands is generally in the order of magnitude of tens of degrees.

Lateral continuity of these sands is a major factor in the evaluation of options to improve the ultimate field recovery. The Tyonek C sands exhibit a wide range of lateral continuity, which poses a significant challenge to implementing an effective waterflood. Figures 8a and 8b demonstrate the variability of channel continuity between reservoirs.

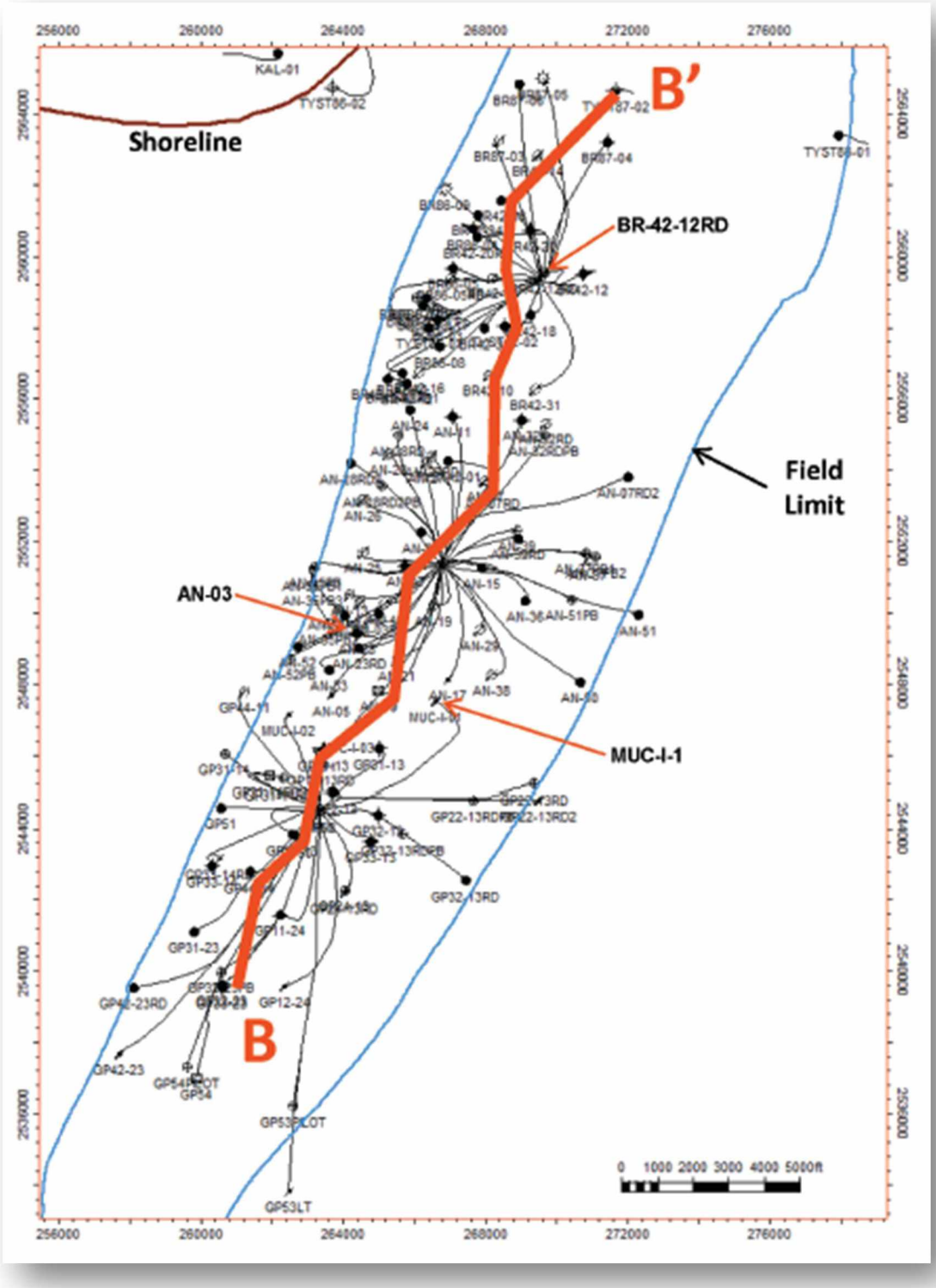

Figure 8a: Index map of Granite Point field showing line of cross section displayed in Figure 8b. Reprinted from "The Granite Point Field, Cook Inlet, Alaska" by M.J. Frankforter and J.C. Waugaman, 2013, in D.M. Stone and D. M. Hite, ed., Oil and gas fields of the Cook Inlet Basin, Alaska: AAPG Memoir 104, p. 263–290.

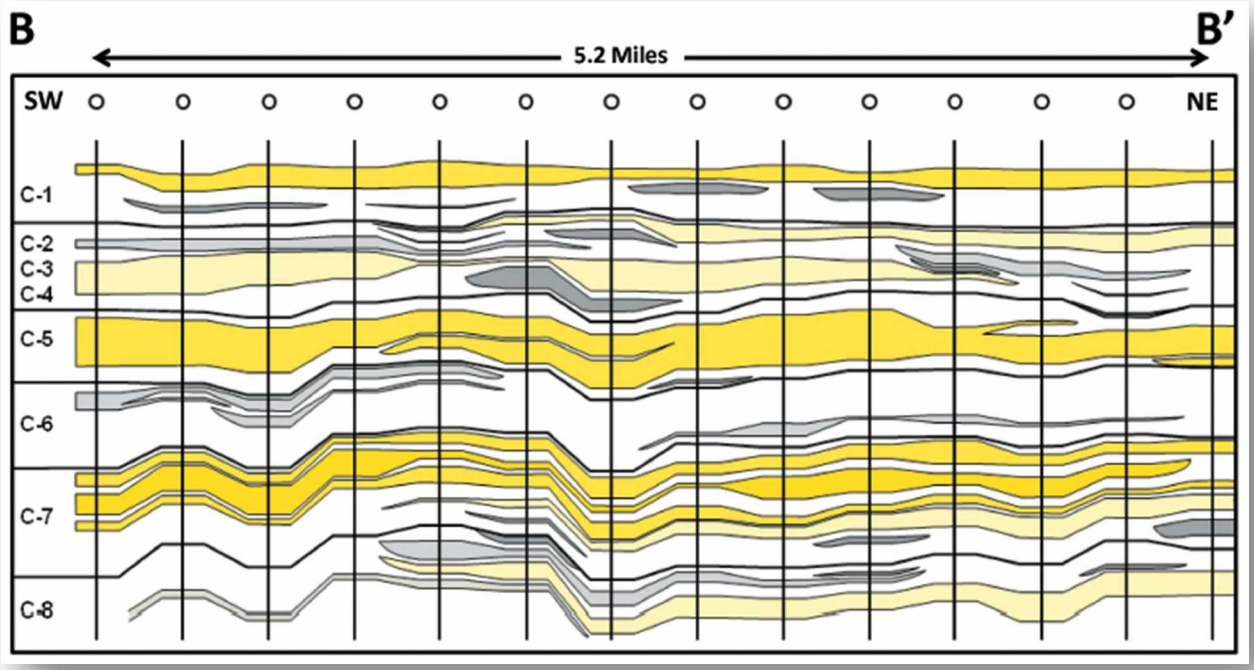

Figure 8b: Schematic cross section through 14 wells along the axial crest of Granite Point field illustrating the continuity of the reservoir sands in the Tyonek C zones. The section location is shown in Figure 8a. The continuity is color coded: Yellow in 11 wells (sand is correlated for 11 contiguous wells), Light Yellow 7-11 wells, Light Gray 3-6 wells, and Gray 1-2 wells. Reprinted from "The Granite Point Field, Cook Inlet, Alaska" by M.J. Frankforter and J.C. Waugaman, 2013, in D.M. Stone and D. M. Hite, ed., Oil and gas fields of the Cook Inlet Basin, Alaska: AAPG Memoir 104, p. 263–290.

As illustrated in Figures 8a and 8b, the lateral continuity of the Tyonek C sands is highly variable. As the sands become thicker they tend to become more laterally continuous and therefore more amenable to a successful waterflood. The thicker sands represent a period of high aggradation, increased coarse sediment, channel confinement, or a varying combination of all three.[1]

In regards to ultimate recovery, the sands become thinner, although more numerous, from the southwest to the northeast of the Granite Point field. This is a critical piece of information for future development.

A total of 41 conventional cores have been recovered from the Granite Point field, predominantly from the C5 and C7 sands as these have proven to be the most prolific reservoirs. From special core analyses completed on these cores, porosity and permeability is primarily influenced by rock facies, diagenesis, and structural deformation. The facies effects include the lithology, grain size, and sorting while the diagenesis effects include grain compaction and cementation. The structural deformation appears to have resulted in a varying degree of tectonically induced fracturing, specifically along the crest of the structure, and a degradation of reservoir quality due to shearing along

the west flank of the structure. C5 zone core acquired along the west flank contained intervals of thin, clay-filled bands related to shearing. Conglomerates contained fractured pebbles along with clay-filled deformation banding.[1]

In core that captured a fully preserved channel deposit a fining-upward sequence is typically seen. In these fluvial sands the deposition environment is chaotic and channel down cutting, lateral channel migration, and variations in flow regimes result in a large degree of lateral heterogeneity.

From petrographic studies the sandstones have been classified as lithic to sublithic arenites consisting of monocrystalline to polycrystalline quartz, K-feldspar, and plagioclase. Porosity is primarily intergranular, with leaching of the feldspar and some other rock fragments resulting in secondary porosity. Grain contacts that are interpenetrating and concavo-convex are evidence of significant primary porosity loss through compaction. Precipitation of mineral cements, predominately kaolinite, quartz overgrowth, and some smectite, has also degraded reservoir quality.[3]

The relationship between porosity and permeability is strongly influenced by grain size and sorting. Conglomerates in the Granite Point field tend to have a lower average porosity, but a greater permeability for a given porosity, when compared to the sandstone (Figure 9). The poorly sorted conglomerates will be more efficiently packed, limiting depositional porosity, while the coarse sand matrix will preserve a higher percentage of large pore throats with mechanical compaction accommodated by the rotation and repacking of larger pebbles and cobbles. Despite the favorable porosity-permeability relationship of the conglomerates, the sandstone lithofacies exhibits the best flow capabilities because of the greater overall pore volume.[1]

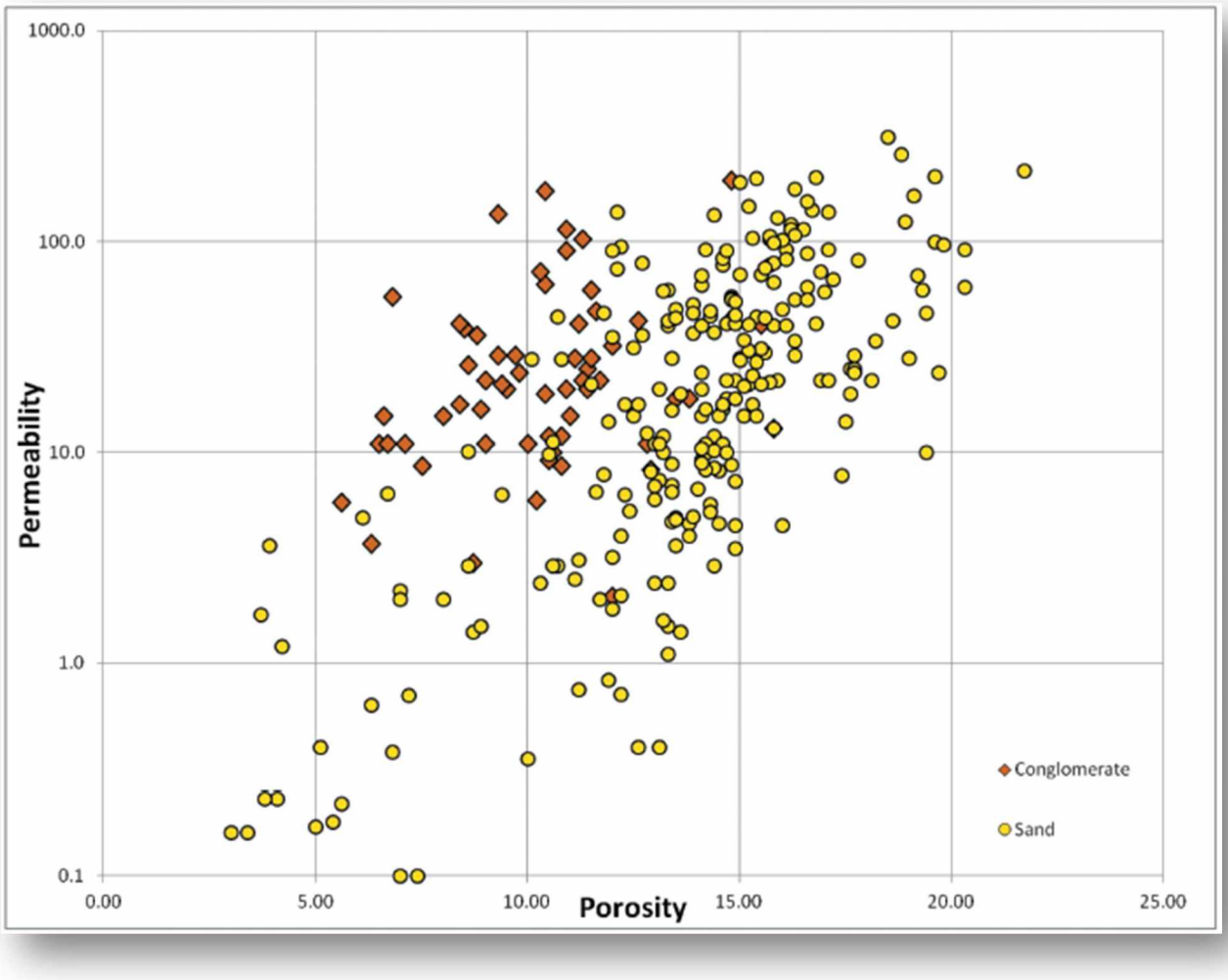

Figure 9: Permeability vs. porosity cross-plot for the Tyonek C zones. Data are from core analysis of conventional core plugs from eight selected wells at the Granite Point field. Reprinted from "The Granite Point Field, Cook Inlet, Alaska" by M.J. Frankforter and J.C. Waugaman, 2013, in D.M. Stone and D. M. Hite, ed., Oil and gas fields of the Cook Inlet Basin, Alaska: AAPG Memoir 104, p. 263–290.

Diagenetic effects on reservoir quality at Granite Point field are mainly the result of compaction and cementation. X-ray diffraction studies indicate that kaolinite comprises 70 to 85% of the clay-size grain fraction, followed by illite (5-10%), chlorite (trace – 3%), and smectite (0-5%).[1] The authors Frankorter and Waugaman stated that sensitivity to aqueous fluids introduced through drilling mud or water flooding is not an issue at the Granite Point field. They contend that kaolinite, along with silt-size feldspar grains will mobilize as water saturation rises when the aquifer or a waterflood front moves through the reservoir, therefore resulting in a reduction in effective permeability. Although fines migration is a potential culprit for the degradation of the effective permeability there is a significant amount of field and special core analysis (SCAL) data that suggests a strongly-water wet reservoir rock is

a primary reason for the degradation of effective permeability. This field and SCAL data will be investigated further in Chapter 3.

The porosity vs. depth relationship at the Granite Point field indicate that the Tyonek C sands were buried much deeper before being uplifted in to the current anticline structure. The average porosity of 13.5% encountered in the Granite Point field at 8,000-9,000 ft in subsea depth should occur at approximately 11,000-12,000 ft based on analog fields without uplift (Figure 10). This indicates an uplift of approximately 3,000 ft has occurred.

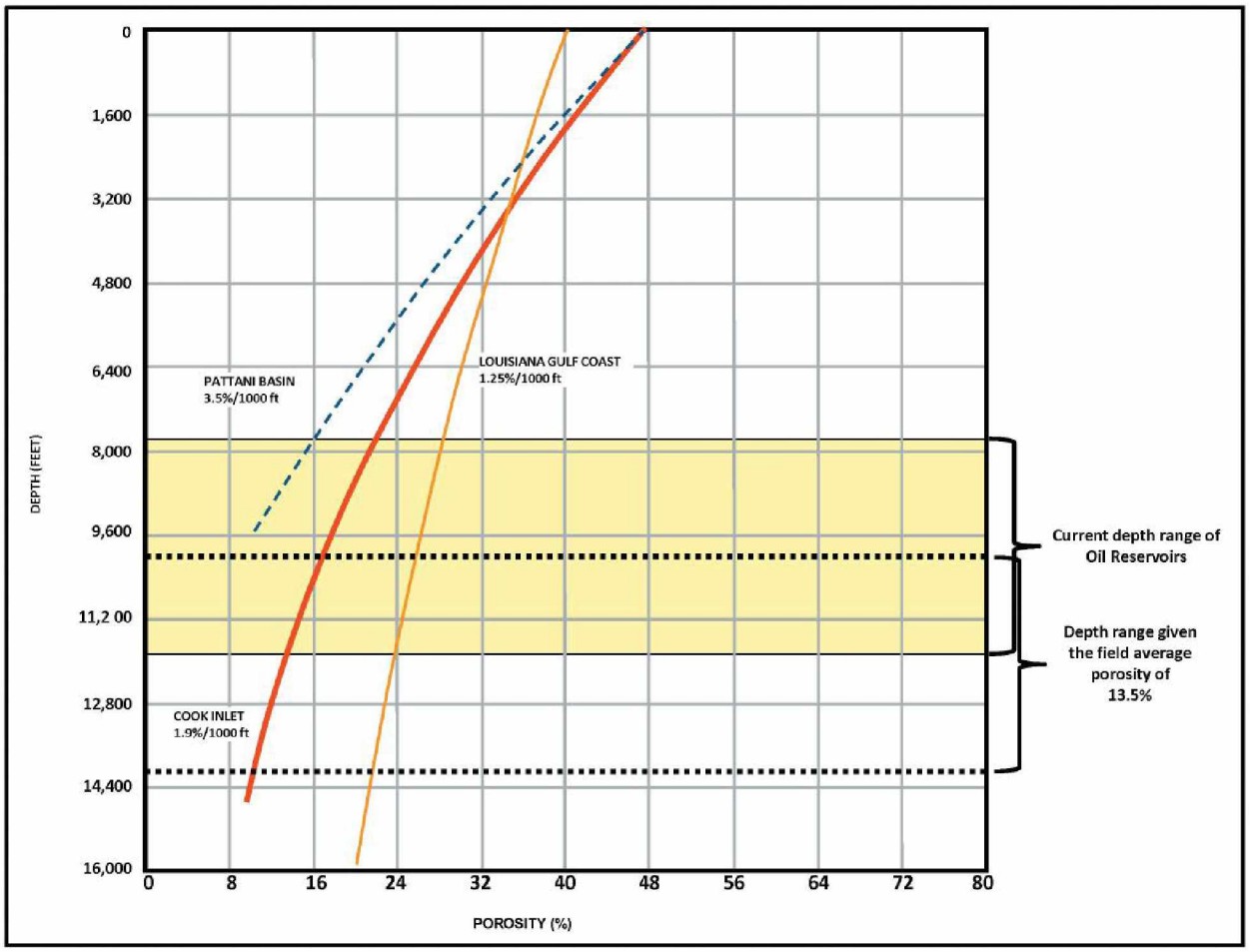

Figure 10: Plot of depth (SSTVD) vs. porosity comparing Cook Inlet Basin trend to the Patani Basin in Thailand and the Louisiana Gulf Coast. The present-day depth range for the Granite Point field Tyonek C zones is indicated by the yellow band. Reprinted from "The Granite Point Field, Cook Inlet, Alaska" by M.J. Frankforter and J.C. Waugaman, 2013, in D.M. Stone and D. M. Hite, ed., Oil and gas fields of the Cook Inlet Basin, Alaska: AAPG Memoir 104, p. 263–290.

In 2008 Chevron completed the most recent petrophysical analysis on the Granite Point field wells. This comprehensive study built upon the efforts of the previous operators and defined a procedure for normalization of

log vintages as a means to provide a log interpretation model that could be applied field-wide. This log model provides the most consistent estimates of lithology, specifically to differentiate conglomerates from sands, along with estimates of total and effective porosities, absolute permeability, shale volume, clay bound water, and water saturation.[1]

The key takeaway from Chevron's petrophysical analysis in regards to productivity and ultimate recovery is the general increase in porosity from northeast to southwest as illustrated for the C5 zone in Figure 11. Although this porosity trend increase is present, there is a much less consistent relationship to the net sand isochore, indicating significant variability in lateral reservoir quality.

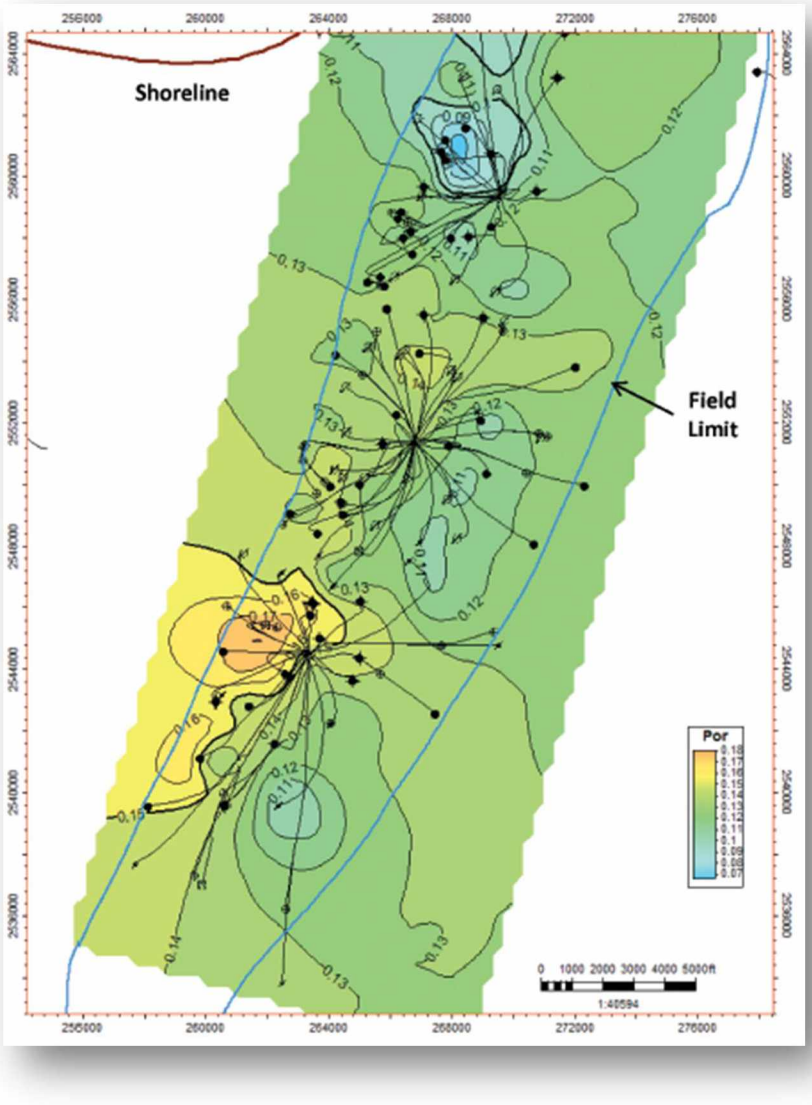

Figure 11: Map of average porosity above 0.08 for the Tyonek C5A zone, Granite Point field. Reprinted from "The Granite Point Field, Cook Inlet, Alaska" by M.J. Frankforter and J.C. Waugaman, 2013, in D.M. Stone and D. M. Hite, ed., Oil and gas fields of the Cook Inlet Basin, Alaska: AAPG Memoir 104, p. 263–290.

2.4 Structure

In addition to well control and the laterally extensive coals that can be correlated across the structure, several 2-D and three 3-D seismic datasets exist. These seismic datasets range in quality from fair to good as there is little shallow gas interference that exists at other oil deposits in the Cook Inlet Basin.

The key takeaways from this data, as it pertains to ultimate recovery, are that the steeply dipping west flank is poorly imaged, two minor high angle reverse fault splays related to the Granite Point fault cut the western limb of the Granite Point structure into separate fault blocks near the Anna and Bruce platforms, and a series of minor northeast-southwest trending faults have been identified, particularly in the northern half of the field. Figures 12a-12e provide an illustrative description of these key findings.

This representation of the structure is supported by field production data. The Granite Point platform exhibits superior waterflood performance to that of the Anna and Bruce Platforms. This is due to a combination of thinner and more laterally discontinuous sands towards the north end of the field along with the fault barriers. Along the west flank of the Anna platform several wells were drilled through the crest of the structure, then steered west to drill through the west flank of the structure. These "hockey stick" wells encountered repeat sections of the Tyonek C sands along the west flank and are illustrated by the western-most well path in Figure 12b.

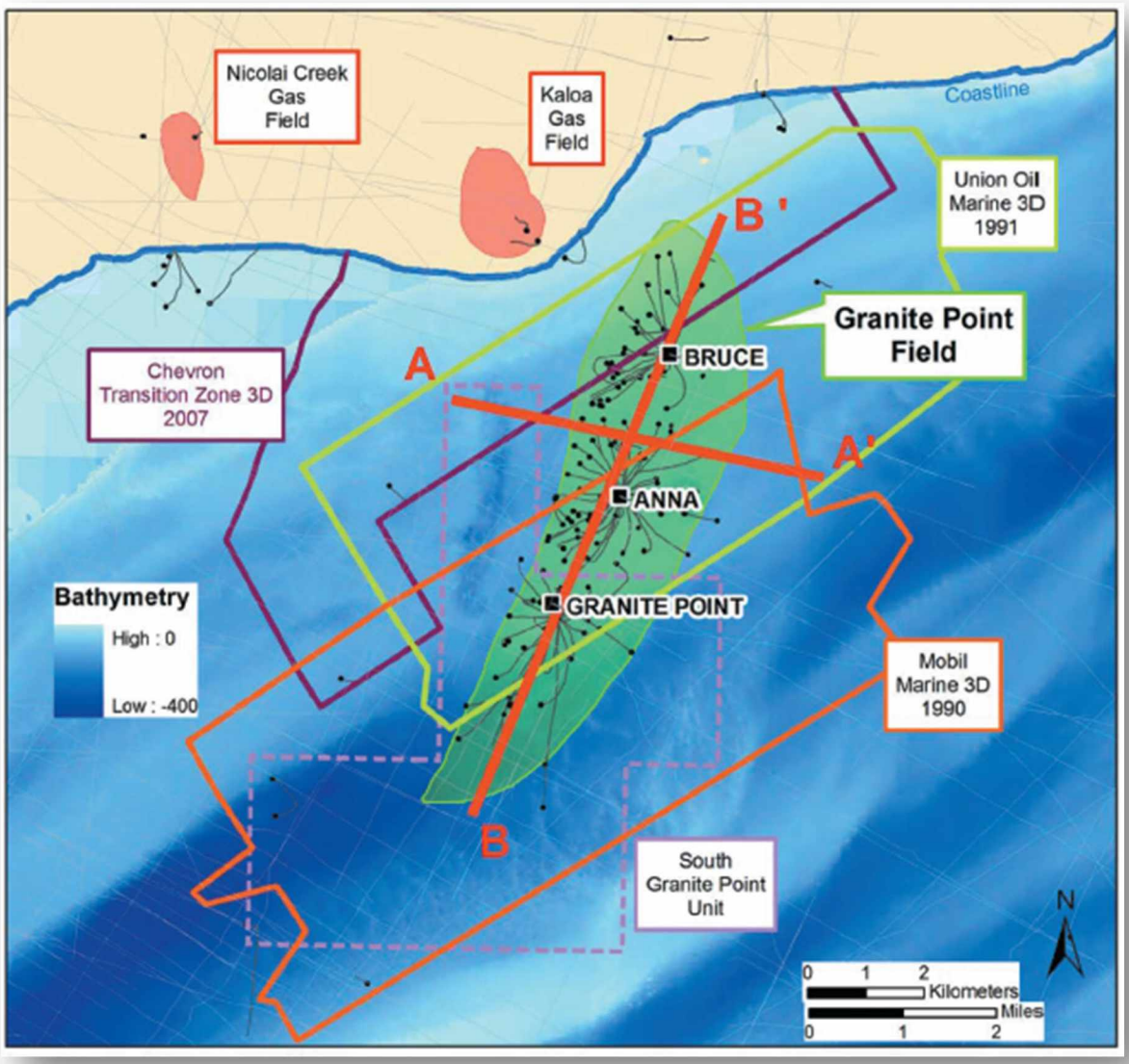

Figure 12a: Two-dimensional (2D) and three-dimensional (3D) seismic coverage map of Granite Point field. Seismic data along the line of section A-A' and B-B' are shown in Figures 12b and 12c, respectively. Seismic survey boundaries are shown in solid lines. Two-dimensional seismic is shown as faint gray lines. Reprinted from "The Granite Point Field, Cook Inlet, Alaska" by M.J. Frankforter and J.C. Waugaman, 2013, in D.M. Stone and D. M. Hite, ed., Oil and gas fields of the Cook Inlet Basin, Alaska: AAPG Memoir 104, p. 263–290.

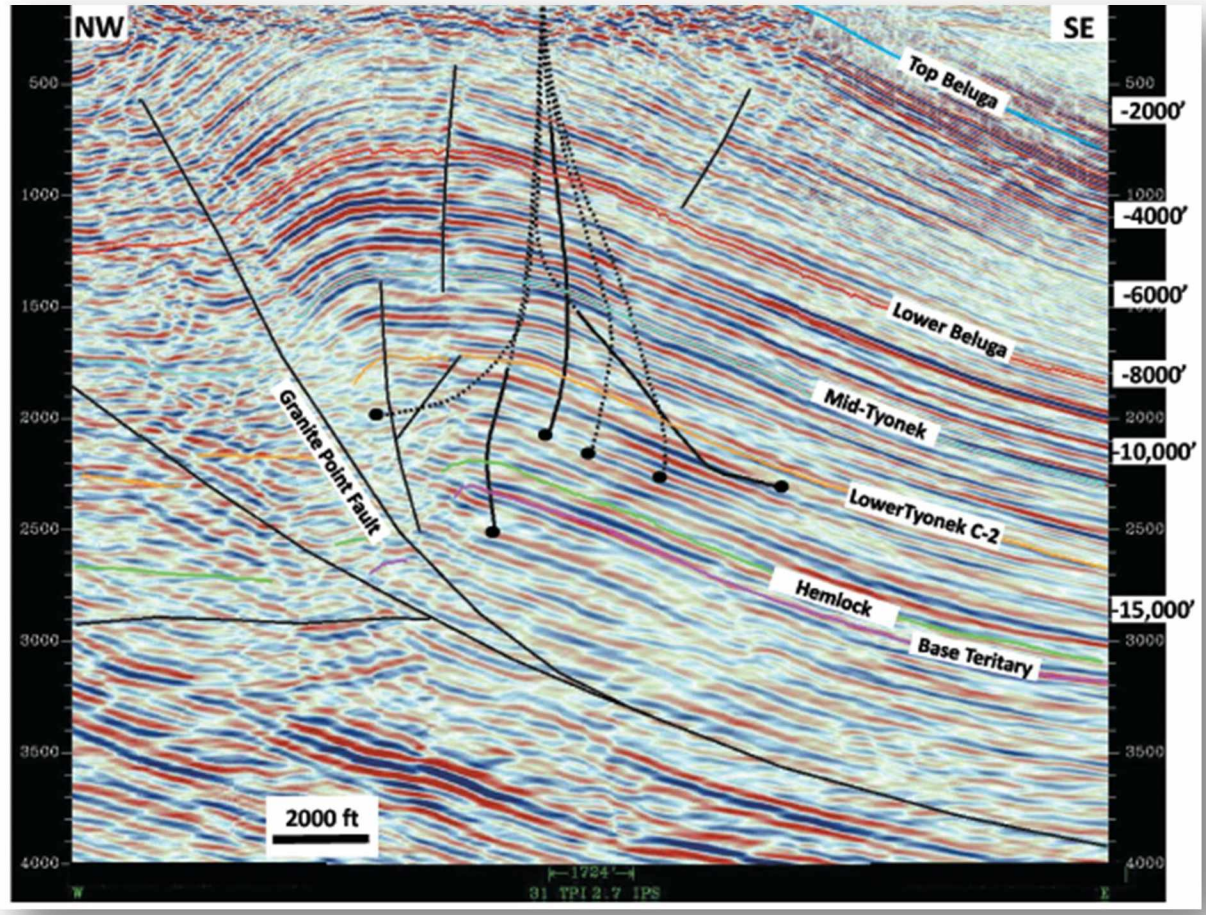

Figure 12b: Representative dip seismic section from the 2007 Chevron 3D seismic survey across the central part of Granite Point field showing the main bounding thrust fault and east dip. The seismic line is the A-A' line defined in Figure 12a. Reprinted from "The Granite Point Field, Cook Inlet, Alaska" by M.J. Frankforter and J.C. Waugaman, 2013, in D.M. Stone and D. M. Hite, ed., Oil and gas fields of the Cook Inlet Basin, Alaska: AAPG Memoir 104, p. 263–290.

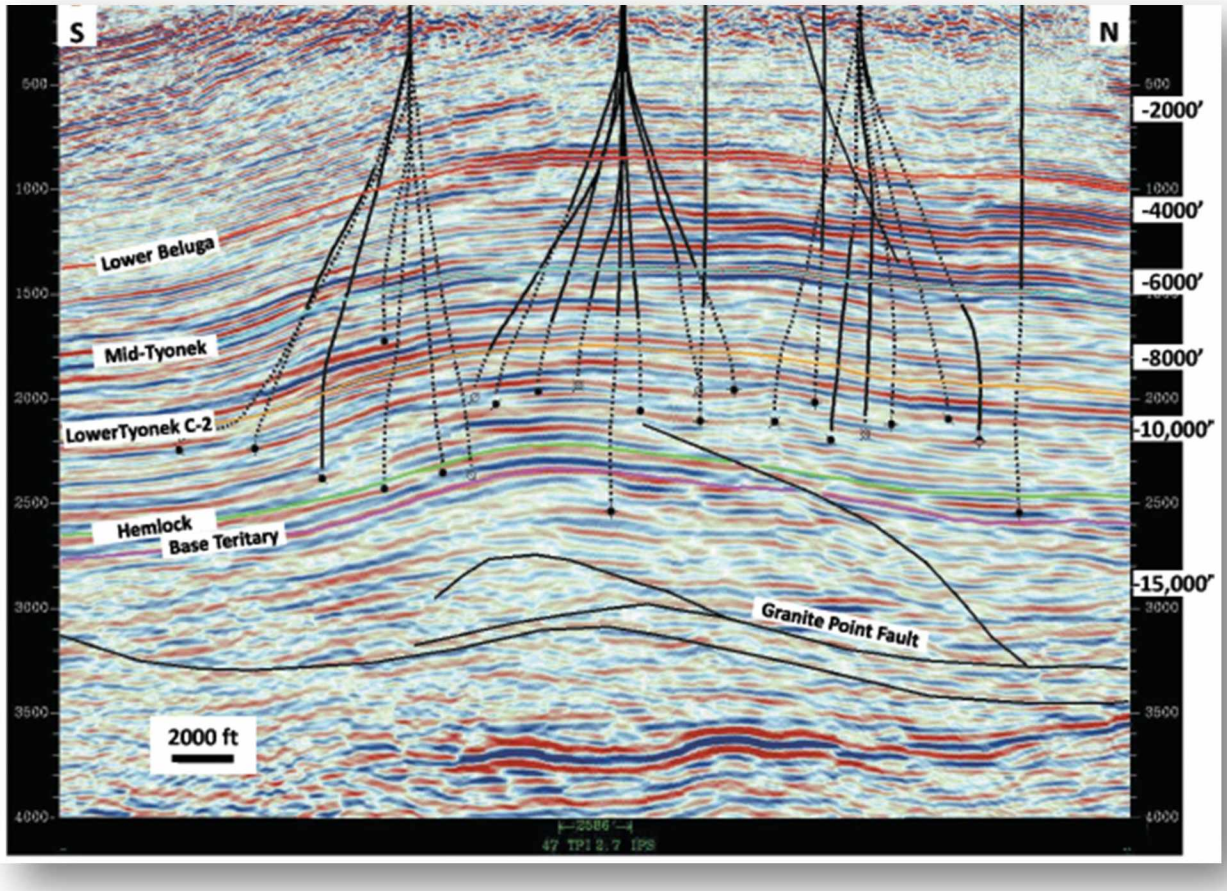

Figure 12c: Representative strike seismic section from the 2007 Chevron 3D seismic survey along the axis of Granite Point field. The seismic line is the B-B' line defined in Figure 12a. Reprinted from "The Granite Point Field, Cook Inlet, Alaska" by M.J. Frankforter and J.C. Waugaman, 2013, in D.M. Stone and D. M. Hite, ed., Oil and gas fields of the Cook Inlet Basin, Alaska: AAPG Memoir 104, p. 263–290.

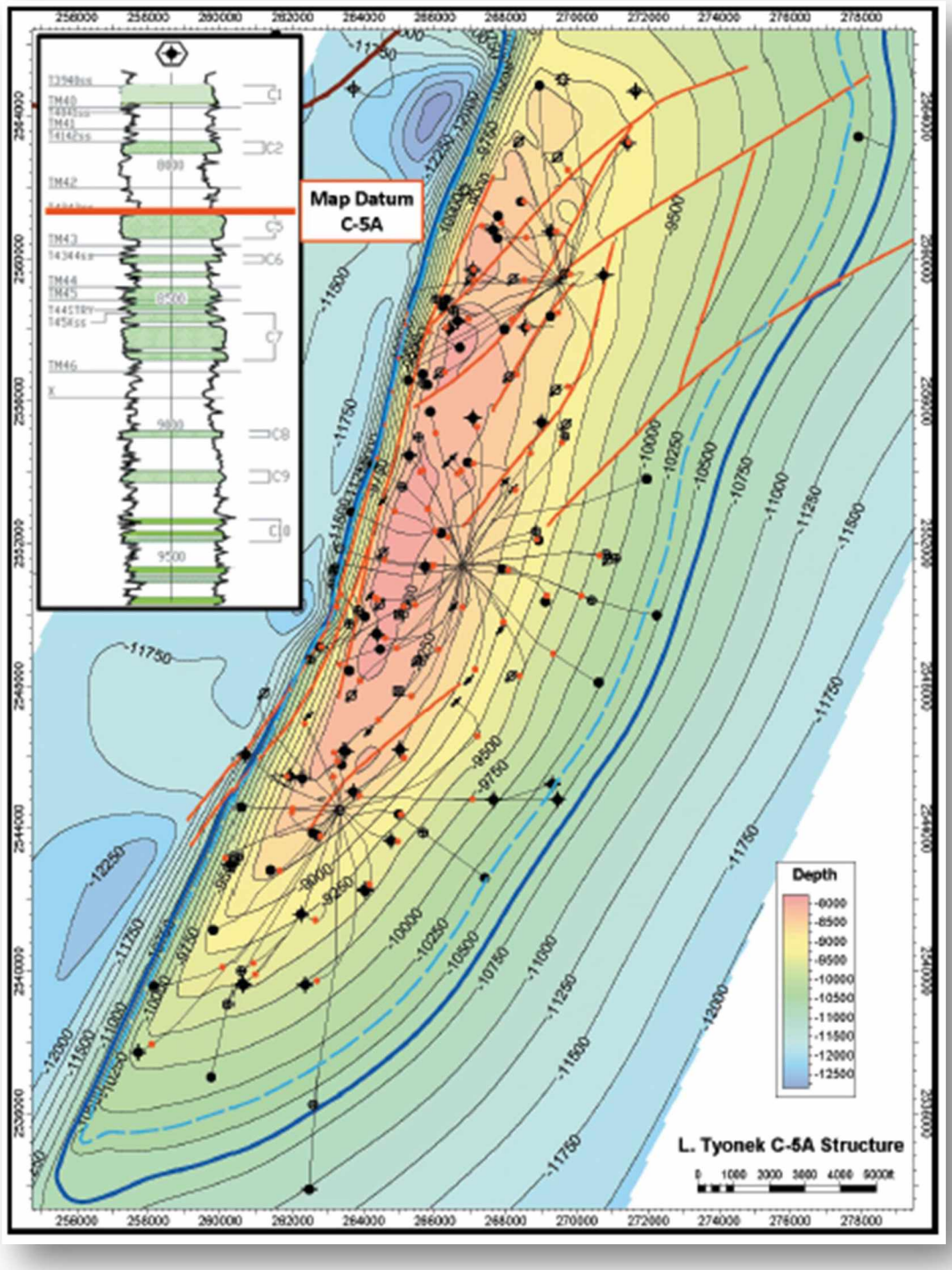

Figure 12d: Top C5A structure map showing platform locations and type log. Blue down-dip dashed and solid lines depict range of uncertainty in the oil-water contacts. Symbols denote: Black dot = producer, black dot with plus sign = abandoned oil well, small red dot = C5A structure intercept, circle with plus sign = abandoned or plugged well. Reprinted from "The Granite Point Field, Cook Inlet, Alaska" by M.J. Frankforter and J.C. Waugaman, 2013, in D.M. Stone and D. M. Hite, ed., Oil and gas fields of the Cook Inlet Basin, Alaska: AAPG Memoir 104, p. 263–290.

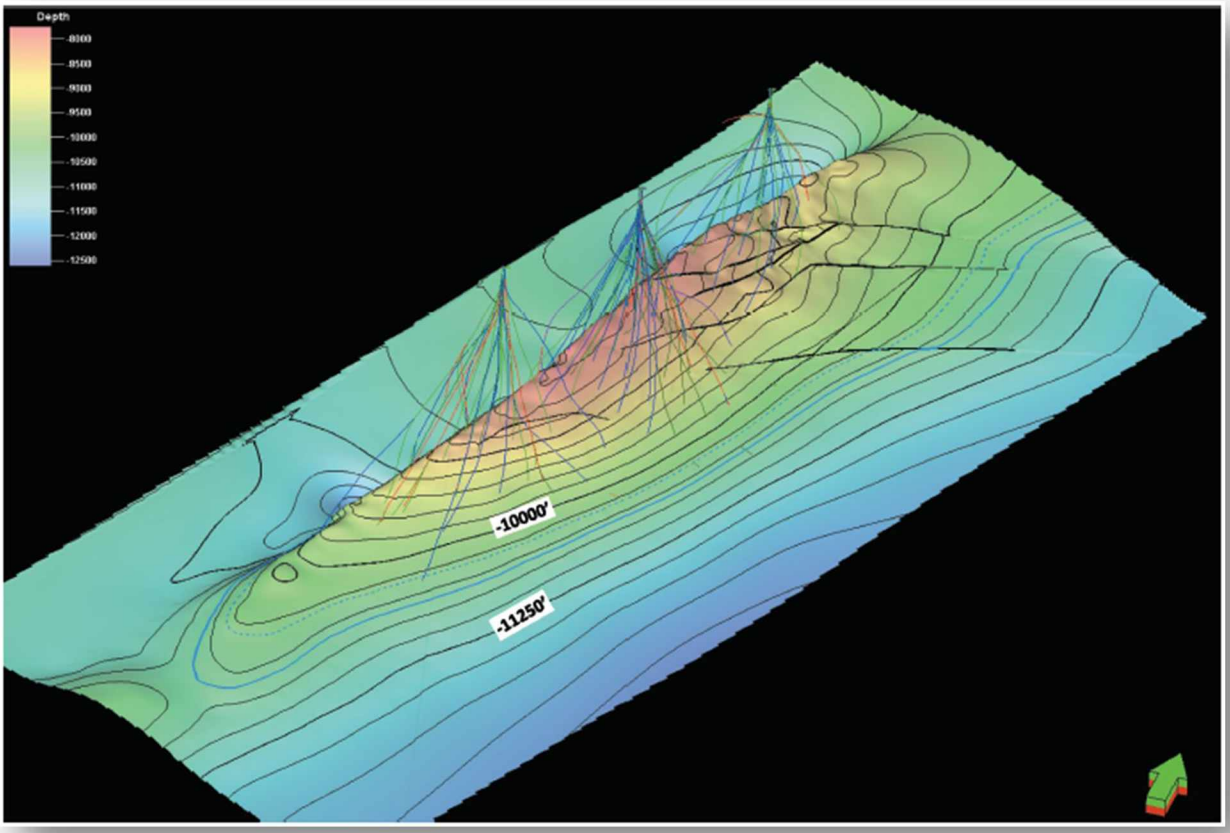

Figure 12e: Three-dimensional representation of Top C5A structure shown in Figure 12d. Reprinted from "The Granite Point Field, Cook Inlet, Alaska" by M.J. Frankforter and J.C. Waugaman, 2013, in D.M. Stone and D. M. Hite, ed., Oil and gas fields of the Cook Inlet Basin, Alaska: AAPG Memoir 104, p. 263–290.

Chapter 3: Reservoir

3.1 Reservoir Chapter Preface

The purposes of Chapter 3 is to understand the movement of fluids within the reservoir and provide a technical foundation for determining methods to improve the ultimate recovery. This chapter builds upon Chapter 2, which has defined the geologic setting of the field, the structure, and characterized the reservoir. Due to the scale of the Granite Point field Chapter 3 will focus on the Granite Point platform section of the field only. The key findings and analytical methodologies established within this chapter can be applied to the Anna and Bruce areas of the field.

3.2 Reservoir Fluids

As demonstrated in Figures 13-16, the Granite Point field oil is of high quality at approximately 39° API at 60° F and a bubble point pressure of 2,389 psia. The viscosity is favorable for waterflooding with a minimum viscosity at saturation pressure of 0.272 cP. Below is a summary of the GP-31-13 PVT analysis[3] in graphical form. This PVT analysis is consistent with other PVT analyses conducted at Granite Point field and is used for defining fluid properties throughout the rest of this project report.

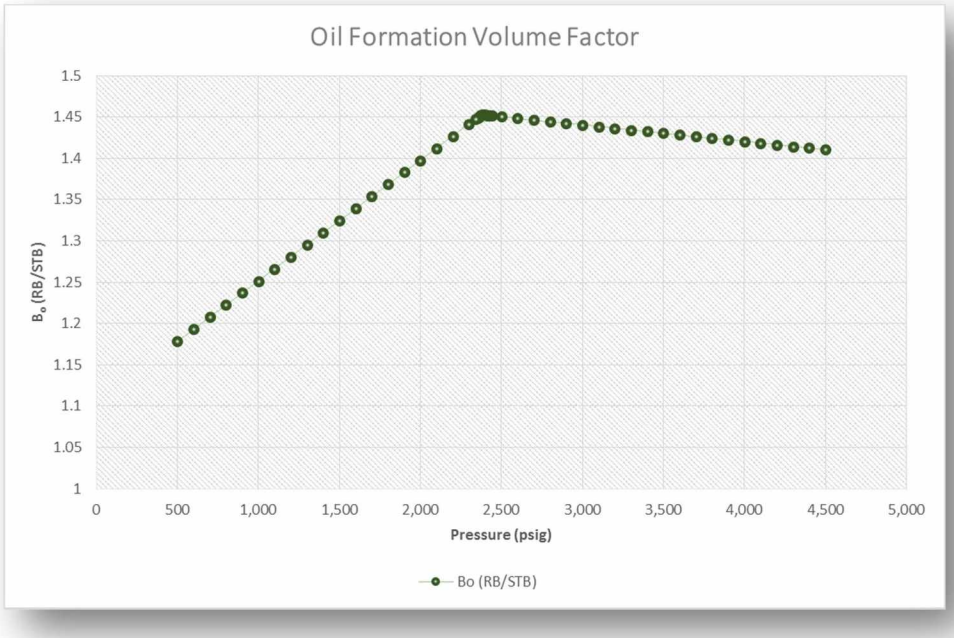

Figure 13: GP-31-13 PVT analysis oil formation volume factor.

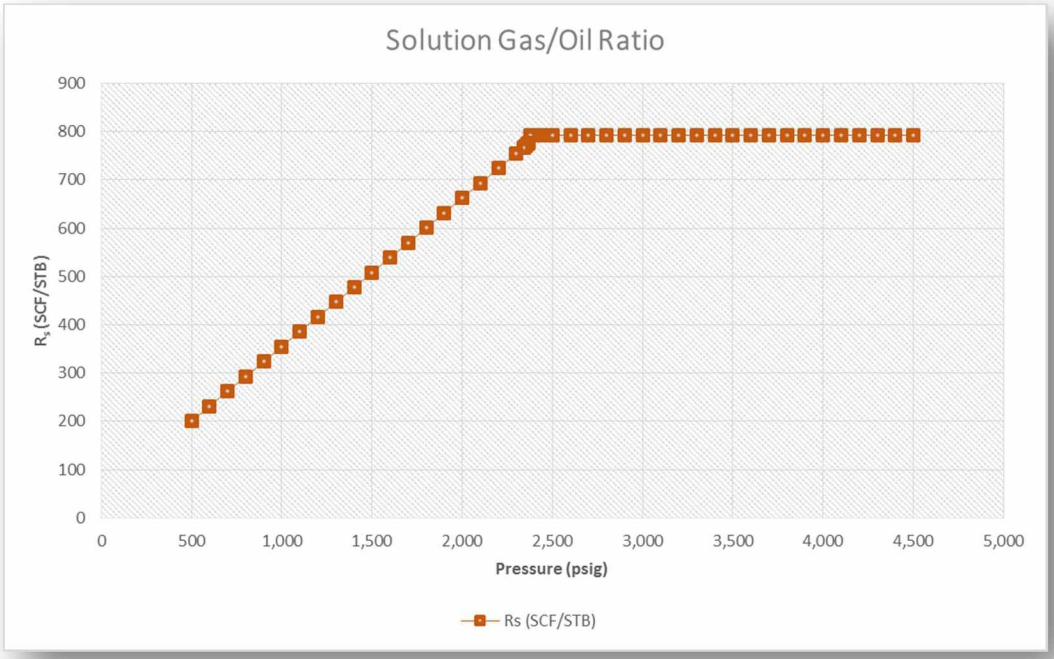

Figure 14: GP-31-13 PVT analysis solution gas-oil ratio.

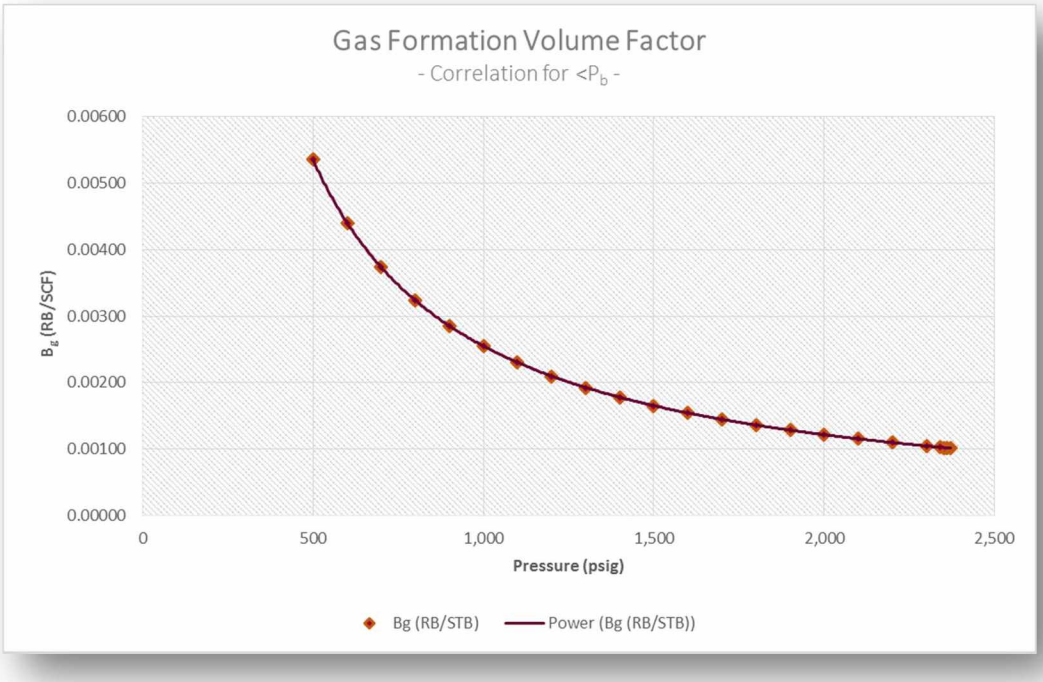

Figure 15: GP-31-13 PVT analysis gas formation volume factor.

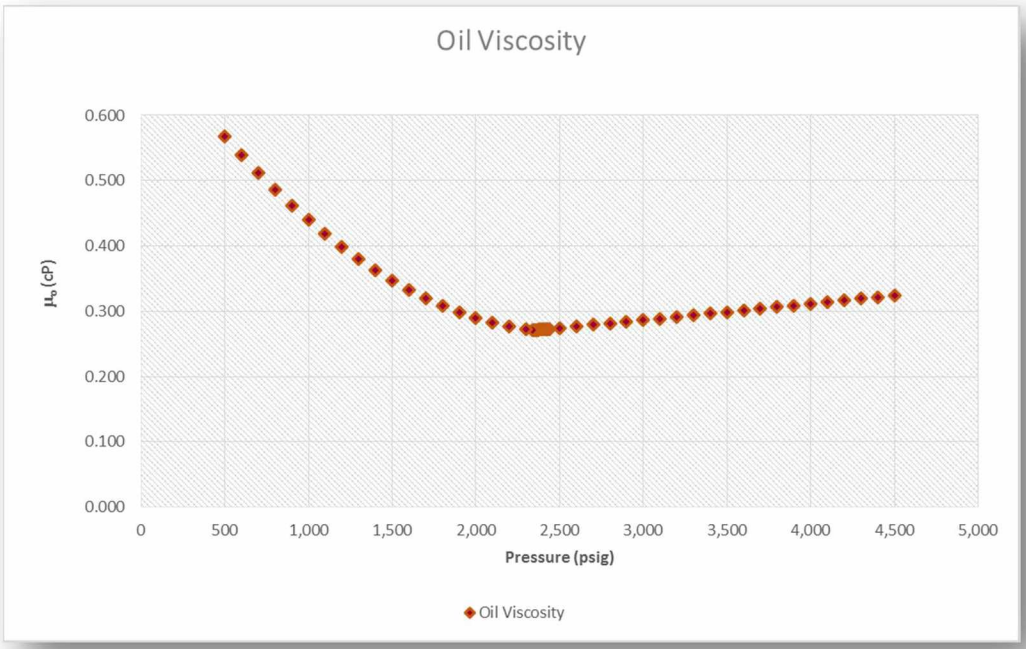

Figure 16: GP-31-13 PVT analysis oil viscosity.

The oil quality of the Tyonek C sands lends itself to be an excellent candidate for gas injection. Testing has been done on this oil that indicates significant swelling properties; however, two reasons preclude pursuing gas injection to increase ultimate recovery:

1.) The value of gas within the Cook Inlet basin
2.) Injecting gas into the proper location on top of structure with down-dip offtake points is not possible in most of the sands at the Granite Point field due to historic water injection locations and volumes.

3.3 Core Analyses

All operators of the Granite Point field conducted conventional (RCAL) and special core analyses (SCAL). These core analyses were investigated to understand the porosity-permeability relationship for: 1.) The effective permeability to oil, and 2.) The effective permeability to water.

The Granite Pont field air permeability has a range of two orders of magnitude for a given porosity (Figure 17); however, the general relationship between permeability and porosity is consistent amongst the sands cored

(Figure 18). The two order of magnitude range in permeability for a given porosity is believed to be attributable to grain size.

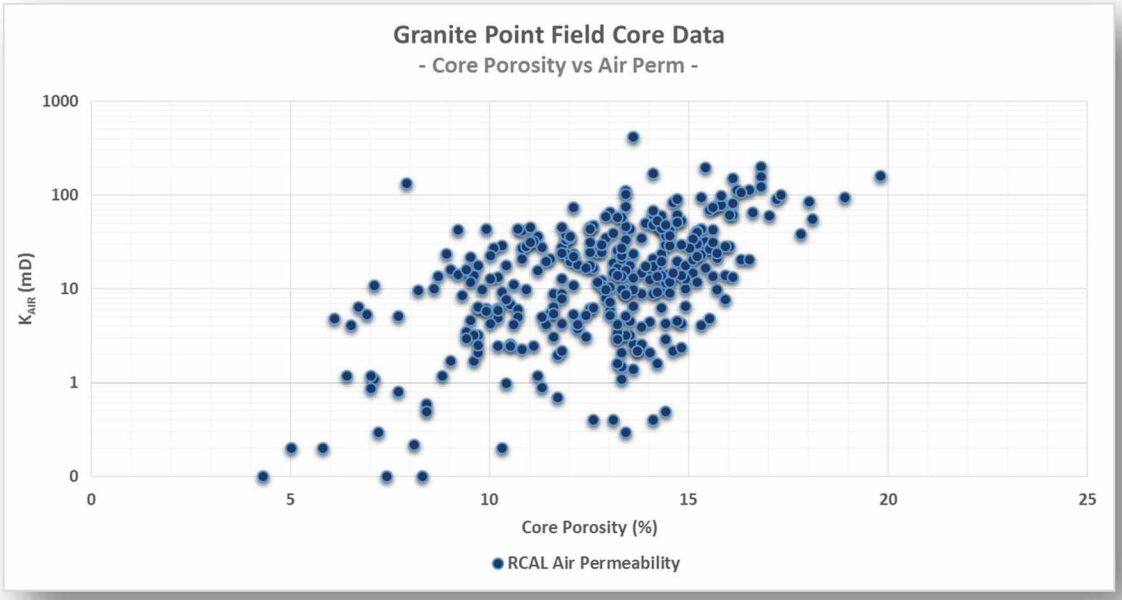

Figure 17: Granite Point field core porosity-permeability relationship.

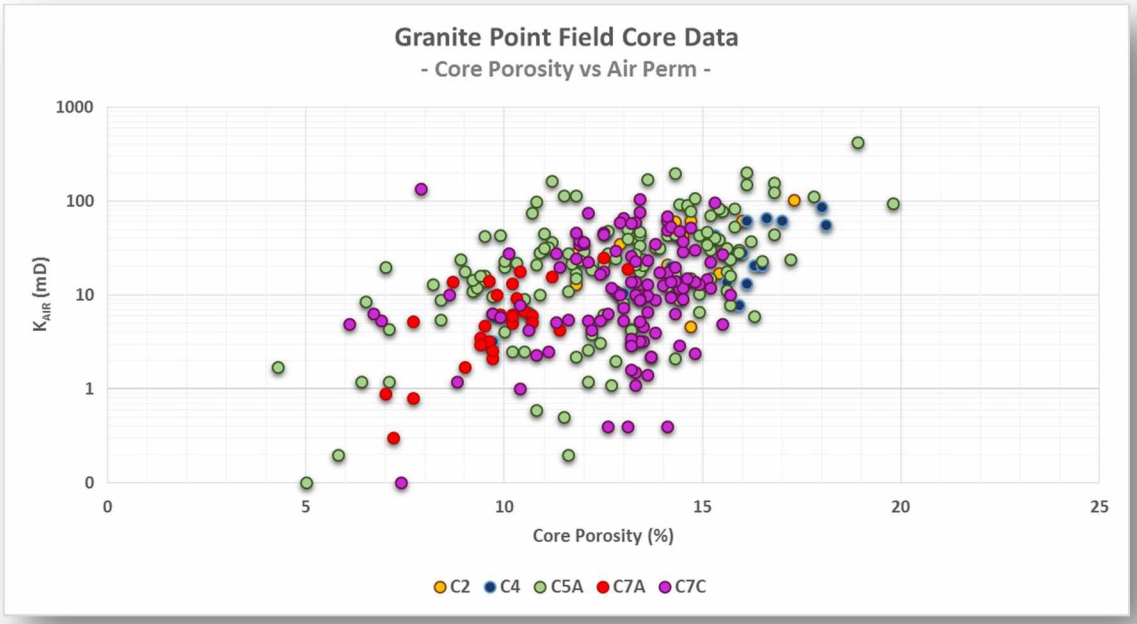

Figure 18: Granite Point field core porosity-permeability relationship by sand.

The GP-1 & GP-31 wells acquired core in the C2, C5, and C7 wells. With this core SCAL studies were completed, providing a relationship between oil permeability and core porosity that fits an exponential regression (Figure 19). Although it is a limited data set, the core evaluated is representative of the Tyonek C sands.

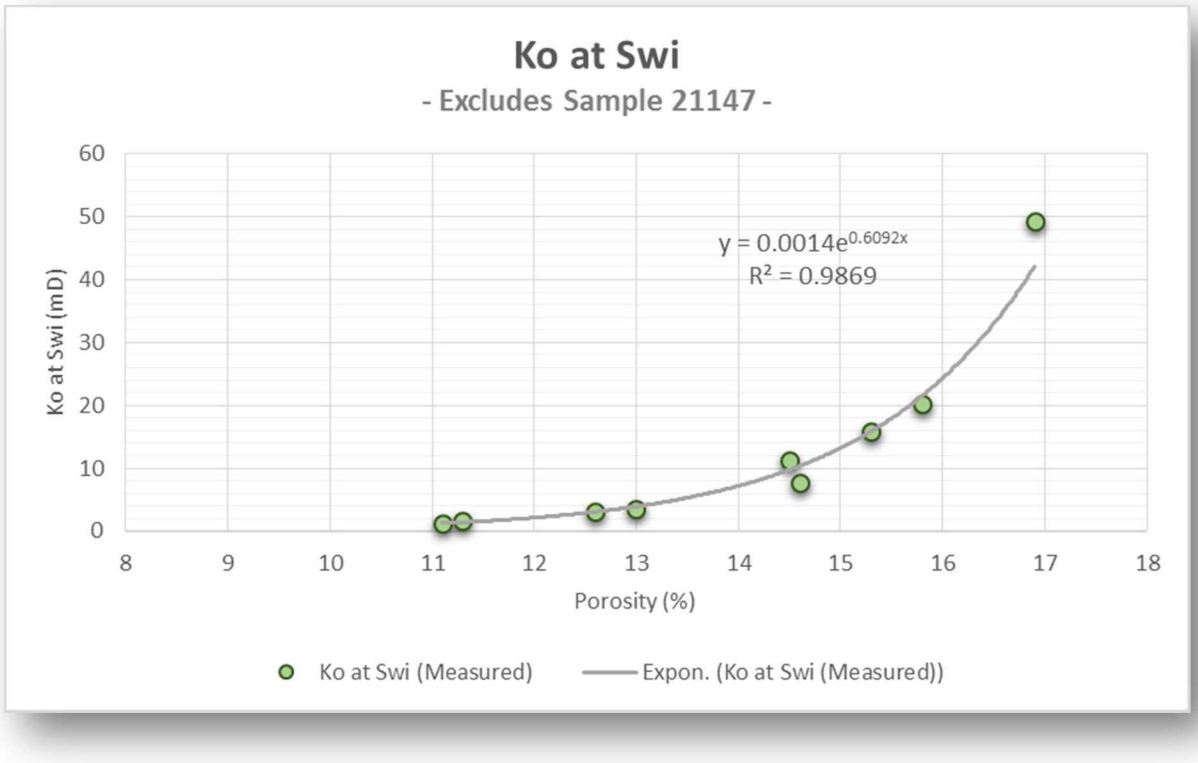

Figure 19: Oil permeability data derived from GP-1 & GP-31 SCAL.

The oil permeability-porosity relationship must be corrected for formation compressibility as the field pressure has declined from approximately 4,200 psi to an average reservoir pressure in 2018 of approximately 1,600 psig. Formation compressibility SCAL data from the AN-32RD C5 sand was used (Table 1). This was the only formation compressibility data uncovered in the field. The initial effective grain pressure at a reservoir depth of 9,400' SSTVD was determined to be 5,155 psi (Pi = 4,245 psig at 9,400' SSTVD and using a 1.0 psi/ft overburden pressure gradient). Current reservoir pressures are estimated to be approximately 1,600 psig, resulting in a current effective grain pressure of 7,800 psi. This increase in grain pressure of 2,645 psi will result in a decrease in porosity and permeability. The AN-32RD SCAL data showed a ~8% decrease in porosity from 400 to 2500 psi and a ~4% decrease in porosity from 2500 to 5000 psi. As the SCAL data does not cover the change in effective grain pressure realized in the field, the data for the change from 2500 to 5000 psi was used as a conservative estimate. This is a conservative estimate as it becomes progressively more difficult to compact the grains further at higher effective

grain pressures. Although the decrease in porosity was only ~4%, the resulting decrease in air permeability was ~32%.

AN-32RD C5 Sand Core Samples

Report: Special Core Analysis Study, AN-32RDPB, Tyonek C Sands, CORE LABORATORIES, April 18th, 1988

		Permeability to Air (mD) Effective Overburden Stress (psi)			Porosity (%) Effective Overburden Stress (psi)				Pemeability (mD Change) Effective Overburden Stress (psi)		Porosity (% Change) Effective Overburden Stress (psi)	
Sample	**Depth**	**400**	**2500**	**5000**	**400**	**2500**	**5000**	**Grain Density**	**400 to 2500**	**2500 to 5000**	**400 to 2500**	**2500 to 5000**
(ID #)	(ft MD)	(mD)	(mD)	(mD)	(%)	(%)	(psi)	(gm/cc)	(mD % Change)	(mD % Change)	(Porosity % Change)	(Porosity % Change)
108	10827.20	34	29.000	28.000	15.4	15.3	15.100	2.64	-14.71%	-3.45%	-0.65%	-1.31%
111	10830.20	28	25.000	23.000	15	14.9	14.500	5.65	-10.71%	-8.00%	-0.67%	-2.68%
127	10846.10	82	74.000	69.000	16	15.7	15.400	2.64	-9.76%	-6.76%	-1.88%	-1.91%
218	10865.00	0.97	0.240	0.120	7.2	6.5	6.200	2.66	-75.26%	-50.00%	-9.72%	-4.62%
224	10871.10	9	4.800	3.500	13.3	12.1	11.700	2.64	-46.67%	-27.08%	-9.02%	-3.31%
306	10882.20	0.25	0.022	0.016	4.2	3.4	3.200	2.68	-91.20%	-27.27%	-19.05%	-5.88%
310	10886.30	1.7	0.690	0.340	12	11.9	11.200	2.67	-59.41%	-50.72%	-0.83%	-5.88%
409*	10910.60	205	151.000	139.000	18.9	18.4	17.100	2.62	-26.34%	-7.95%	-2.65%	-7.07%
514	10925.20	0.26	0.120	0.080	8.8	8.5	8.200	2.67	-53.85%	-33.33%	-3.41%	-3.53%
809	10967.00	0.1	0.013	0.007	5.1	4.3	4.100	2.69	-87.00%	-43.85%	-15.69%	-4.65%
810	10968.00	0.23	0.037	0.012	5.5	4.7	4.4	2.69	-83.91%	-67.57%	-14.55%	-6.38%
*Fractured and irregular								Average (Excludes 409):	-53.25%	-31.80%	-7.55%	-4.02%

Table 1: AN-32RD C5 sand formation compressibility SCAL data.

In the absence of core study data quantifying the formation compressibility effects upon oil permeability, a method was developed to transform the data in Table 1 to an oil permeability corrected for current overburden stress. To accomplish this a relationship between core porosity and the change in air permeability needed to be derived. This was done by plotting the change in air permeability versus core porosity from Table 1 for the change from 400 psi to 2500 psi and 2500 to 5000 psi (Figure 20). A linear regression is an acceptable fit over the applicable 2500 to 5000 psi data set. As the relationship between gas and liquid permeability fits a linear regression as well (Figure 21), the core derived oil permeability at initial water saturation can then be multiplied by the linear regression in Figure 20 to determine the formation compressibility corrected oil permeability as shown in Figure 22.

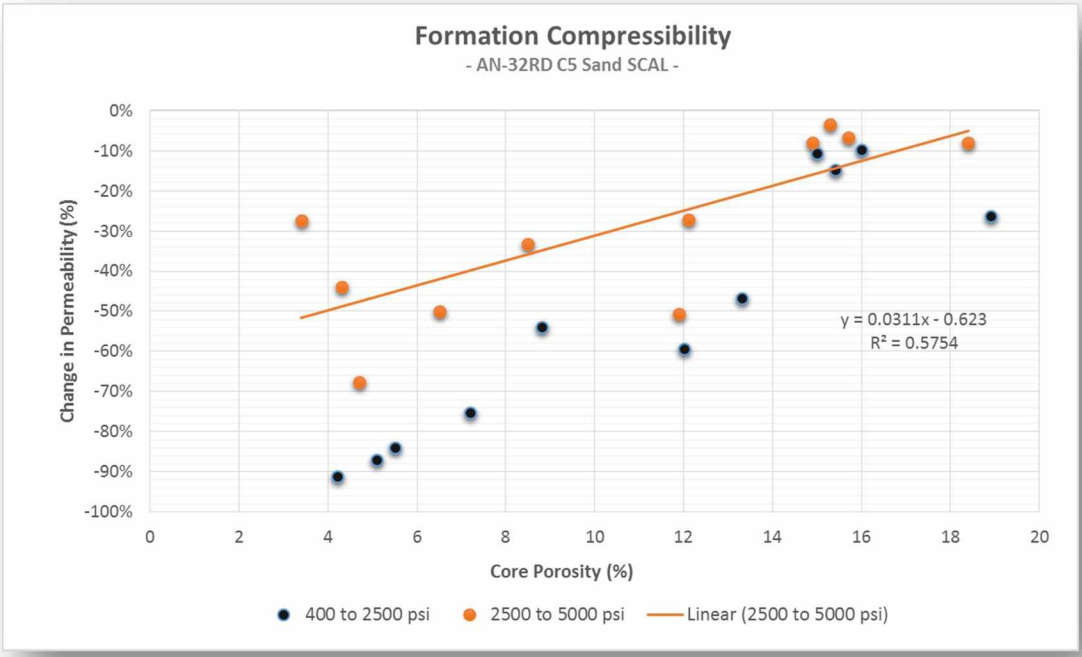

Figure 20: AN-32RD C5 sand change in permeability (%) vs. core porosity.

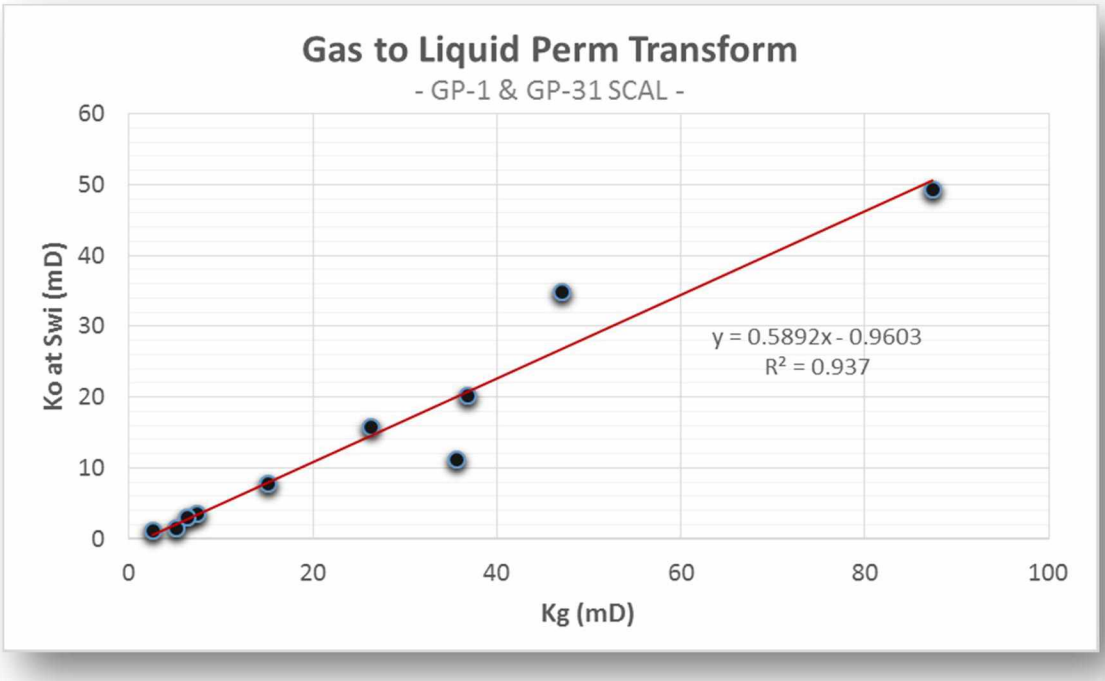

Figure 21: Gas to liquid permeability transform derived from GP-1 & GP-31 SCAL.

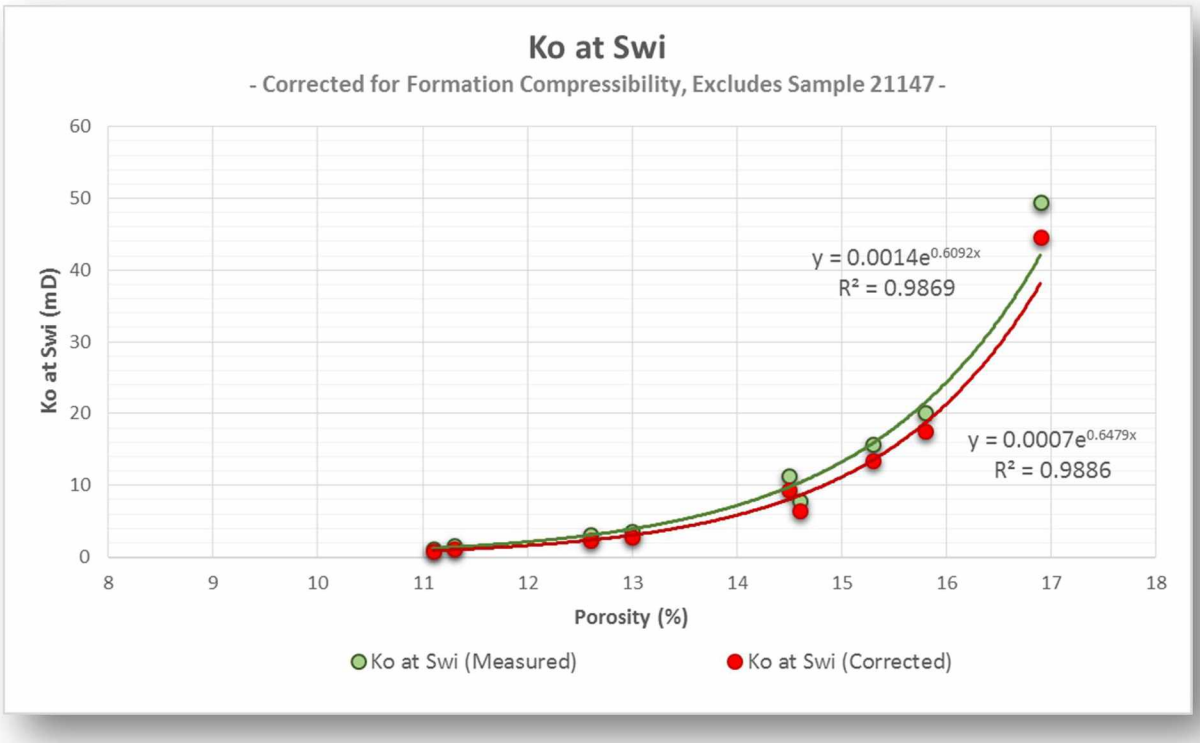

Figure 22: Oil permeability at initial water saturation vs. core porosity, corrected for formation compressibility at current reservoir pressures.

3.4 Productivity

The next step was to validate that the oil permeability derived from formation compressibility corrected SCAL data matches empirical field production data. An evaluation methodology was constructed to compare the SCAL derived oil permeability with the permeability determined from the Vogel[4] (Equation 1) oil inflow performance expression for a two-phase reservoir. As the reservoir pressure dropped below bubble point pressure by 1973 (see Section 3.6), using an expression that accounts for two-phase flow is necessary. The permeability derived from the Vogel expression was determined by iterating the permeability to match empirical oil rates. All other variables within the Vogel expression are well understood. The skin was set to zero as minimal skin damage has been identified in pressure build-up analyses at Granite Point field producers, the average reservoir pressure was derived from pressure surveys (see Section 3.6), and the drainage radius was determined from pressure build-up analyses.

$$q_o = \frac{k_o hp\left[1 - 0.2\left(\frac{p_{wf}}{p}\right) - 0.8\left(\frac{p_{wf}}{p}\right)^2\right]}{254.2\mu(p)B_o(p)\left(ln\left(\frac{0.472r_e}{r_w}\right) + s\right)}$$

Equation 1: Vogel oil inflow performance expression for a two-phase reservoir.

Where;

k_o = Oil permeability [mD]

h = Net reservoir thickness [ft]

p = Average reservoir pressure [psig]

p_{wf} = Bottomhole flowing pressure [psig]

$B_o(p)$ = Formation volume factor at average reservoir pressure [RB/STB]

$\mu_o(p)$ = Oil viscosity at average reservoir pressure [cP]

r_e = Drainage radius [ft]

r_w = Wellbore radius [ft]

s = Skin [Dimensionless]

From this comparison it was determined that the oil permeability derived from matching empirical vertical well performance is ~50-70% less than the permeability derived from SCAL at current reservoir conditions. Ten slant wells along the crest of the structure were analyzed to arrive at this conclusion. The period matched was the pseudo-steady state oil production period with 0% water cut to represent k_o at S_{wi} as shown in Figure 23. The reason the horizontal permeability required to achieve a match with empirical data is lower than the SCAL data is likely attributable to one or both of the following reasons:

1.) An increasing gas saturation in the near wellbore region
2.) Fines migration, as suggested in historical research papers

The example well in Figure 23, GP-44-14, summarizes this evaluation methodology. Well GP-44-14 is a slant well completed in 1968 at the top of the structure and drilled from the Granite Point platform. It is a commingled producer with offtake from the C2, C5, C6, C7, and C8 sands. The actual oil rate was matched by iterating the permeability to oil. As shown in Figure 23 below, the SCAL derived permeability would result in an oil production rate significantly greater than actual. The oil rate drops off as expected as water cut increases as the water will impact the efficiency of the artificial lift and the thickness of the sand that is contributing oil.

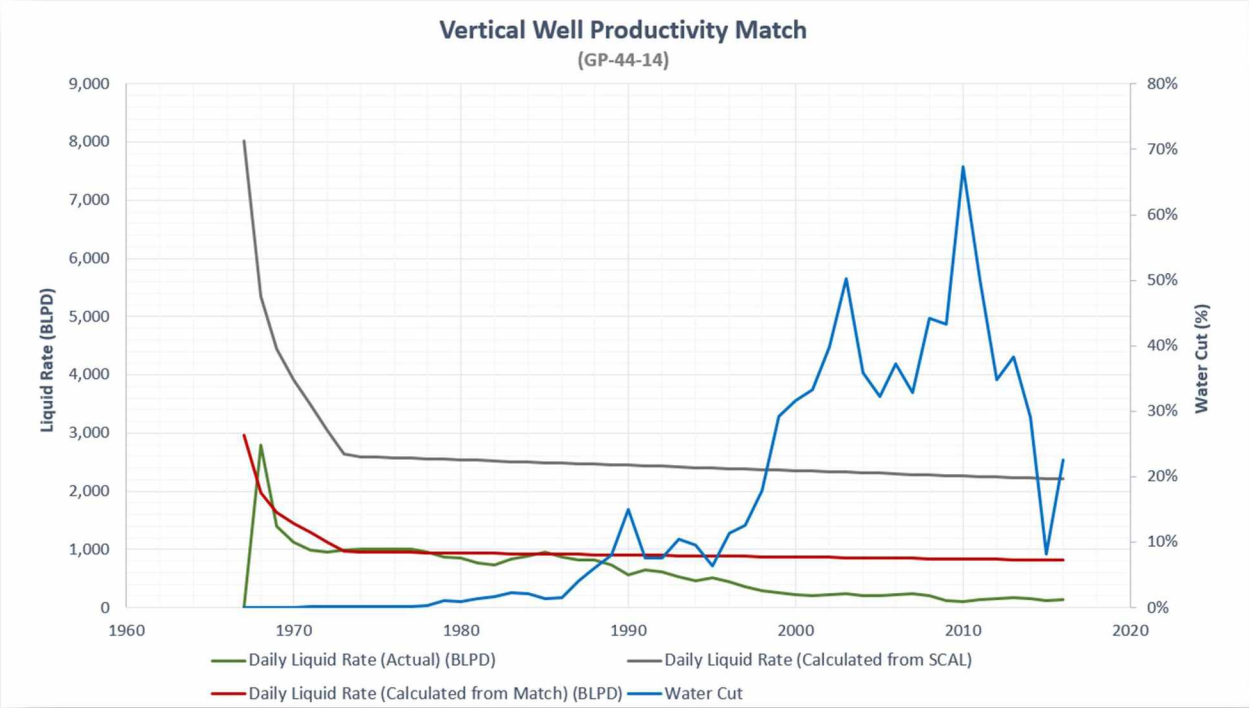

Figure 23: Example vertical well productivity match. The oil permeability derived from matching production data is 50-70% less than the SCAL derived value.

3.5 Relative Permeability & Fractional Flow

The water-oil relative permeability relationship is a critical component of the Granite Point field. The water relative permeability at S_{or} is approximately 0.10. The low relative permeability, as illustrated in Figure 24, combined with the low absolute permeability, results in an extremely low effective permeability to water.

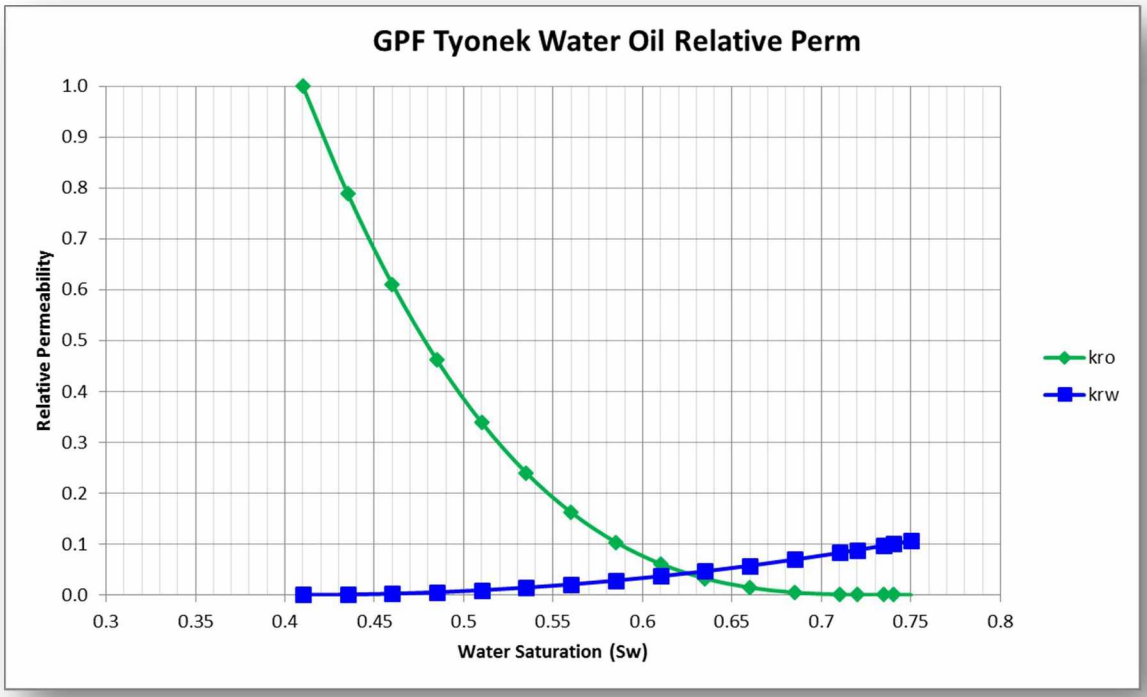

Figure 24: Granite Point field Tyonek C sands oil-water relative permeability curves.

Although the effective permeability to water is low, the fractional flow curve suggests an efficient oil displacement (Figure 25). Using the core samples the recovery factor at breakthrough was calculated vs. pore volumes injected (Figure 26). The average recovery factor at water breakthrough is 52% while at 10 pore volumes injected it is 57%. This marginal increase in oil recovery after breakthrough suggests that individual sands can be thought of qualitatively as producing oil up until water breakthrough, and afterwards will produce water only. This conclusion is supported by field production history. When water breakthrough occurs the oil rate effectively goes to zero for that sand.

The oil recovery versus pore volumes injected data illustrated in Figure 26 aligns with the experimental results, in that essentially all of the oil was produced at breakthrough, with the exception of one sample, (No. 21147). This sample had an unusually high oil permeability in comparison with the specific gas permeability; also, relative permeabilities to injection waters – relative to the oil permeability – were much higher than the majority. The converse to sample No. 21147 was sample No. 21759.

The high oil permeability realized in sample No. 21147 may be the result of fractures within the core during the process of acquiring and handling the core, or they could represent natural fractures within the formation.

These two samples were visually similar to other plugs; however, because of the anomalous behavior of samples No. 21147 and No. 21759, only the remaining eight samples were used for averaging purposes.

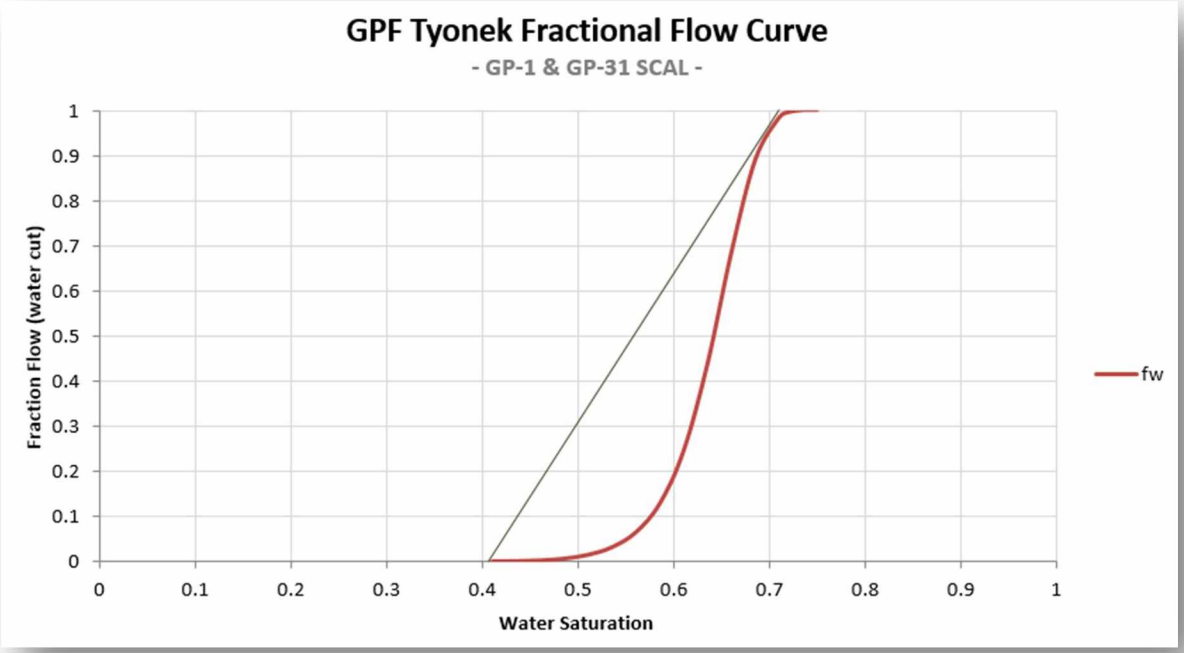

Figure 25: GP-1 & GP-31 SCAL fractional flow curve to water for the Tyonek C sands.

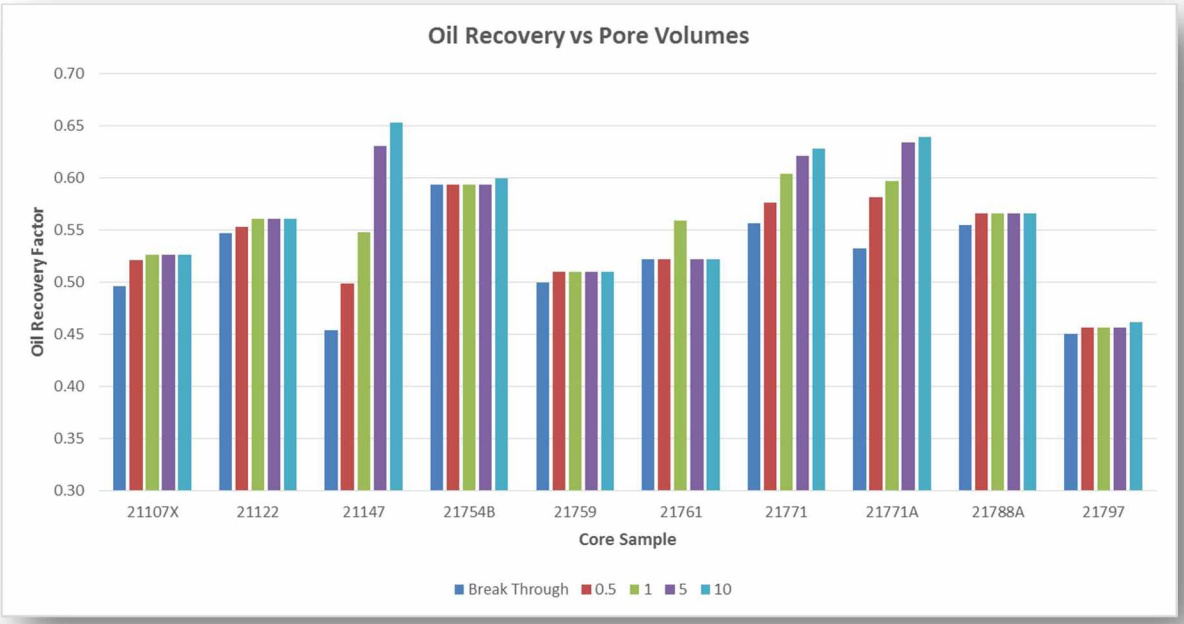

Figure 26: GP-1 & GP-31 SCAL oil recovery factor vs. pore volumes injected for the Tyonek C sands.

3.6 Reservoir Pressure

The reservoir pressure history obtained from the Granite Point platform area of the field indicates a nearly constant reservoir pressure of 1,500-1,800 psig at the producers from 1973 to 2018. The pressure at the injectors is significantly higher. This is expected as the relative permeability (to be discussed in following sections) to water is small and therefore the pressure will take a significant period of time to equalize throughout the reservoir. This is illustrated in Figure 27 for the Granite Point Platform.

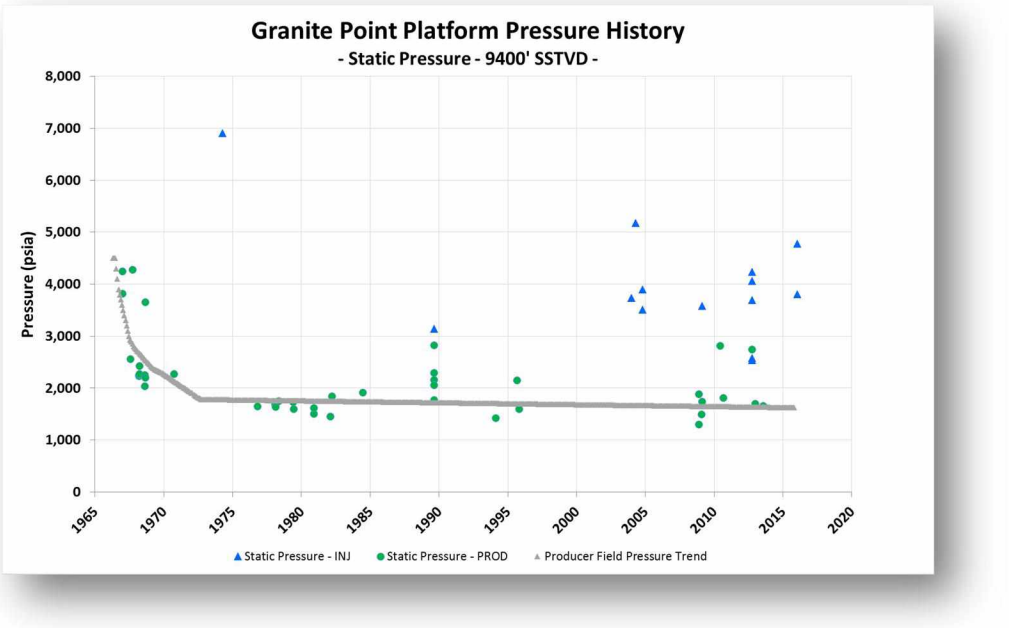

Figure 27: Granite Point platform pressure history. The gray line is representative of the average producer pressure trend with injector pressures omitted from this average.

This reservoir pressure trend is only possible if the injection withdrawal ratio has been maintained close to unity, the tank size is much larger than currently mapped, there is aquifer support, or some combination of all three. To determine which of these factors predominate a material balance analysis was completed as discussed in Section 3.5.

3.5 Drive Mechanism

The static reservoir pressure history, low rate of production decline, stable GOR, and infill wells encountering aquifer water at shallower depths than were encountered during the initial development wells suggest aquifer support is present. As an example, during the 2017 Granite Point Platform drilling campaign aquifer contacts were encountered up-dip of the original LKO's in the C5, C6, and C7 sands. The aquifer water is identifiable

from its much lower NaCl content than filtered Cook Inlet water that was used historically for injection water. The NaCl equivalent of the aquifer water is 4,000-6,000 ppm versus the filtered Cook Inlet water used for injection, which has a NaCl equivalent of 18,000-20,000 ppm.

To further investigate the aquifer a material balance was performed on the Granite Point platform area of the field. The Granite Point Platform area of the field has sufficient static reservoir pressure and PVT data. The Anna and Bruce platforms utilize downhole jet pumps for artificial lift resulting in a more interpretive estimate of reservoir pressure than downhole gauge data that can be acquired in the gas lifted wells at the Granite Point platform.

The most appropriate expression of the material balance to history match the performance of this reservoir is the Havlena and Odeh, defined below.[5]

$$N_p\left[B_o + (R_p - R_s)B_g\right] + W_pB_w = N\left[(B_o - B_{oi}) + (R_{si} - R_s)B_g\right] + mNB_{oi}\left(\frac{B_g}{B_{gi}} - 1\right) + \frac{(1+m)NB_{oi}(c_wS_{wc} + c_f)\Delta p}{1 - S_{wc}} + W_eB_w + W_i + G_iB_{gI}$$

$$\textit{Or More Simply, } F = N(E_o + mE_g + E_{fw}) + W_eB_w$$

$$\textit{Where, } F = N_p\left[B_o + (R_p - R_s)B_g\right] + W_pB_w \qquad \text{[RB]}$$

$$E_o = \left[(B_o - B_{oi}) + (R_{si} - R_s)B_g\right] \qquad \text{[RB/STB]}$$

$$E_g = B_{oi}\left(\frac{B_g}{B_{gi}} - 1\right) \qquad \text{[RB/STB]}$$

$$E_{fw} = (1+m)B_{oi}\frac{(c_wS_{wc} + c_f)\Delta p}{1 - S_{wc}} \qquad \text{[RB/STB]}$$

Equation 2: Havlena and Odeh Material Balance.

Where;

N_p = Cumulative oil [STBO]

B_o = Oil formation volume factor at average reservoir pressure [RB/STB]

R_p = Cumulative gas divided by cumulative oil [SCF/STB]

R_s = Solution GOR [SCF/STB]

B_g = Gas formation volume factor [RB/SCF]

W_p = Cumulative water [STBW]

B_w = Water formation volume factor [RB/STB]

N = Original oil in place [STBO]

B_{oi} = Initial oil formation volume factor [RB/STB]

R_{si} = Initial solution GOR [SCF/STB]

m = Ratio of gas cap volume/oil volume at initial conditions [vol/vol]

c_w = Water compressibility [psi-1]

S_{wc} = Connate water saturation [% of pore volume]

c_f = Formation compressibility [psi-1]

Δp = Pressure differential from original reservoir pressure [psi]

W_e = Water encroachment from aquifer [RB]

W_i = Cumulative injection water [STB]

G_i = Cumulative gas injection [SCF]

B_{gi} = Gas formation volume factor at initial conditions [RB/SCF]

With the data monitoring of the field having been sufficient, the expression is left with two unknowns, the STOIIP, N, and the cumulative water influx, W_e. There are several methods available to quantify the rate of water influx; however, limited empirical data is available to define the aquifer properties and any attempt made to quantify these properties would be highly subjective. Furthermore, due to the numerous sands and their variable quality, each sand will have its own associated aquifer properties. Therefore, the opening move was to verify that the reservoir has exhibited aquifer support. This was done by plotting the underground withdrawal divided by the oil and formation water expansion terms, $F/(E_o+E_{fw})$, vs cumulative production, N_p (Figure 28). The variance through time can be used qualitatively to determine the type of drive mechanism. If the points lie on a horizontal straight line it implies that the aquifer encroachment is zero and therefore a depletion drive mechanism. If the points rise it indicates the reservoir has been energized. This energy could come from abnormal pore compaction, water influx, or a subtle combination of the two.[4]

The plot in Figure 28 shows an increase in $F/(E_o+E_{fw})$ prior to the startup of water injection and again after the cessation of water injection. These two time periods support the qualitative observations from the field's low production decline rate, infill wells encountering aquifers at shallower depths than were encountered during the initial development wells, static reservoir pressure history, and stable GOR. Furthermore, the constant positive slope of the $F/(E_o+E_{fw})$ vs N_p curve when water injection is not active suggests an infinite acting aquifer.[4] Special core analysis does not indicate abnormal pore compaction and therefore the source of the energy must be derived

from aquifer influx.

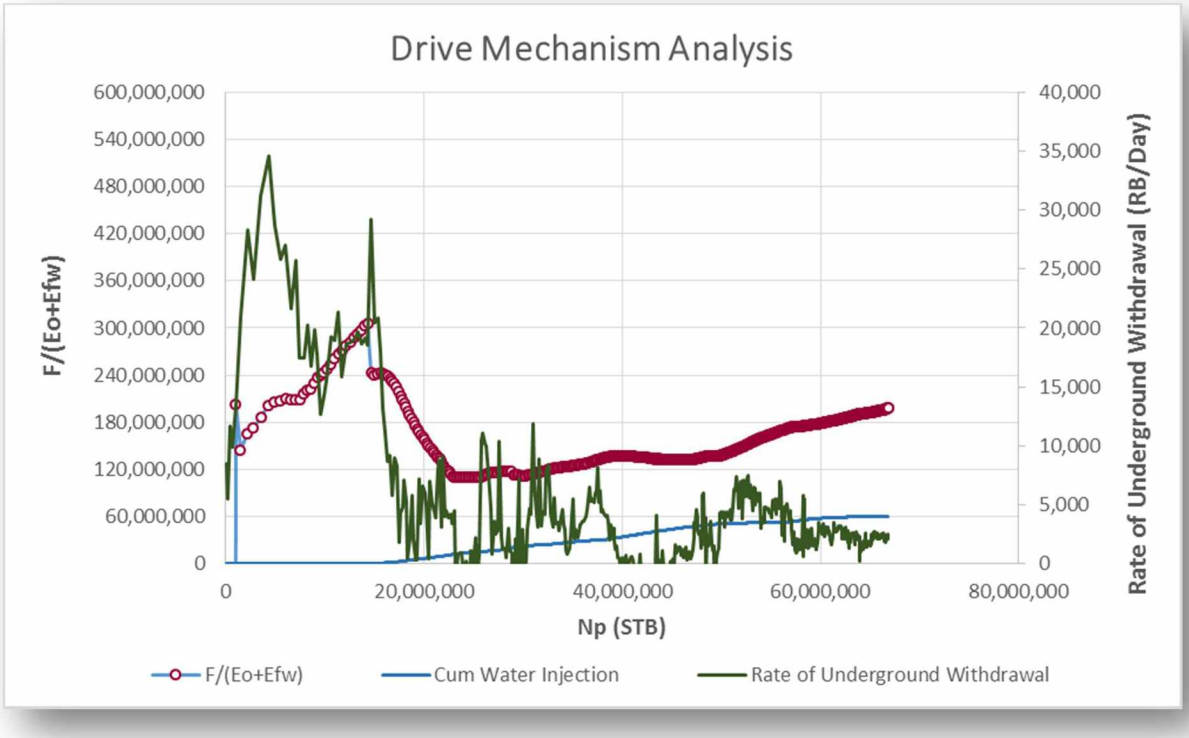

Figure 28: Drive mechanism analysis results.

This plot can be further utilized by assessing the intercept of $F/(E_o+E_{fw})$ at Np equals zero. This estimates the Granite Point Platform's STOIIP to be approximately 150 MMSTBO. This value is only the amount of oil that is in pressure communication with the wells in which the reservoir pressure data points were taken. Any oil not contributing to the reservoir pressure data points are not incorporated into the material balance and is therefore upside potential.

3.6 Oil-Water Contacts

As evidenced by the infill development wells, the oil-water contacts vary considerably by individual sand. Contacts encountered in development wells indicate hydrocarbon fill ranging from 40% to 70% of closure. The most reliable data for determination of these contacts is well control.

Within the Granite Point platform area of the field the primary zones of interest are the C2, C5, C6, and C7. With the three phases of development, along with the 2017 drilling campaign, an understanding of the oil-water contacts can be achieved.

The C2 sand original oil-water contact was -9,596' SSTVD (Figures 29 and 30). Due to the relatively thin C2 sand, and relatively high porosity and permeability, the sand is nearly entirely swept by injection water. This is supported by 1990's GP-50 and GP-51 development wells that encountered the C2 sand wet on the top of the structure.

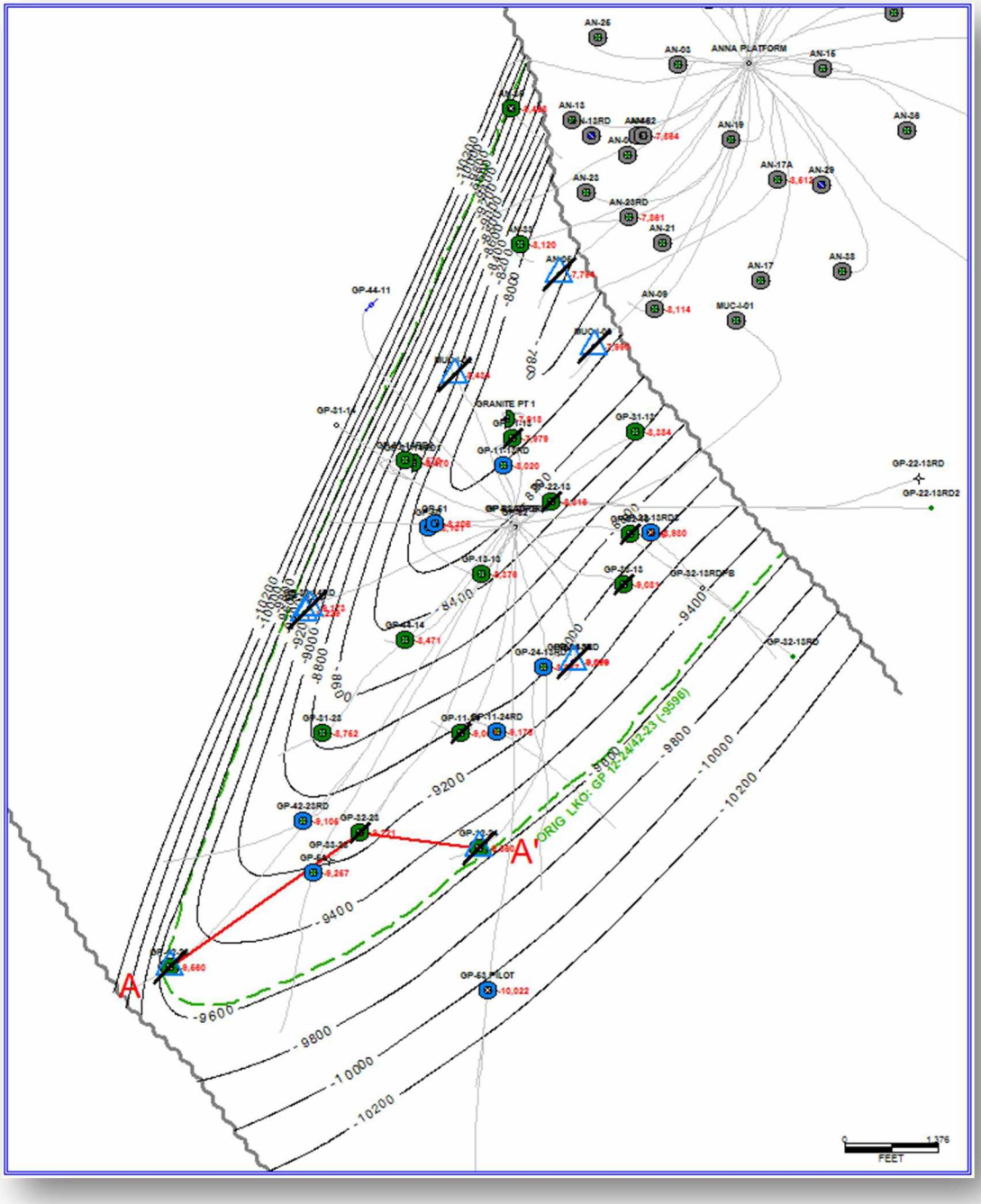

Figure 29: Granite Point platform C2 structure map, well locations, and original lowest known-oil. This lowest known-oil is illustrated by the green dashed line. The cross section in Figure 30 is through A-A'.

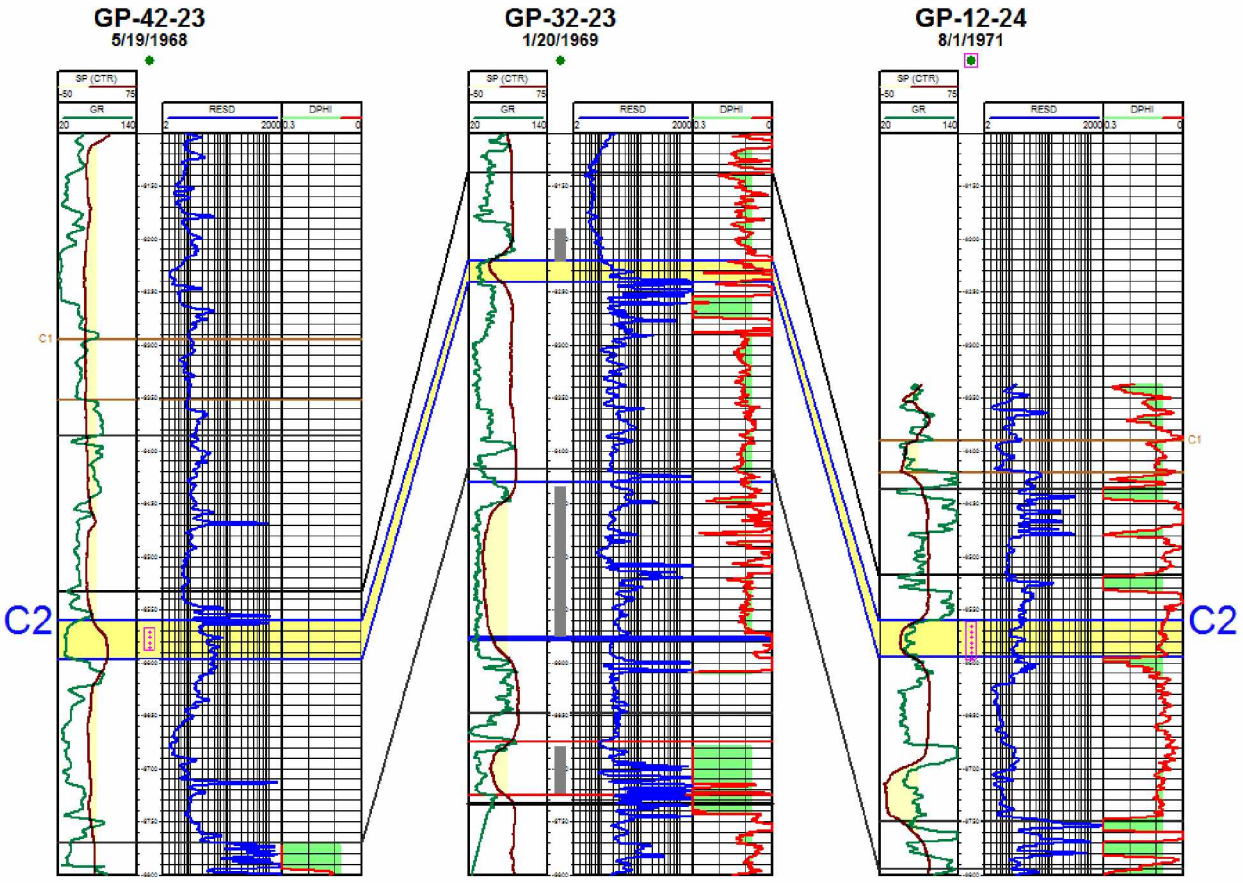

Figure 30: Granite Point platform C2 well logs along the cross section A-A' in Figure 29. Track 1 consists of the Gamma Ray and SP curves, track 2 is the depth (SSTVD) and perforated intervals (pink boxes), track 3 is the resistivity curve, and track 4 is the density porosity curve.

The original C5 sand lowest-known oil was found at -10,576' SSTVD in the GP-42-23 well drilled and completed one year after the platform was brought into production (Figure 31). The C5 sand current oil-water contact of -10,290' SSTVD is predicated upon the GP-11-24RD well that was drilled and completed in 2017 (Figure 32). Evidence of aquifer support is present as the GP-32-13RD, a C5 only horizontal well drilled along the west flank, was completed in 1992 and encountered the oil-water contact at -10,395' SSTVD. GP-54, a C5 only horizontal well along the southern nose of the structure drilled to -10,070' SSTVD and did not encounter the aquifer, supporting the GP-11-24RD current oil-water contact.

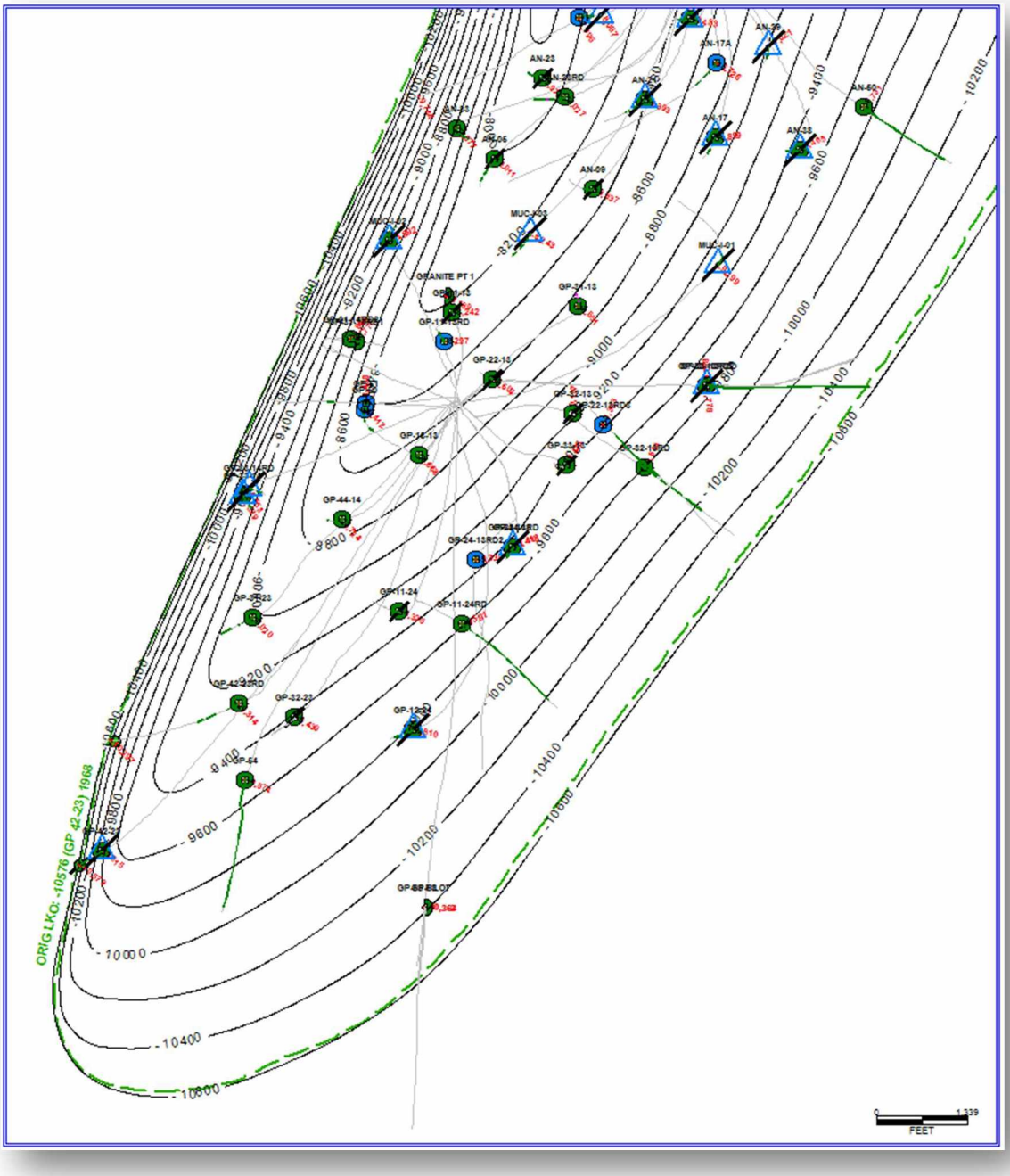

Figure 31: Granite Point platform C5 structure map, well locations, and original lowest known-oil. The channel edge is defined by the gray line. This lowest known-oil is illustrated by the green dashed line.

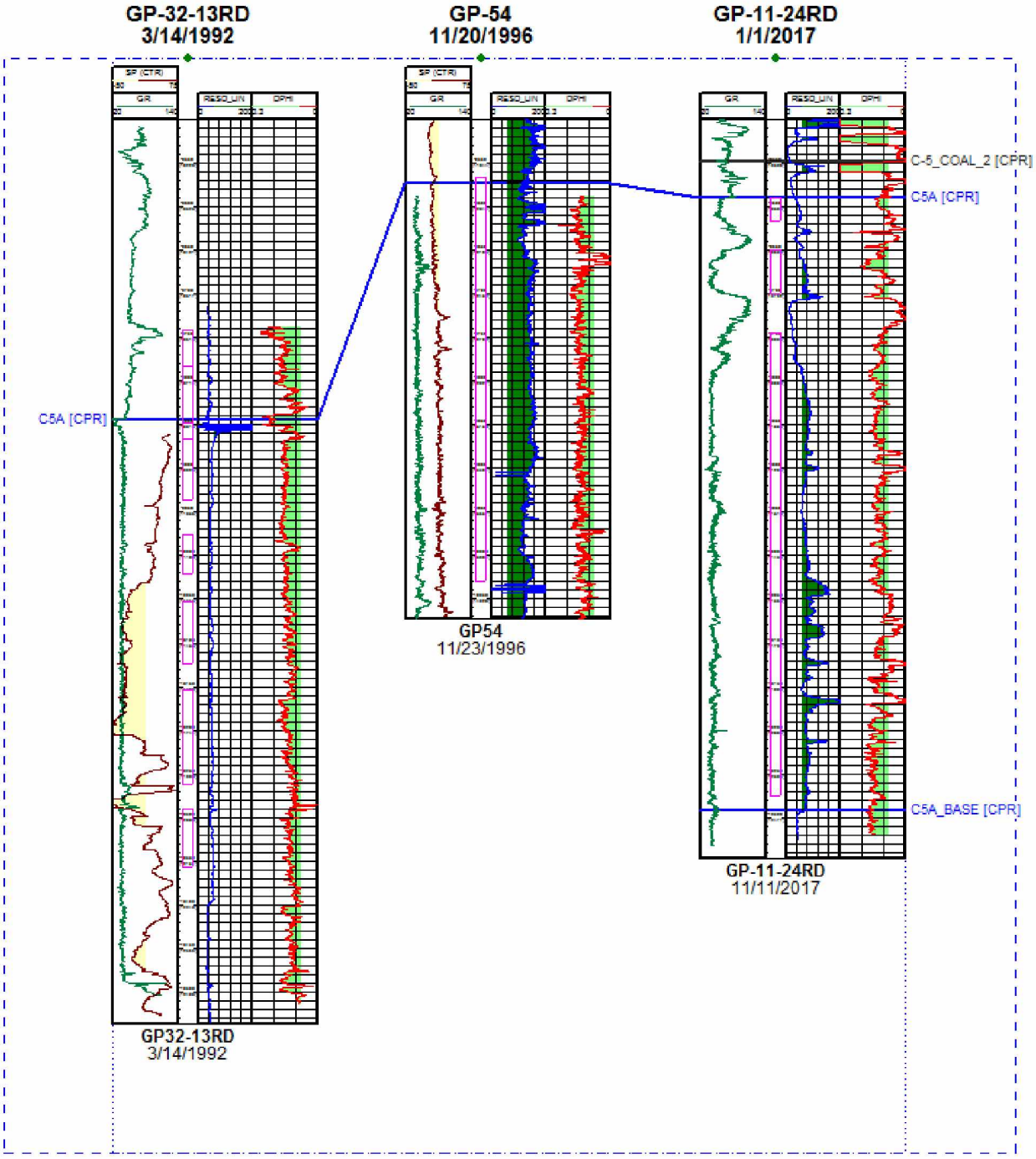

Figure 32: Granite Point platform C5 horizontal well logs. Track 1 consists of the Gamma Ray and SP curves, track 2 is the depth (SSTVD) and perforated intervals (pink boxes), track 3 is the resistivity curve, and track 4 is the density porosity curve.

The C6 contact has not been encountered; however, the lowest-known oil was encountered in the GP-12-24 well along the eastern flank at -10,088' SSTVD. Figures 33 and 34 below show the map and cross section detailing this lowest-known oil.

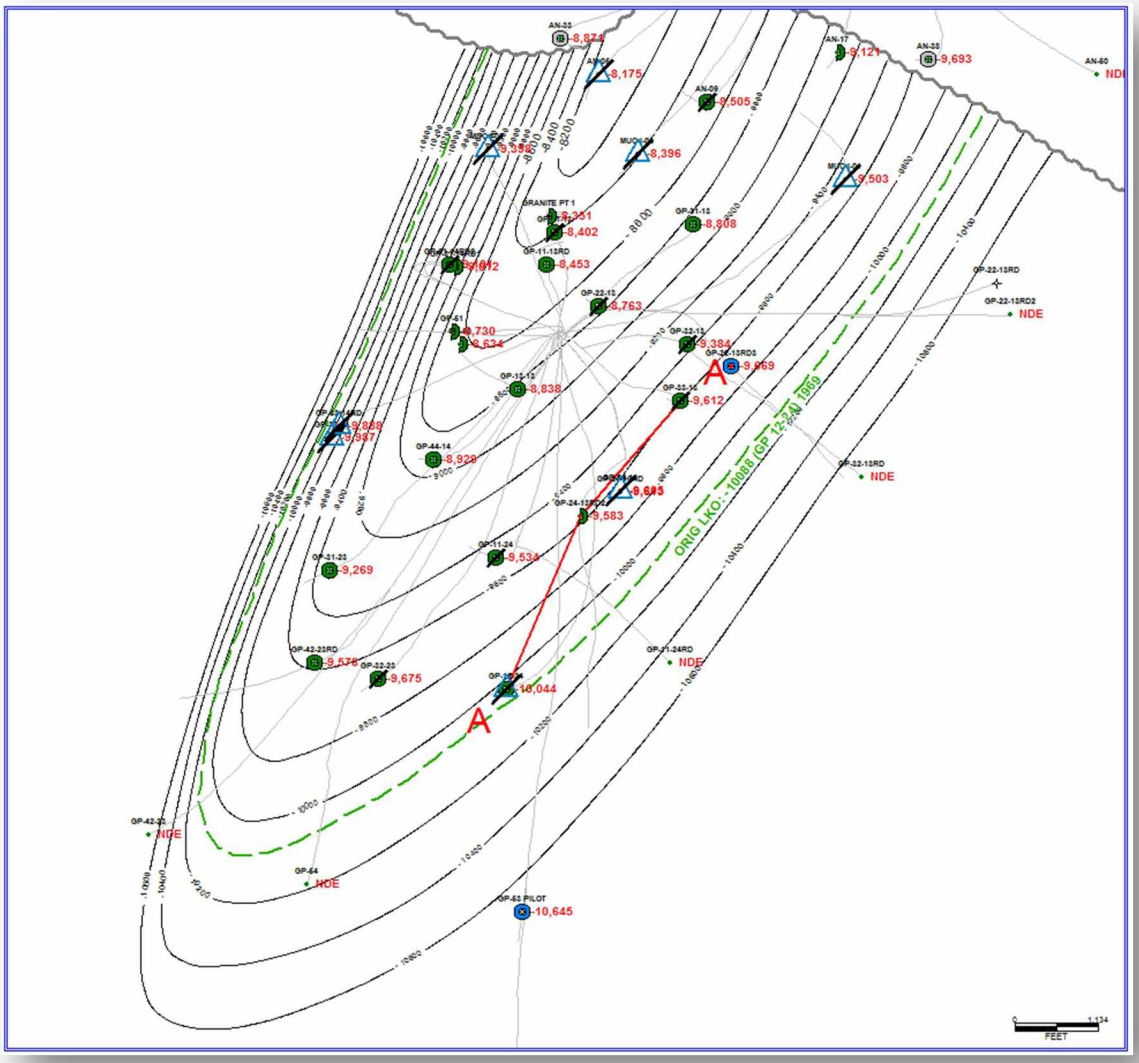

Figure 33: Granite Point platform C6 structure map, well locations, and original lowest known-oil. This lowest known-oil is illustrated by the green dashed line. The channel edge is defined by the gray line. The cross section in Figure 34 is through A-A'.

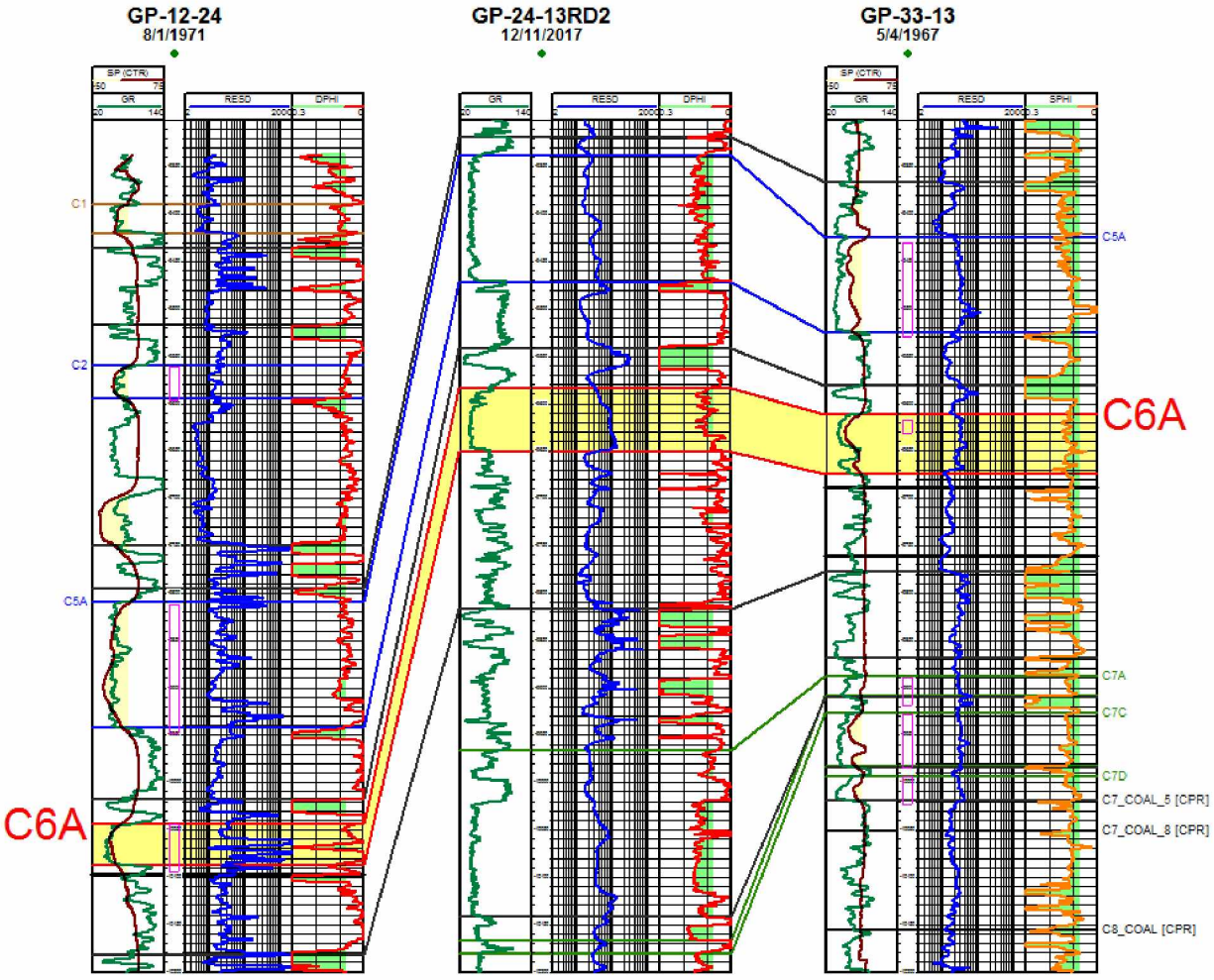

Figure 34: Granite Point platform C6 horizontal well logs. Track 1 consists of the Gamma Ray and SP curves, track 2 is the depth (SSTVD) and perforated intervals (pink boxes), track 3 is the resistivity curve, and track 4 is the density porosity curve.

The C7 contact was encountered in 2017 with the GP-24-13RD2 well at -10,350' SSTVD. The original lowest-known oil was encountered in the GP-33-14 well along the western flank at -10,505' SSTVD. Figures 35 and 36 below show the map and cross section detailing this original lowest-known oil.

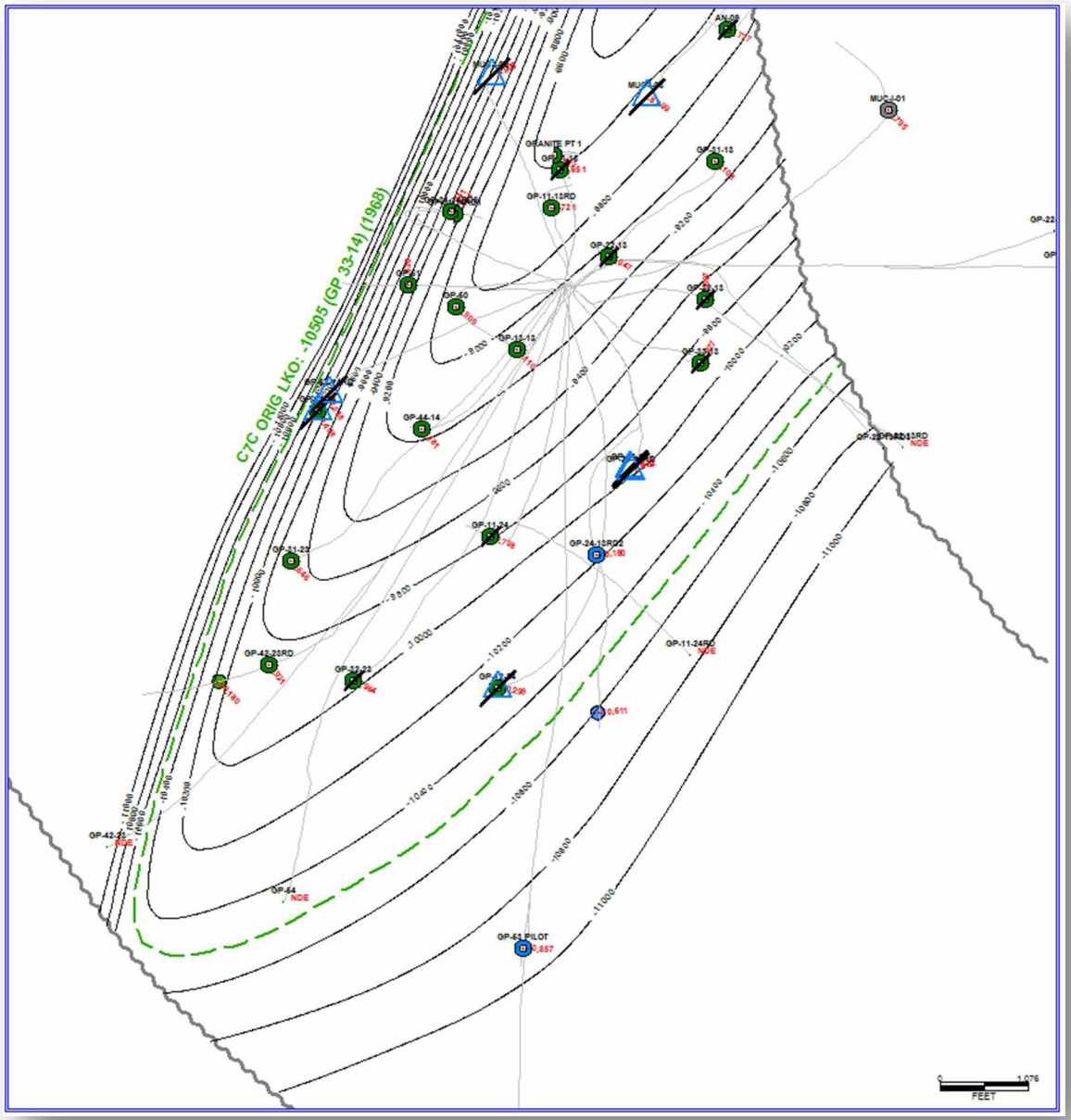

Figure 35: Granite Point platform C7C structure map, well locations, and original lowest known-oil. The channel edge is defined by the gray line. This original lowest known-oil is illustrated by the green dashed line.

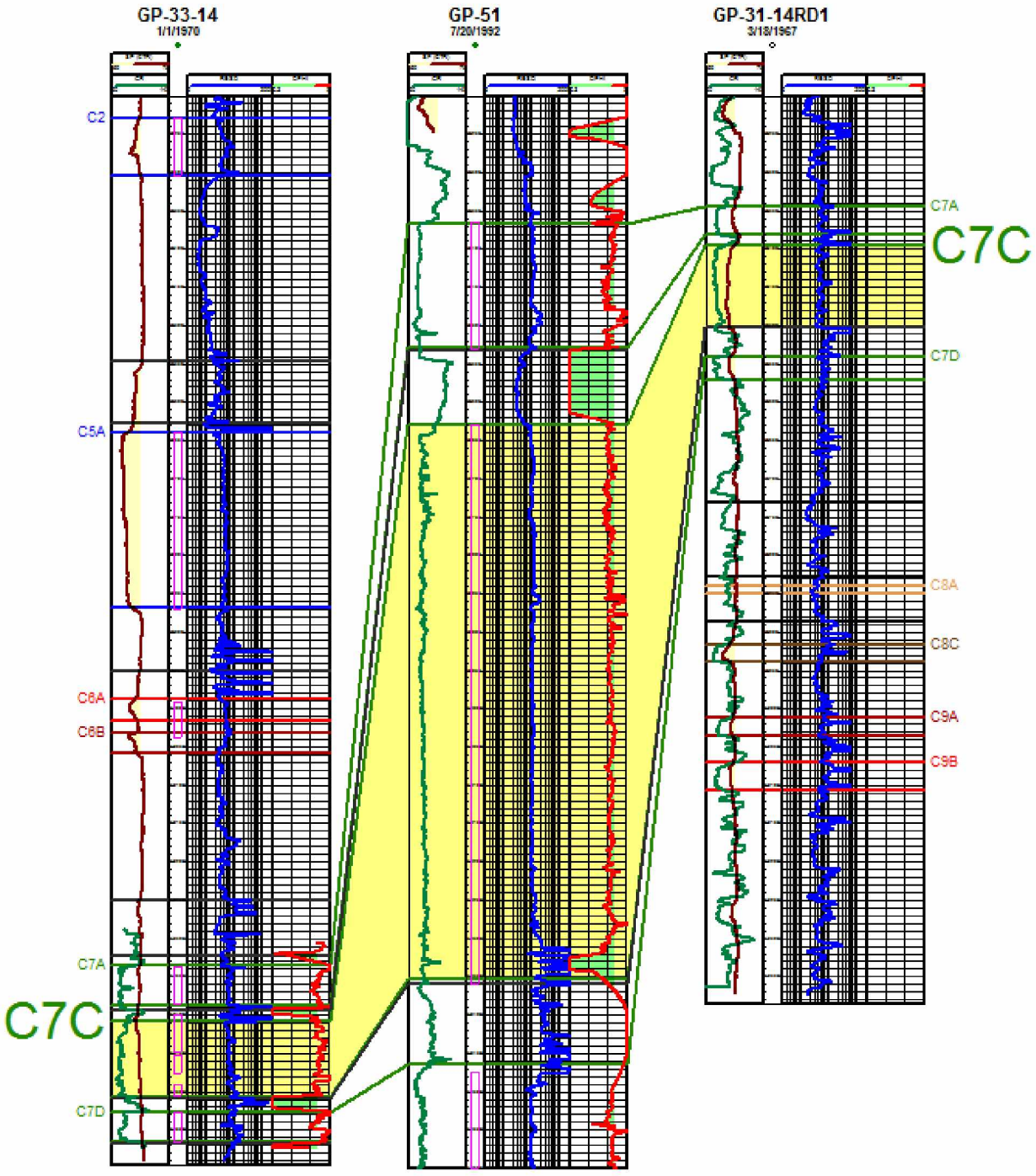

Figure 36: Granite Point platform C7C horizontal well logs. Track 1 consists of the Gamma Ray and SP curves, track 2 is the depth (SSTVD) and perforated intervals (pink boxes), track 3 is the resistivity curve, and track 4 is the density porosity curve.

3.7: Waterflood Areal Extent

Prior to performing simulation to define the extent of the waterflood an analytical approach was developed. This analytical approach allocated injection volumes into each sand that was perforated, at each injector, by weighting the relative quality of the sands perforated and multiplying this value by the cumulative volume of water injected into each well. The relative quality of the sands was determined by calculating the product of each sand's respective k-h, and dividing it by the sum of the k-h values for all sands perforated in the injector. The value of h for each sand was derived from calculating the true stratigraphic thickness (TST) of each perforated sand using an 8% porosity cutoff. The k value used for this analysis was the k_w at S_{or} as derived from the GP-1 and GP-31 SCAL data. Using the porosity-k_w exponential relationship defined in Figure 37 below, the average net sand porosity can be derived from the well logs then the k_w value calculated.

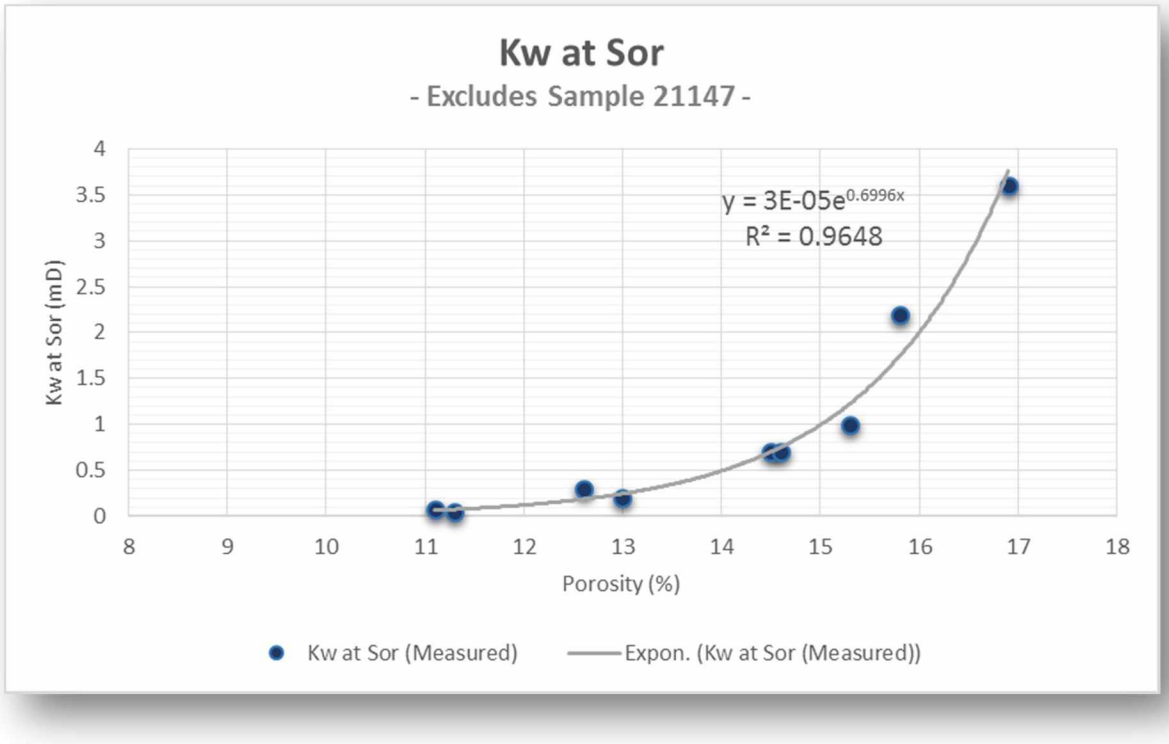

Figure 37: GP-1 and GP-31 k_w at S_{or} vs. porosity relationship for the Tyonek C sands.

As an example, the GP-24-13 injector's C5A sand has a k-h value of 10.1 (k_w at S_{or} = 0.13 mD, h = 76'), while the sum of all of the present sands' k-h is 44.7. Therefore, 23% (10.1/44.7) of the 8,253 MSTBW injected into the GP-24-13 well has been allocated to the C5A sand (Figure 38).

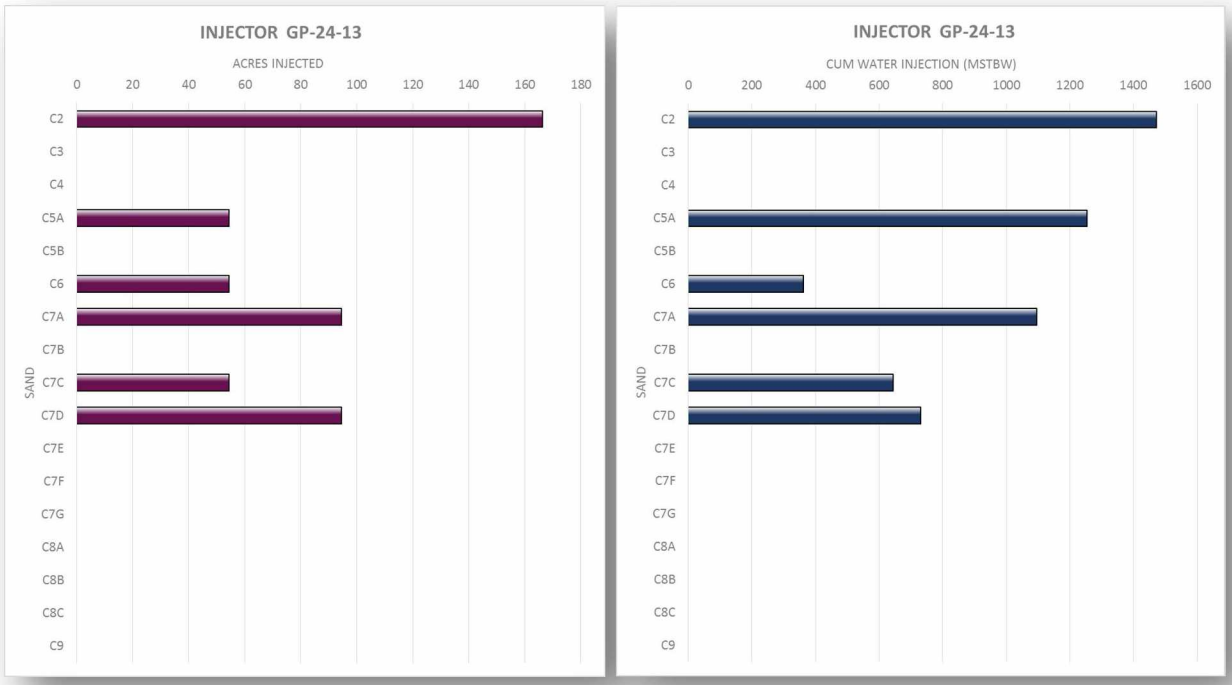

Figure 38: Waterflood areal extent for the GP-24-13 injector.

This approach is only possible due to the extreme water wetness of the Granite Point Field Tyonek C sands and the favorable mobility ratio. Due to the favorable mobility ratio the injection water will not outrun the oil. This combined with the fractional flow curve indicating that the difference in water saturation within the formation between breakthrough and >90% f_w is negligible when determining swept rock volume. This assumes the porosity is relatively uniform throughout each individual sand (the Tyonek C sands are not a dual-porosity system). Furthermore, this approach was validated with the GP-24-13RD2 horizontal producer in 2017. This producer was drilled through the area swept by injection to reach the target area, thus delineating the areal extent of the injection. The actual areal extent of the waterflood was within 100 feet of the calculated areal extent. Furthermore, this approach matches other development well control fairly well.

Pulling the geologic understanding, reservoir fluid, and core data together, the extent of the waterflood can now be mapped. This analytical approach is not intended to replace simulation, it is simply meant to aid in defining the simulation input parameters and identify potential infill development opportunities at a high level. An example is shown in Figure 39 below for the C5A sand in the Granite Point platform area of the Granite Point field.

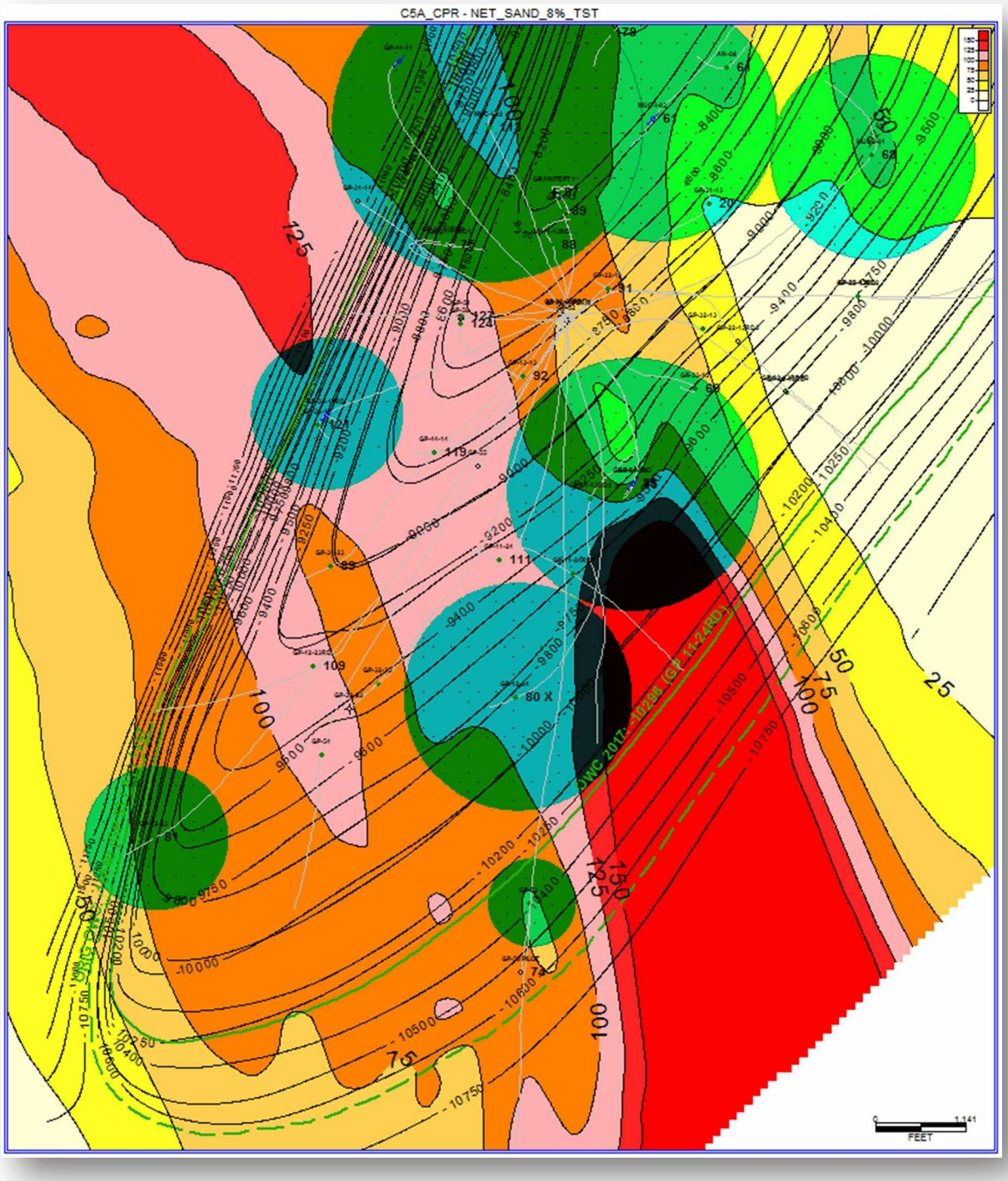

Figure 39: Granite Point platform area C5A sand waterflood areal extent. The structure contours are in black, the blue-green circles are the calculated injection acreage, the yellow-to-red shading is the net sand in true stratigraphic thickness, the solid green contour line is the current oil-water contact, and the dashed green line is the original oil-water contact.

Water injection at the Granite Point field was reduced to a negligible amount in 2008, and was curtailed at several points in time throughout the field's history due to mechanical problems and skepticism as to whether the waterflood was effective.[6] Although digital data of the wellhead injection pressures no longer exists, hall plots were constructed by previous operators that indicated severe plugging, as illustrated in Figure 40 below. This is as expected based upon the extremely low effective permeability to water, lateral heterogeneity in sand quality and thickness, sand discontinuities pertaining to the fluvial deposition environment, the potential for fines migration, and the faulting present along the west flank and north end of the field. In order to inject into the formation 6,000-10,000 psi at surface was required which required high pressure piping and pumping equipment that was costly to maintain for the operators.[6]

Reviewing of injection logs indicate an injection conformance that is expected based upon the exponential relationship between porosity and effective water permeability. The lower porosity sands were unable to take significant quantities of water. These aforementioned geologic hurdles make secondary recovery with water injection challenged; however, in areas with well-defined sand channels of higher porosity, waterflood can be extremely effective as evidenced by the fractional flow curve.

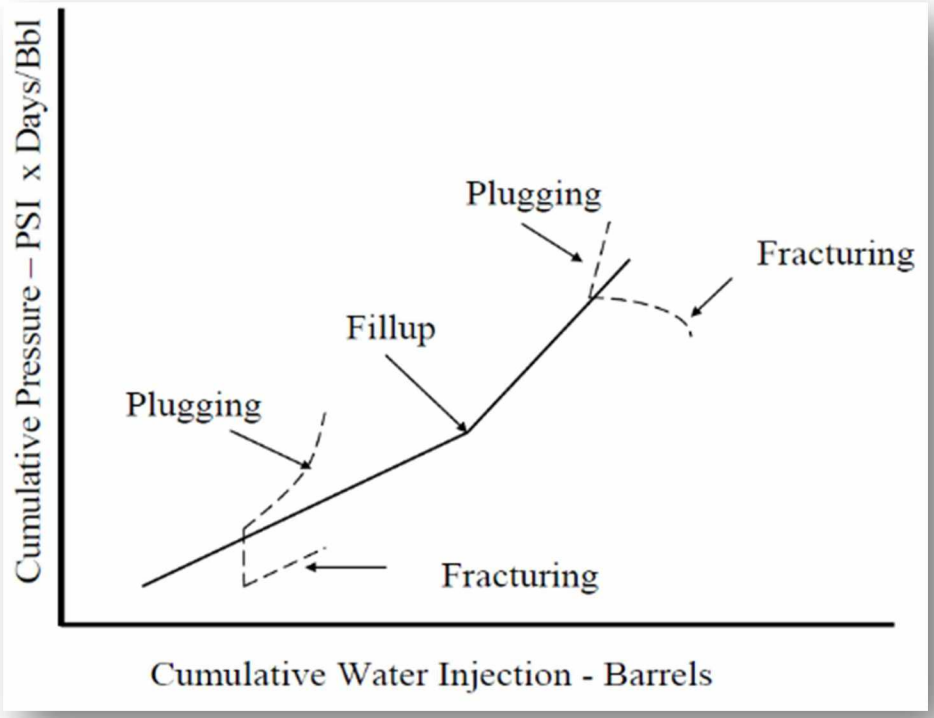

Figure 40: Illustrative example of plugging in an injector hall plot.[7]

3.8: Horizontal Wells

As of year-end 2017 there were thirteen horizontal wells drilled at Granite Point field, eight of which can be classified as an economic success. Four of the five failures were attributable to drilling into the aquifer (unknown OWC) and one failure was attributable to the inability to successfully complete the well. The eight wells that can be classified as economic successes are still online and have produced between 415 – 2,662 MSTBO of cumulative oil per well, as shown in Figure 41 below. Seven of these eight wells and their associated production data were chosen to determine the horizontal permeability to oil. The eighth well, GP-11-24RD, was excluded as it was brought online in November 2017 at an initial production rate of 1,200 BOPD (0% water cut) and is still in its transient phase.

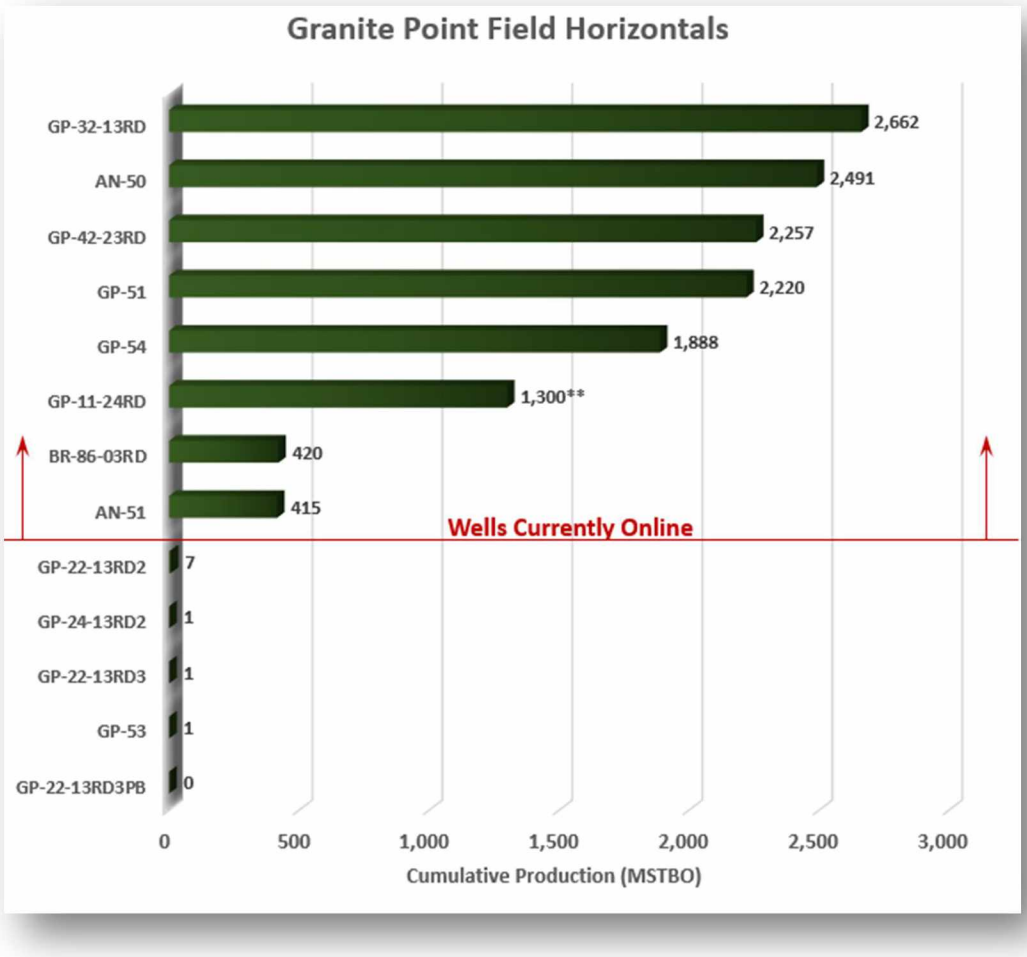

Figure 41: Granite Point field horizontal wells current cumulative oil recovery.

From these successes it is apparent that horizontal wells, when steered away from injection swept areas and the aquifer, can improve the ultimate recovery of the Granite Point field. To forecast the incremental rate from

these horizontal wells the Economides, Deimbacher, Brand, and Heinemann (1991) variation of the Joshi horizontal well equation can be used.[8]

$$q_h = \frac{k_h h(p_e - p_{wf})}{141.2\mu B_o \left(ln\left(\frac{a + \sqrt{a^2 - \left(\frac{L}{2}\right)^2}}{\frac{L}{2}} \right) + \frac{h * \sqrt{\frac{k_h}{k_v}}}{L} * ln\left(\frac{h * \sqrt{\frac{k_h}{k_v}}}{r_w\left(\sqrt{\frac{k_h}{k_v}} + 1\right)} \right) + s \right)}$$

Equation 3: Economides, Deimbacher, Brand, and Heinemann (1991) variation of the Joshi horizontal well equation.

Where;

$$\text{a} = \frac{L}{2}\left\{0.5 + \left[0.25 + \left(\frac{r_e}{\frac{L}{2}}\right)^4\right]^{0.5}\right\}\text{^0.5}$$

k_h = Horizontal oil permeability [mD]

h = Net reservoir thickness [ft]

p_e = Average reservoir pressure [psig]

p_{wf} = Bottom hole flowing pressure [psig]

$B_o(p)$ = Formation volume factor at average reservoir pressure [RB/STB]

$\mu_o(p)$ = Oil viscosity at average reservoir pressure [cP]

L = Length of lateral in net sand [ft]

k_v = Vertical oil permeability [mD]

r_e = Drainage radius [ft]

r_w = Wellbore radius [ft]

s = Skin [Dimensionless]

Each variable within this expression was analyzed to determine the effect on oil rate at the Granite Point field, as illustrated in the tornado chart in Figure 42. The high, low, and mean values for each variable was derived from field data. For example, the Granite Point wells have a wellbore radius ranging from 0.4 – 0.7 ft., the oil viscosity and B_o vary with pressure over a range of 0.5 – 0.3 cP and 1.45 – 1.28 RB/STB, respectively, and the reservoir thickness varies from 30 ft. – 120 ft. The resultant high (green bars) and low (red bars) production rates

for each variable were determined by using the mean value for all other variables and changing the specific variable of interest to its high and low value. The lateral length of 1000' of net sand was set as a fixed parameter.

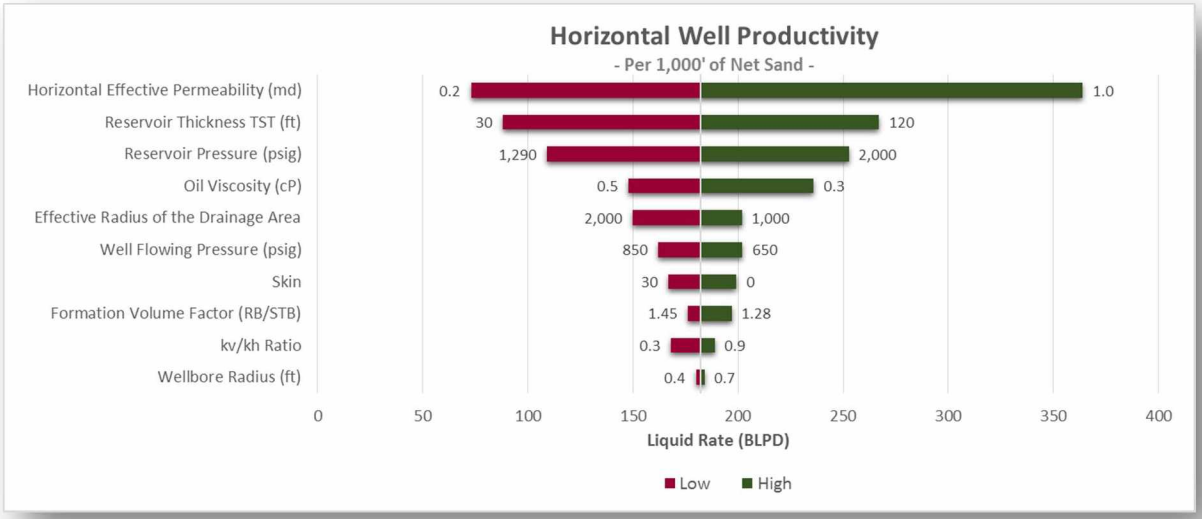

Figure 42: Granite Point field horizontal well productivity analysis tornado chart.

This tornado chart reveals that the range of permeability, reservoir thickness, and reservoir pressure have the most leveraging impact on the oil productivity. The mean value is 182 BLPD/1000' of net sand.

As there is sufficient well control in the field to accurately estimate net sand thickness, and historic reservoir pressure data depicts a fairly narrow range of reservoir pressures, the oil permeability for these horizontal wells remain the critical variable that requires a thorough understanding.

The average horizontal oil permeability for the horizontal wells was determined to be 0.7 mD, with a range of 0.20 – 1.0 mD (Table 2). This match was achieved by setting the wellbore radius (r_w), oil viscosity (μ), formation volume factor (B_o), wellbore flowing pressure (p_{wf}), effective drainage radius (r_{eH}), and skin (s) at the mean expected value, then determining from well data the net perforated footage (L), reservoir thickness (TST), and average porosity of the net footage with a 9% porosity cutoff. This allowed isolation of the oil permeability value, which can then be iterated to achieve a match with empirical data with all other variables set to their most likely estimate. The setting of the aforementioned variables as constants was possible due to the narrow range of these variables amongst these horizontal wells and the relatively small impact on the production rate as shown in the tornado chart in Figure 42. The one exception to this would be the effective drainage radius; however, accurate empirical data is lacking to accurately assess each well's effective drainage radius and therefore an average value of 1,250 ft was chosen based upon well spacing and the subsequent assumed equipotential pressure contours.

Well (Name)	ϕ (Average) (%)	k_t (mD)	k_v (mD)	h (TST) (ft)	r_e (ft)	μ (cP)	B_o (RB/STB)	L (Net) (ft)	p_{wf} (psi)	r_w (ft)	a (ft)	s (Dimensionless)
GP-32-13RD	14%	1	0.6	84	0.523	0.4	1.4	1,115	750	1250	1314	15
AN-50	11%	0.9	0.54	120	0.523	0.4	1.4	941	750	1250	1295	15
GP-42-23RD	14%	0.8	0.48	109	0.523	0.4	1.4	902	750	1250	1291	15
GP-51	10%	0.8	0.48	95	0.523	0.4	1.4	492	750	1250	1262	15
GP-54	14%	0.5	0.3	110	0.523	0.4	1.4	1,843	750	1250	1430	15
BR-86-03RD	10%	0.7	0.42	82	0.523	0.4	1.4	187	750	1250	1252	15
AN-51	11%	0.2	0.12	83	0.523	0.4	1.4	779	750	1250	1281	15
GP-11-24RD	13%	0.5	0.3	105	0.523	0.4	1.4	1,319	750	1250	1340	15

Table 2: Granite Point field horizontal well effective permeability determination.

A key note on this approach is that this match was done on the time period when the well was flowing 100% oil and had reached a pseudo-steady state flow rate. In other words, the flush production period in which the drainage radius was established was excluded, as demonstrated in Figure 43 below. The calculated liquid rate, in red, uses the average field producers' reservoir pressure over time from when the field was brought online through 2018 and therefore has a steep decline during the early years of the field's production history.

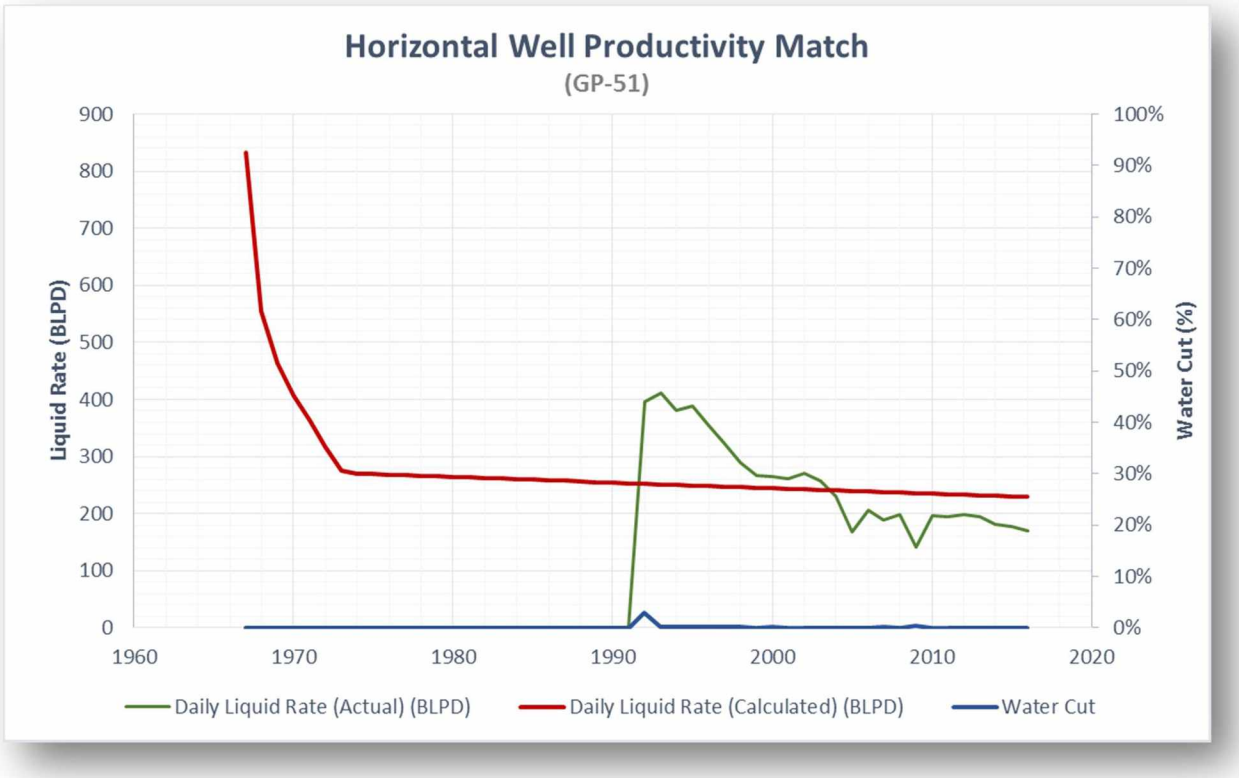

Figure 43: Horizontal well productivity match example.

The period of flush production lasted from 1-3 years in the horizontal wells analyzed. Although this flush production period has a positive effect on the economics of future development wells, it was excluded due to the highly subjective process of determining flush production rates and duration.

The good agreement between the value of the horizontal effective permeability from the horizontal wells and the vertical wells, 0.7 mD and 1.2 mD, respectively, supports calibrating the effective horizontal permeability to empirical data rather than relying upon core data. For the forecasting of horizontal wells' initial production rates, excluding flush production, a range of 0.20 to 1.0 mD should be used, with a mean value of 0.70 mD.

To further assess whether the application of the Economides, Deimbacher, Brand, and Heinemann variation of the Joshi Model is applicable, as well as to identify any outlying data sets, the horizontal wells' liquid production rate was normalized against a number of variables. The first normalization was done by dividing the actual liquid production rate by the net footage perforated with a 9% porosity cutoff (Figure 44). This showed well GP-51 as an outlier with a greater normalized productivity than the rest of the data set, and the AN-51 well as an outlier with a lower normalized productivity.

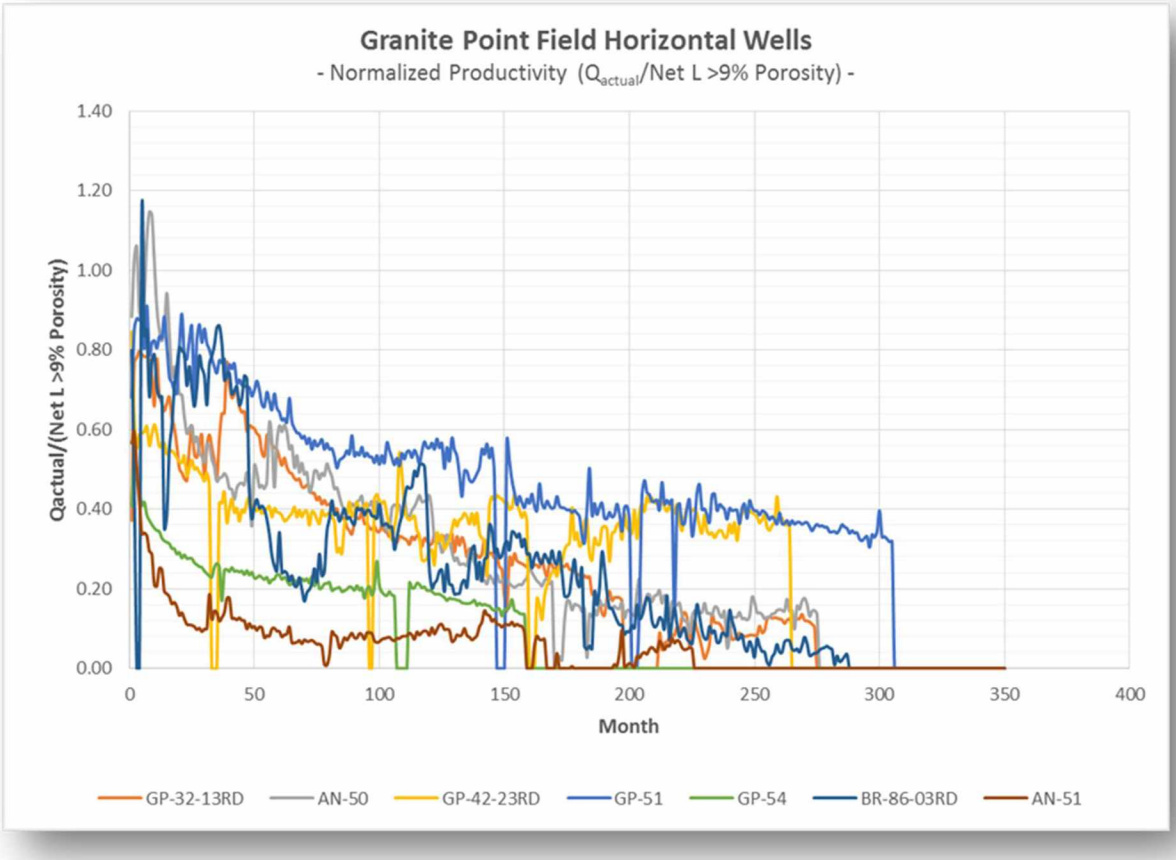

Figure 44: Normalized Productivity (Q_{ACTUAL}/Net L >9% Porosity)

To understand why the GP-51 and AN-51 wells were outliers, further normalization was done. Due to the productivity impairment from water imbibition into the reservoir rock, the second normalization eliminated production data in which the water cut exceeded 5%. Plotting this data (Figure 45) the low outlier AN-51 was removed as it only produced at less than 5% water cut for brief periods of time. In addition, the late time data of a number of wells in which productivity degradation was realized was excluded as the water cut exceeded the 5% threshold. These results aligned with other field data that suggests productivity will degrade when water comes into contact with the formation and/or the introduction of water into the wellbore degrades the ability to draw the well down as much as with an oil column.

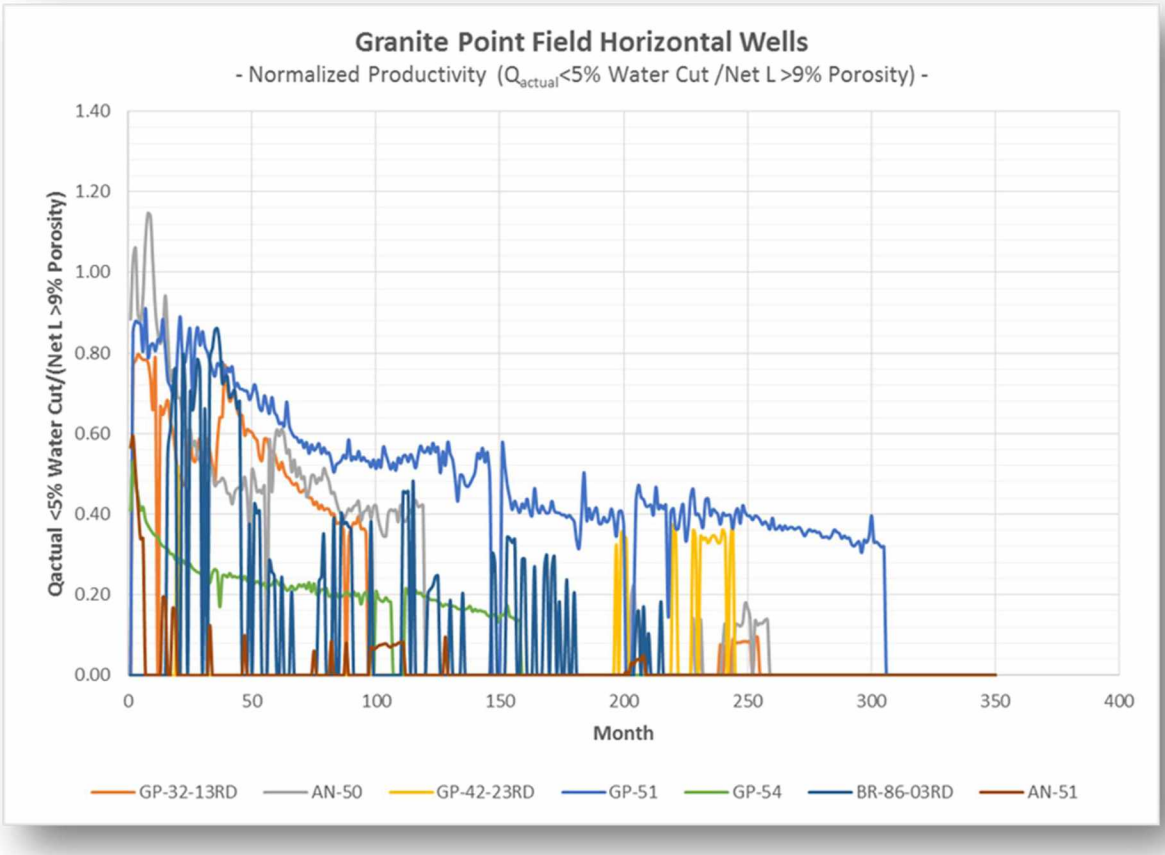

Figure 45: Normalized Productivity (QACTUAL<5% Water Cut/Net L >9% Porosity)

The high outlier, GP-51 appeared abnormally productive on a per foot basis. After further investigation, it appears that the porosity cutoff of 9% is too high, and that 8% porosity is a more reasonable cutoff. By applying a

8% porosity cutoff, both the GP-51 and the early time data from BR-86-03RD align more closely with the other wells' normalized productivity data as shown in Figure 46.

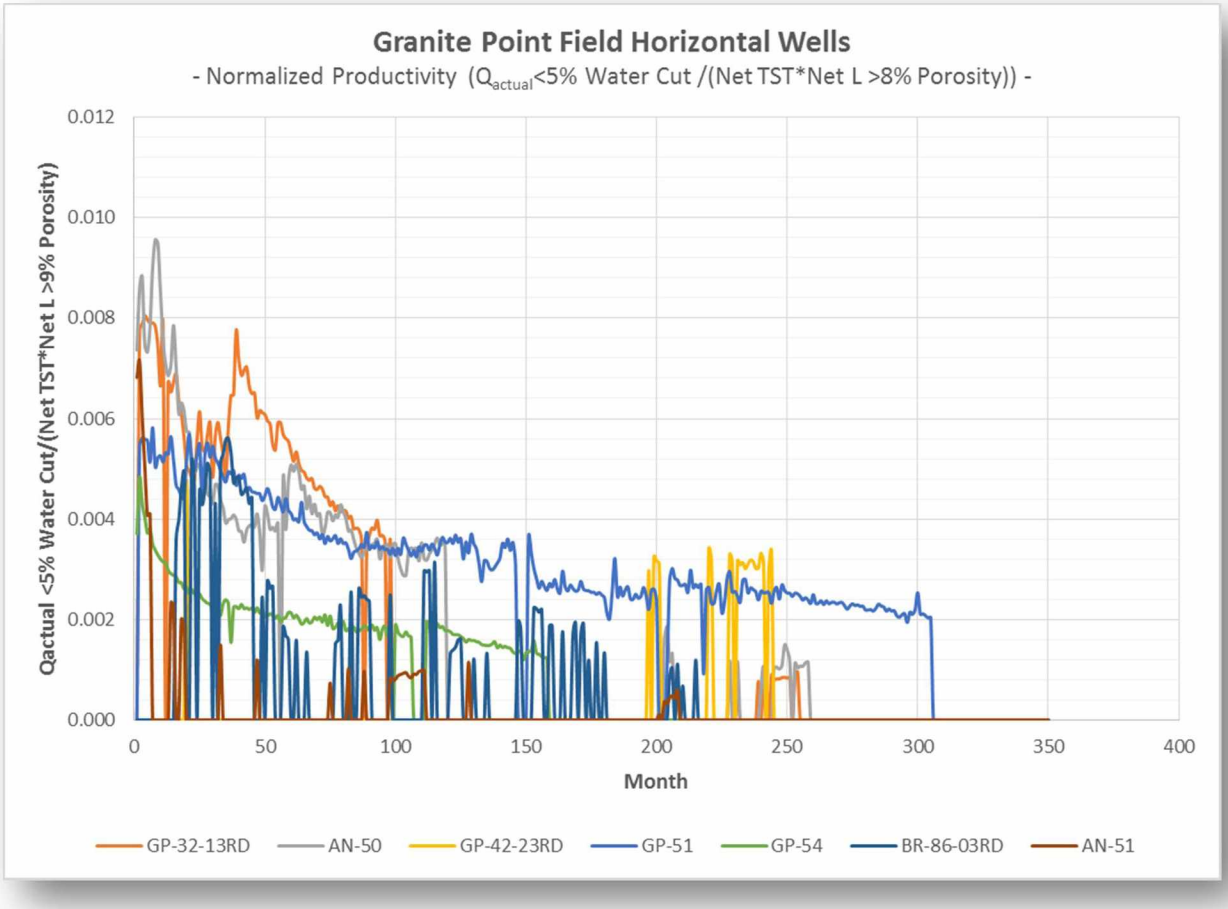

Figure 46: Normalized Productivity (Q_{ACTUAL}/Net L >8% Porosity).

Chapter 4: Development Simulation

4.1 Simulation Objectives

With the geologic understanding as outlined in Chapter 2, and the analytical approaches undertaken to define the fundamentals of the reservoir in Chapter 3, an effective reservoir simulation can be constructed. This effort was undertaken with the main objectives being to understand the movement of water within the reservoir as a means to identify un-swept areas. These un-swept areas can be targeted with additional horizontal wells to improve the ultimate recovery. With the analytical work completed, and 53 years of production history, the reservoir simulation can be properly history matched.

4.2 Simulation Construction

A preliminary reservoir model was built that incorporated the C2, C5, C6, and C7 sands. The grid was defined around the Granite Point Platform producing area. An average porosity, absolute permeability, and kv/kh ratio was applied to each layer (Figure 47), with the C2 and C5 being of generally better reservoir quality than the C6 and C7 sands. A natural boundary dividing the Granite Point platform area of the field from the Anna platform area to the north is established by three injectors that were drilled along the lease boundaries. These injectors were brought online early in the life of the field and so can be considered an equipotential boundary.

	Grid Thickness	Porosity	Permeability I	Permeability J	Permeability K
UNITS:	ft		md	md	md
SPECIFIED:	X	X	X	X	X
HAS VALUES:	X	X	X	X	X
Whole Grid					
Layer 1 (C2)	(O:\Alaska\Fields\Granite Point\R...	0.13	5.86	5.86	0.586
Layer 2 (C2)	(O:\Alaska\Fields\Granite Point\R...	0.13	5.86	5.86	0.586
Layer 3 (C2)	(O:\Alaska\Fields\Granite Point\R...	0.13	5.86	5.86	0.586
Layer 4 (C5)	(O:\Alaska\Fields\Granite Point\R...	0.13	5.86	5.86	0.586
Layer 5 (C5)	(O:\Alaska\Fields\Granite Point\R...	0.13	5.86	5.86	0.586
Layer 6 (C5)	(O:\Alaska\Fields\Granite Point\R...	0.13	5.86	5.86	0.586
Layer 7 (C5)	(O:\Alaska\Fields\Granite Point\R...	0.13	5.86	5.86	0.586
Layer 8 (C5)	(O:\Alaska\Fields\Granite Point\R...	0.13	5.86	5.86	0.586
Layer 9 (C5)	(O:\Alaska\Fields\Granite Point\R...	0.13	5.86	5.86	0.586
Layer 10 (C6)	(O:\Alaska\Fields\Granite Point\R...	0.125	2.48	2.48	0.248
Layer 11 (C6)	(O:\Alaska\Fields\Granite Point\R...	0.125	2.48	2.48	0.248
Layer 12 (C6)	(O:\Alaska\Fields\Granite Point\R...	0.125	2.48	2.48	0.248
Layer 13 (C6)	(O:\Alaska\Fields\Granite Point\R...	0.125	2.48	2.48	0.248
Layer 14 (C7)	(O:\Alaska\Fields\Granite Point\R...	0.125	2.48	2.48	0.248
Layer 15 (C7)	(O:\Alaska\Fields\Granite Point\R...	0.125	2.48	2.48	0.248
Layer 16 (C7)	(O:\Alaska\Fields\Granite Point\R...	0.125	2.48	2.48	0.248
Layer 17 (C7)	(O:\Alaska\Fields\Granite Point\R...	0.125	2.48	2.48	0.248
Layer 18 (C7)	(O:\Alaska\Fields\Granite Point\R...	0.125	2.48	2.48	0.248
Layer 19 (C7)	(O:\Alaska\Fields\Granite Point\R...	0.125	2.48	2.48	0.248

Figure 47: General property specification for the Granite Point Platform reservoir model.

Using well control, a preliminary interpretation of the net sand thicknesses were created and imported into the reservoir model to define the grid thicknesses. Figure 48 below represents the grid thickness for the C7 sand from a northwest perspective. The fluvial deposition environment makes this interpretation challenging; however, with the significant amount of well control a fairly accurate representation can be made.

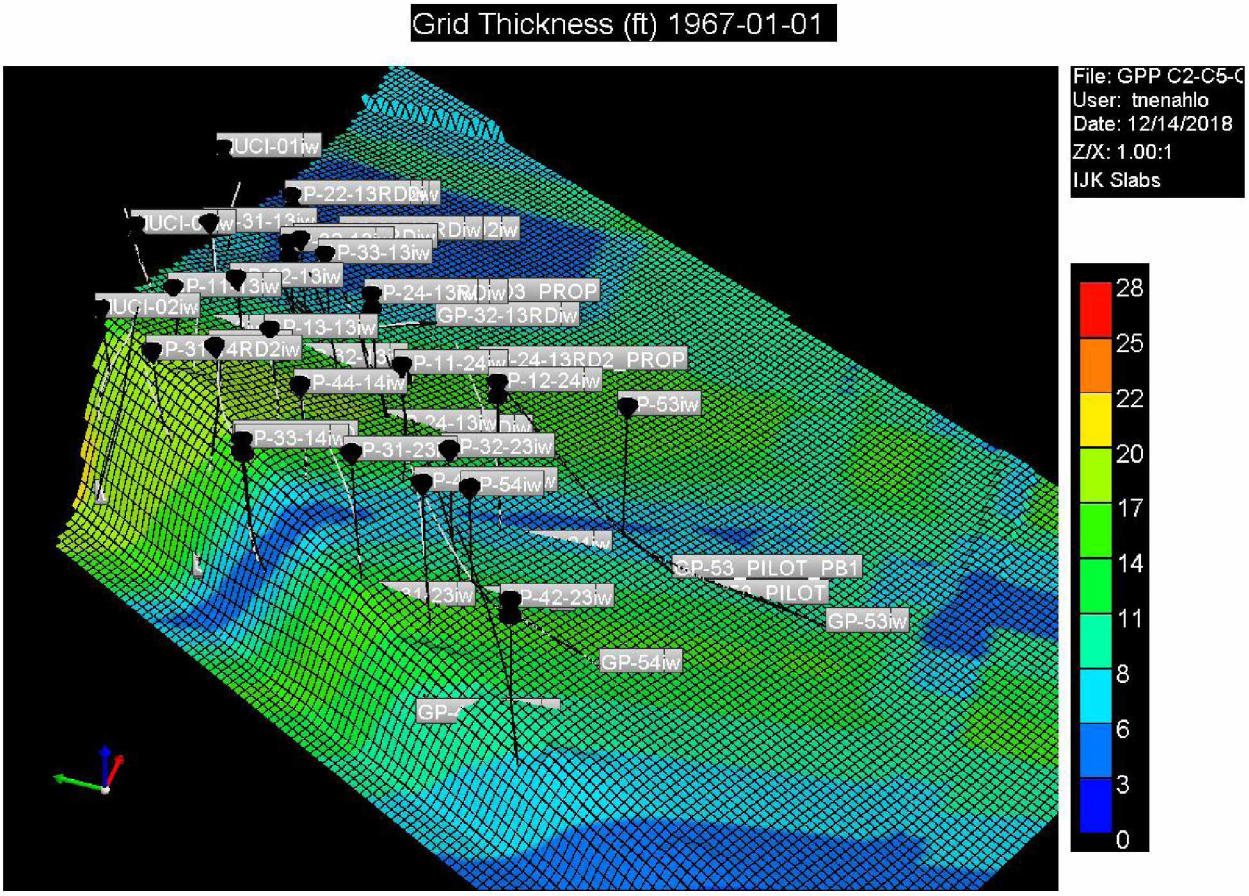

Figure 48: C7 sand grid thickness for reservoir simulation.

The model was constructed as a Black Oil model with no free gas present. The initial reservoir pressure was defined as 4,631 psi at a reference depth of 9,800 ft SSTVD with a bubble point pressure of 2,400 psi. The PVT and relative permeability were derived from the analytical work outlined in Sections 3.1 – 3.8. The aquifer contacts were defined using well control where the oil water contact was established, or a lowest-known oil where the contact was not known. The depths of the oil-water contacts for each sand is a critical assumption in this model and future iterations of the simulation should investigate the effects of changing the contact depths.

The production and injection history was imported into the model. The MUCI injectors that lie along the lease boundary between the Granite Point and Anna Platforms had their injection volumes reduced to 50%. This assumes that 50% of the injection went to the south and 50% of the injection went to the north.

Aquifer properties were defined to simulate the encroachment that has supported reservoir pressure. The aquifer properties were iterated to achieve an adequate history match.

4.4 Simulation History Matching

With the oil rate specified, a match to bottomhole pressure was achieved through iterating the aquifer properties (influx) and making adjustments to the water injection rates. The next step was to match the water injection breakthrough timing. The infill well data is critical for history matching, specifically in reference to the objectives of the simulation to find un-swept areas of oil. This match was achieved in the C2, C5, and C6 sands, but not in the C7 sands, as shown below in Figure 49. Simulation shows that water has moved along the crest of the structure whereas infill development wells drilled in the 1990s, along with production histories of the wells along the top of structure indicate that the C7 sand is un-swept along the top of the structure south of the GP-50 and GP-51 wells. Further investigation needs to be completed to understand this water movement.

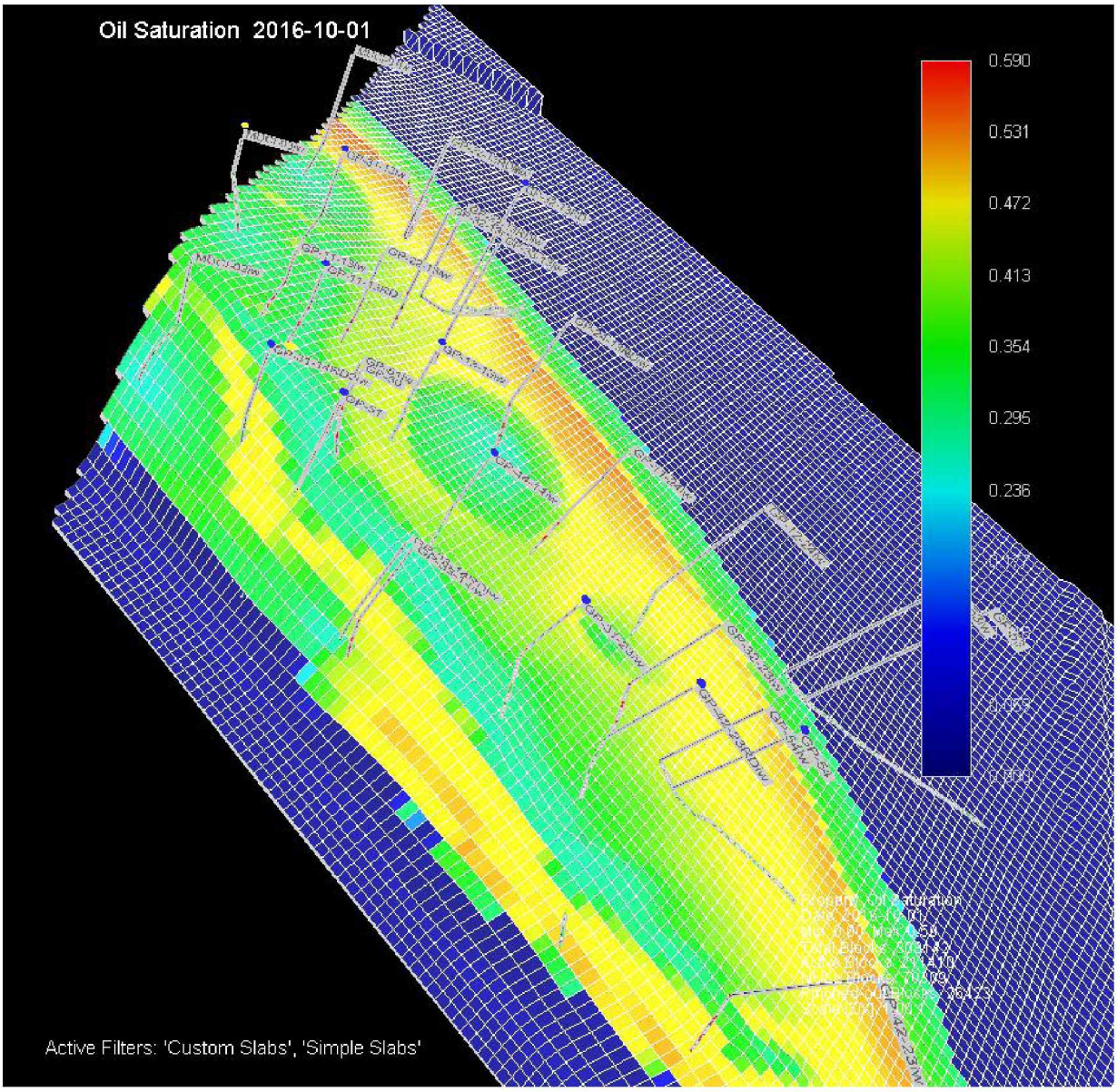

Figure 49: Granite Point platform reservoir simulation, oil saturation map, time step 2016.

4.4 Simulation Key Findings

The results of this simulation align well with the analytical approach in predicting the areal extent of the injection, with the exception being water movement along the top of structure in the C7. The simulation has identified areas along the east and west flanks, as well as the southern nose of the Granite Point platform area structure for potential infill horizontal wells as shown for the C5 sand in Figure 50. As further confirmation of the accuracy of the model, the GP-11-24RD well was drilled into the east flank in 2017 and encountered initial oil saturation along its trajectory, as suggested by the model as well as the analytical approach.

To improve model accuracy, as a means to ensure development success by placing horizontal wells in the optimal location, the following needs to be completed:

- A porosity array needs to be applied to each sand using well control to guide the interpretation. The subtle variation in porosity will have a large impact on the movement of water.
- The thinner sands (e.g. C7A, C8, etc.) must be included into the model to ensure water injection and oil production are allocated properly to each sand.

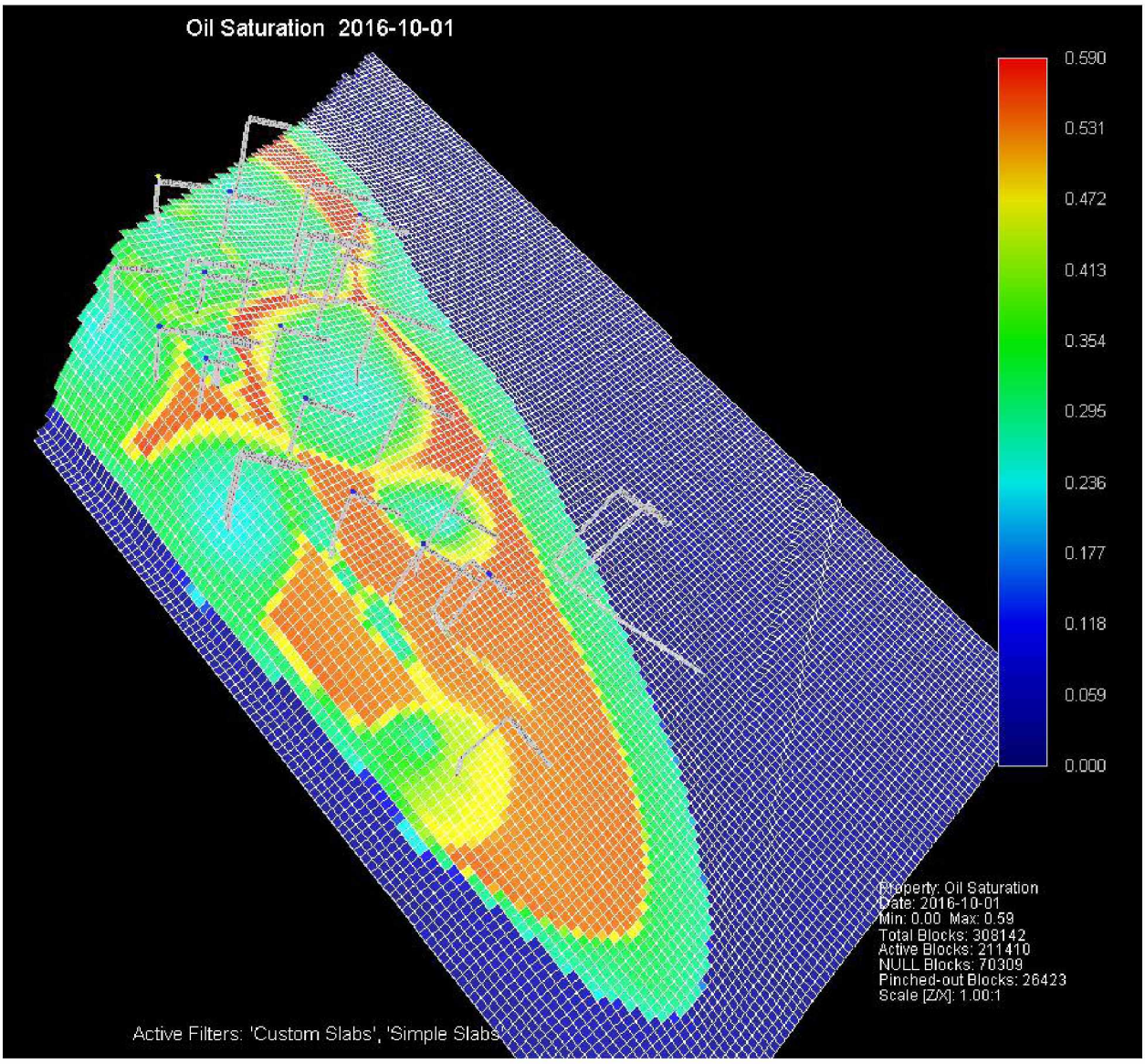

Figure 50: Granite Point platform C5 sand reservoir model match to year 2016. The red indicates initial oil saturation (see color scale on right).

Chapter 5: Conclusions

5.1 Historical Field Review Findings

- The anticline structure of the Granite Point field is generally well defined through extensive seismic data and well control. The steeply dipping west flank is the exception.
- The deposition environment is fluvial in nature with a generally northwest-southeast depositional axes as the primary source of the sediment came from the Alaska Range Complex.
- The Tyonek C sands are composed of primarily sandstone, conglomerate, and small amounts of siltstone.
- Conglomerates in the Granite Point field tend to have a lower average porosity, but a greater permeability for a .given porosity, when compared to the sandstone.
- The wide range in permeability for the sandstone at a given porosity is believed attributable to the grain size.
- The Tyonek C sands are thicker, fewer in number, and generally of higher quality to the southwest and become thinner, more numerous, and of poorer quality to the northeast.
- The reservoir rock quality of the Granite Point field is analogous to fields that are 3,000' deeper, indicating the reservoir has been substantially uplifted.
- Faulting is present along the west flank of the structure near the crest, and in the north of the field. These faults likely are baffling to sealing in nature and pose a challenge to reservoir connectivity.

5.2 Summary of Key Findings

- The Granite Point field oil is of high quality with a 39° API gravity at 60° F and a bubblepoint pressure of 2,389 psia. The viscosity is favorable for waterflooding with a minimum viscosity at saturation pressure of 0.272 cP.
- The oil in the Tyonek C sands could benefit from gas injection due to swelling properties.
- An exponential relationship exists between porosity and effective oil and water permeability.
- SCAL derived effective permeability to oil will overestimate well productivity.
- The fractional flow curve suggests an efficient oil displacement.
- The average recovery factor at water breakthrough is 52% while at 10 pore volumes injected it is 57%. This marginal increase in oil recovery after breakthrough suggests that individual sands can be thought of qualitatively as producing oil up until water breakthrough, and afterwards will produce water only.
- The reservoir pressure history obtained from the Granite Point Platform area of the field indicates a nearly constant reservoir pressure of 1,500-1,800 psig at the producers from 1973 to 2018.

- The static reservoir pressure history, low rate of production decline, stable GOR, and infill wells encountering aquifer water at shallower depths than were encountered during the initial development wells suggest aquifer support is present.
- Limited empirical data is available to define the aquifer properties and any attempt made to quantify these properties to determine aquifer influx would be highly subjective.
- Material balance drive mechanism analysis indicates aquifer support is present prior to startup of water injection and after water injection cessation. The constant positive slope of the $F/(E_o+E_{fw})$ vs N_p curve when water injection is not active suggests an infinite acting aquifer. The aquifer appears to be weak in its influx capabilities, likely attributable to the unfavorable effective permeability to water.
- An analytical approach to injection allocation and areal coverage is possible due to the favorable mobility ratio and efficient displacement as indicated by the fractional flow curve.
- Injection logs indicate an injection conformance that is expected based upon the exponential relationship between porosity and effective water permeability. The lower porosity sands were unable to take significant quantities of water.
- Geologic hurdles make secondary recovery with water injection challenged; however, in areas with well-defined sand channels of higher porosity, waterflood can be extremely effective as evidenced by the fractional flow curve.
- Hall plots were constructed by previous operators that indicated severe plugging.
- The fracture gradient of the Tyonek C sands is approximately 1.0 psi/ft, along with the extremely low effective permeability to water, making fracture stimulation challenging.
- Horizontal wells, when steered away from injection swept areas and the aquifer, can improve the ultimate recovery of the Granite Point field.
- The average effective horizontal permeability for the horizontal wells was determined to be 0.7 mD, with a range of 0.20 – 1.0 mD
- Permeability, reservoir thickness, and reservoir pressure have the most leveraging impact on the liquid productivity for horizontal wells at Granite Point field.
- The good agreement between the value of the horizontal effective permeability from the horizontal wells and the vertical wells, 0.7 mD and 1.2 mD, respectively, supports calibrating the effective horizontal permeability to empirical data rather than relying upon core data.
- Based upon normalized productivity data for horizontal wells, an 8% porosity cutoff is recommended.
- Reservoir simulation results align well with the analytical approach to mapping the waterflood.
- To improve model accuracy, as a means to ensure development success by placing horizontal wells in the optimal location, the following needs to be completed:
    - A porosity array needs to be applied to each sand using well control to guide the interpretation. The subtle variation in porosity will have a large impact on the movement of water.

- The thinner sands (e.g. C7A, C8, etc.) must be included into the model to ensure water injection and oil production are allocated properly to each sand.

5.3 Methods to Improve Ultimate Recovery

Upon completion of this work, there are four methodologies identified that could be employed to improve the ultimate recovery of the field. A summary of these methodologies are as follows:

- Fracture Stimulation:
  - On principle fracture stimulation should improve productivity and therefore ultimate recovery within the Tyonek C sands; however, the nature of the geology makes the execution of a successful fracture stimulation challenging. The fracture gradient of the Tyonek C sands is approximately 1.0 psi/ft and the reservoir rock has an extremely low effective permeability to water. Dead crude has been used to deliver a 30,000# frac at the BR-08-86 well; however, no uplift in production was realized. This size frac was likely not enough to overcome the low effective permeability to oil.
- Gas Injection:
  - The under-saturated oil within the Tyonek C sands has a high swelling potential, based upon testing that was not covered in detail the body of this report. Gas injection was not investigated due to the market value of gas within the Cook Inlet basin. To inject gas into an oil reservoir would be costly as a significant investment in pipelines, injection facilities, and recompletions and/or new wells would be required, not including the lost revenue from injecting gas that could be sold. Furthermore, injecting the gas into the proper location on top of structure with down-dip offtake points is not possible in most of the sands at the Granite Point field due to historic water injection locations and volumes.
- Horizontal Wells:
  - Horizontal wells are the key to improving ultimate recovery at the Granite Point field. The flat production profile indicates a weak aquifer drive. Leveraging this aquifer drive and drilling significant footage will yield economic results. Thorough quantification of injection and aquifer movement is required on a sand-by-sand level to ensure optimal placement of laterals. For the north end of the field, as the sands become thinner and of lower porosity, economic results with prevailing rotary well costs may not meet operators' economic thresholds. More cost effective solutions to drill horizontal wells, such as coiled tubing drilling, may prove lucrative.
- Water Injection:

- Although the Tyonek C sand have an extremely low effective permeability to water, secondary recovery with water injection was successful in the early stage of development, and can be in the future, but only when applied between wells that are connected by a sand of acceptable porosity.

List of References

1.) Matthew J. Frankforter, James C. Waugaman, 2013, The Granite Point field, Cook Inlet, Alaska, in D.M. Stone and D. M. Hite, ed., Oil and gas fields of the Cook Inlet Basin, Alaska: AAPG Memoir 104, p. 263–290.

2.) Nokleberg, W. J., L. M. Parfenov, J. W. H. Monger, I. O.Norton, A. I. Khanchuk, D. B. Stone, C. R. Scotese, D. W. Scholl, and K. Fujita, 2000, Phanerozoic tectonic evolution of the circum-north Pacific: USGS Professional Paper 126, 122 p.

3.) Reservoir Fluid Study, Mobil Oil Corporation & CORE Laboratories; Granite Point State No. 31-13 well, Granite Point Field, Cook Inlet, Alaska; August 16th, 1967.

4.) Economides, Hill, Zhu. *Petroleum Production Systems, Second Edition.* Boston: Prentice Hall, 2013. Print. 55p.

5.) Dake, L.P. *The Practice of Reservoir Engineering (Revised Edition).* Amsterdam: Elsevier BV, 2001. Print.

6.) Granite Point Field Historical Review Memo, Unocal, circa 1998.

7.) Hall Plots. Retrieved from http://www.petroleumengineers.ru/sites/default/files/u198/hall_plot.png

8.) Economides, Hill, Zhu. *Petroleum Production Systems, Second Edition.* Boston: Prentice Hall, 2013. Print. 98p.

9.) Reservoir Fluid Study, Mobil Oil Corporation & CORE Laboratories; Granite Point State No. 31-13 well, Granite Point Field, Cook Inlet, Alaska; August 16th, 1967.

10.) Trevena, A. S., and A. F. Walden, 1994, Description and formation evaluation of cored intervals from the Tyonek, Hemlock, and West Foreland Formation, Granite Point field, Cook Inlet, Alaska: Unocal Technical Memorandum PDT 94-210M

11.) Dake, L.P. *The Fundamentals of Reservoir Engineering.* Amsterdam: Elsevier BV, 1978. Print.

Acknowledgements

There are many individuals I would like to acknowledge for their help in this research. Firstly, I would like to thank Matthew Brown, the Asset Team Lead for Hilcorp Alaska's Cook Inlet Offshore Assets. The access to the field historical information and the associated data made this research possible.

I would also like to thank the faculty of the University of Alaska Fairbanks, specifically Dr. Abhijit Dandekar and Dr. Samson Ning. These two professors dedicated a tremendous amount of their personal time to help me in becoming a better engineer.

Lastly, I would like to thank the College of Petroleum Engineering and Geosciences, King Fahd University of Petroleum and Minerals, for the time dedicated by Professor Shirish Patil, Saudi Aramco Chair Professor of Petroleum Engineering, for serving as my co-advisor for this research.